Reliability Problems in Earthquake Engineering

J. E. Hurtado

Monograph CIMNE IS-63, 2010

Monografías de Ingeniería Sísmica
Editor A. H. Barbat

Reliability Problems in Earthquake Engineering

J. E. Hurtado

Monograph CIMNE IS-63, 2010

CENTRO INTERNACIONAL DE MÉTODOS NUMÉRICOS EN INGENIERÍA
Edificio C1, Campus Norte UPC
Gran Capitán s/n
08034 Barcelona, Spain

MONOGRAFÍAS DE INGENIERÍA SÍSMICA
Editor A. H. Barbat

ISSN: 1134-3249

RELIABILITY PROBLEMS IN EARTHQUAKE ENGINEERING
Monografía CIMNE IS63

ISBN: 978-84-96736-86-3
Depósito legal: B-18792-2010

Introduction

This monograph deals with the problem of reliability analysis in the field of Earthquake Engineering. Chapter 1 is devoted to a summary of the most widely used reliability methods, with emphasis on Monte Carlo and solver surrogate techniques used in the subsequent chapters. Chapter 2 presents a discussion of the Monte Carlo from the viewpoint of Information Theory. Then, a discussion is made in Chapter 3 on the selection of random variables in Earthquake Engineering. Next, some practical methods for computing failure probabilities under seismic loads are reported in Chapter 4. Finally, a method for reliability-based design optimization under seismic loads is presented in Chapter 5.

Contents

Chapter 1

Basic concepts of structural reliability

This introductory chapter summarizes some well-established concepts and methods for structural reliability computations for the better understanding of the discussions and ideas exposed in the following chapter for the specific field of Earthquake Engineering.

1.1 Performance and limit-state functions

The main problem in stochastic mechanics is the estimation of the probability density function of one or several structural responses. If the case under analysis is a dynamical one, then the aim would be to calculate the evolution of such densities. This kind of problem can be termed *full probabilistic analysis*. A derived, more practical problem is to find a specific probability of exceeding a response threshold that can be considered critical for the serviceability or the stability of the system. This is the *reliability analysis*. Notice that, in principle at least, the second problem could be solved after the first, as the probability of failure can eventually be obtained by integration of the probability density function of the observed response. However, most reliability methods developed in the last decades attempt to estimate directly the failure probability or related reliability

indices without calculating first the response density function for reasons explained in the sequel.

In the reliability problem the input random variables (called also *basic variables*) are collected in a set $\underline{\boldsymbol{x}}$, whose deterministic counterpart is the vector $\boldsymbol{x}$. This defines the *input space*. Let us define a *performance function* $g(\boldsymbol{x})$ that incorporates both the response $r(\boldsymbol{x})$ and a critical threshold for it, $\bar{r}$, in such a way that $g(\boldsymbol{x}) > 0$ means that the sample $\boldsymbol{x}$ is in the safe domain and $g(\boldsymbol{x}) < 0$ implies failure. Hence there is a boundary $g(\boldsymbol{x}) = 0$ between the two domains $\mathcal{S} = \{\boldsymbol{x} : g(\boldsymbol{x}) > 0\}$ and $\mathcal{F} = \{\boldsymbol{x} : g(\boldsymbol{x}) < 0\}$ that is termed *limit-state function*.

For structural components, the performance function writes

$$g(\boldsymbol{x}) = S(\boldsymbol{x}) - R(\boldsymbol{x}) \tag{1.1}$$

where $\boldsymbol{x} = [x_1, x_2, \ldots, x_d]$ is the vector of d input variables, $S(\boldsymbol{x})$ is a load effect on the component and $R(\boldsymbol{x})$ the strength capacity to withstand it. In the case of complex structures the performance function is given only implicitly through a finite element (or similar) code in the form

$$g(\boldsymbol{x}) = \bar{r} - r(\boldsymbol{x}) = 0 \tag{1.2}$$

in which $r(\boldsymbol{x})$ the implicit function and $\bar{r}$ is a critical threshold for the response $r(\cdot)$ whose surpassing indicates failure. Notice, however, that for structural components the load effects $S(\boldsymbol{x})$ in Eq. (1.1) depend on the overall structural response and hence they are also known only implicitly (The only exception to this rule are the simple statically determinate structures, as is well known). As a consequence, a correct probabilistic description of the load effects on each component also passes through several finite element solutions.

For solving the above reliability problem two kinds of methods have been developed, according to which of the two functions is used as a reference. In the *methods based on the limit-state function* the shape of the function $g(\boldsymbol{x}) = 0$ in the $\boldsymbol{x}-$space is of paramount importance, since the purpose is to compute the integral

$$P_{\mathrm{f}} = \int\limits_{g(\boldsymbol{x})\leq 0} p_{\underline{\boldsymbol{x}}}(\boldsymbol{x})\mathrm{d}\boldsymbol{x} \tag{1.3}$$

that yields the probability of failure. Here $p_{\underline{\boldsymbol{x}}}(\boldsymbol{x})$ is the joint probability of the random variables. In this family we have the methods which are most widely applied, such as those based on the Taylor expansion of the performance function

(FORM and SORM) and some variants of Monte Carlo methods (Importance Sampling, Directional Simulation, etc). In the *methods based on the performance function* one observes the random variable $\underline{g}(\underline{\boldsymbol{x}})$ and defines the failure probability as

$$P_{\mathrm{f}} = P[\underline{g} \leq 0] \tag{1.4}$$

Notice that to this purpose it is not necessary to consider the form of the limit-state function $g(\boldsymbol{x}) = 0$ in the $\boldsymbol{x}$ space. This has an important advantage from the practical viewpoint, which is that the probabilities of failure corresponding to several limit-states can be obtained at the same computational cost that for a single one, because it is only a matter of observing several responses $\underline{g}_i, i = 1, 2, \ldots$ instead of one. In principle, any stochastic mechanics method giving the probability density function of the observed response, normally through moments or cumulants, can be used for estimating the reliability by integration. Although, most reliability methods published to-date belong to the former category. This is due to the fact that in this approach there are some bye-product measures such as reliability indices and, in particular, design points that provide useful insight into the structural reliability problem, that are not obtained with the performance function approach. This is especially true in the particular case of incomplete statistical information.

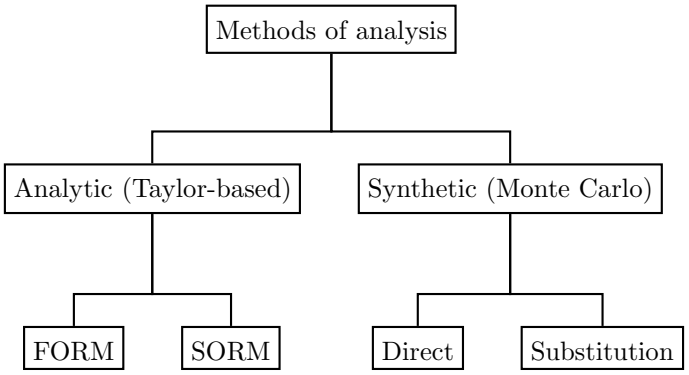

Figure 1.1: Methods based on the limit-state function.

1.2 Methods based on the limit-state function

The methods based on the limit-state function that have been proposed so far in the international literature can be grouped into two general families which can be named as *analytic* and *synthetic*, according to whether the random variable set $\underline{\boldsymbol{x}}$ and its effects are treated with the tools of Probability Theory or with those of Statistics (see Fig. 1.1). In the first case we have two families of methods based on the Taylor-series expansion of the limit state function, which are known as FORM (First-Order) and SORM (Second-Order Reliability Method). The FORM method requires information on the value of the performance function and its gradient in the vicinity of the so-called *design point* and the SORM method needs also the knowledge of the second-order derivatives. In the second case, sample sets of the basic variables are generated and processed by a numerical solver of the structural model in order to obtain a population of structural responses over which statistical analyses can be conducted (Monte Carlo simulation). An important consequence of this approach, not sufficiently stressed nor evaluated in many papers on the subject, is that the failure probability becomes a random variable with normally a high coefficient of variation.

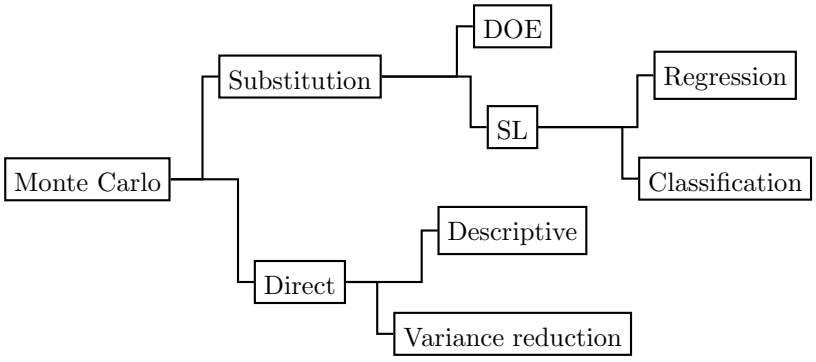

Figure 1.2: Taxonomy of Monte Carlo methods.

Monte Carlo methods in structural reliability comprehend those oriented to an overall statistical description of the response, such as Latin Hypercube ([1]; [2]; [3]) or Descriptive Sampling [4], and those specially purported at solving the integral (1.3), which are commonly known as *variance reduction methods*. These include Importance Sampling ([5]; [6]), Directional Sampling [7] and Subset Simulation [8]. Advanced versions of the descriptive methods, however, have been recently proposed for the reliability problem [9]. All these methods can be applied either to the numerical solver of the structural model to obtain the samples of the structural responses (*direct simulation*) or to a suitable *solver surrogate* thereof (Fig. 1.2). In this latter case a simple function that yields estimates of the structural response of interest in the reliability analysis is calculated. The above mentioned randomness of the failure probability points out the importance of this alternative, because even when applying variance-reduction methods there is a need of repeating the entire simulation some times in order to produce an average of the failure probability or the reliability index, because the coefficient of variation of the failure probability tends to be the higher, the lower the target probability [10]. If the solver is substituted by an approximating function, these additional runs and a large part of the first one can be performed without resort to the finite element code but using the function instead.

The construction of a surrogate of the finite-element solver has been attempted in the last decades by means of the Response Surface Method (RSM) developed in the field of Design of Experiments (DOE) (see e.g. [11], [12]). In recent years it has been proposed to develop alternative solver-surrogates using Statistical Learning (SL) techniques such as Neural Networks or Support Vector Machines, which emerge as alternatives to such purpose with several distinguishing advantages [13, 14, 15, 16]. One of them is the possibility of approaching the reliability problem either with regression or with classification tools, as shown later in this chapter.

After introducing these classification of the reliability methods, a summary of their basic traits and limitations will be examined in the next paragraphs.

1.3 Transformation of basic variables

The application of some reliability methods, such as FORM and SORM, requires that the basic variable vector $\boldsymbol{x}$, defined by its joint density function or an approximate model thereof, be transformed into a set of independent Normal variables $\boldsymbol{u}$. Such transformations are also very useful when applying Statistical Learning tools.

This is due to the fact that some of these learning devices employ some special functions that are active in a limited range and hence it is convenient to standardize the input variables before training them. For this reason it is important to examine briefly some standardization techniques.

The transformation of the basic variables from $\boldsymbol{x}$ to $\boldsymbol{u}$ can be performed in several ways, according to the available statistical information. For the simple case of independent Normal variables, the transformation is simply the standardization

$$\underline{u}_i = \frac{\underline{x}_i - \mu_{\underline{x}_i}}{\sigma_{\underline{x}_i}} \tag{1.5}$$

where $\mu_{\underline{x}_i}, \sigma_{\underline{x}_i}$ are respectively the mean and standard deviation of the variable $\underline{x}_i$. If the variables are correlated, the set $\underline{\boldsymbol{u}}$ is obtained by a linear transformation of the form

$$\underline{\boldsymbol{u}} = \boldsymbol{T}(\underline{\boldsymbol{x}} - \boldsymbol{\mu}_{\underline{\boldsymbol{x}}}) \tag{1.6}$$

where $\boldsymbol{T}$ is a matrix obtained from the Choleski or the spectral decomposition of the covariance matrix of the set $\underline{\boldsymbol{x}}$. This latter leads to the Principal Component Analysis that allows a direct generation of a small subset of important random variables in a transformed space, thus operating an effective dimensionality reduction. Such an important prerogative is not exhibited by the Choleski decomposition.

In the case where the variables are non-Normal, but are independent, the Normal tail transformation [17] is applicable:

$$\underline{u}_i = \Phi^{-1}\left(P_{\underline{x}_i}(x_i)\right) \tag{1.7}$$

Here $P_{\underline{x}_i}(x_i)$ is the distribution of $\underline{x}_i$ and $\Phi(\cdot)$ is the standard Normal distribution. A similar transformation using a non-standard Normal distribution instead of the standard one is used in the context of FORM algorithms [18].

If the joint density function of all variables is known the Rosenblatt transformation can be applied [19]. The transformation is based on the fact that the multivariate distribution $P_{\underline{x}_1,\underline{x}_2,\cdots\underline{x}_n}(x_1, x_2, \cdots x_n)$ is equivalent to $P_{\underline{x}_1}(x_1)P_{\underline{x}_2|\underline{x}_1}(x_2|x_1)\cdots P_{\underline{x}_n|\underline{x}_1,\underline{x}_2,\cdots\underline{x}_{n-1}}(x_n|x_1, x_2, \cdots x_{n-1})$. Therefore, the transformation can be performed in the following recursive form:

$$\begin{aligned} u_1 &= \Phi^{-1}\left(P_{\underline{x}_1}(x_1)\right) \\ u_2 &= \Phi^{-1}\left(P_{\underline{x}_2|\underline{x}_1}(x_2|x_1)\right) \\ &\vdots \\ u_m &= \Phi^{-1}\left(P_{\underline{x}_m|\underline{x}_1,\underline{x}_2,\cdots\underline{x}_{m-1}}(x_m|x_1,x_2,\cdots x_{m-1})\right) \end{aligned} \tag{1.8}$$

where, e.g. $P_{\underline{x}_i|\underline{x}_j,\underline{x}_k}(x_i|x_j,x_k)$ is the the conditional distribution of x_i given x_j and x_k. These functions can only be obtained in some particular cases. Also, it must be taken into account that the order of inclusion of the variables in the recursion can facilitate or complicate the solution.

A more common case is that of variables whose joint density function is not known (in fact, there are only few continuous multivariate probability models (see e.g. [20]) so that it is not likely that any of them fits the problem in hand), but the marginals and the correlation structure are known. To such situation the Nataf transformation [21] has been found to be very convenient in stochastic mechanics ([22];[23]). It consists in transforming the give variables $\underline{x}_i$ to

$$z_i = \Phi^{-1}\left[P_{\underline{x}_i}(x_i)\right] \tag{1.9}$$

The set $\underline{\boldsymbol{z}}$ has zero mean, unit standard deviations and correlation matrix

$$\boldsymbol{R}_{\underline{\boldsymbol{z}}} = \begin{pmatrix} 1 & \bar{\rho}_{12} & \cdots & \bar{\rho}_{1,m} \\ \bar{\rho}_{21} & 1 & \cdots & \bar{\rho}_{2,m} \\ \vdots & \vdots & \ddots & \vdots \\ \cdots & \cdots & \cdots & 1 \end{pmatrix} \tag{1.10}$$

in which the correlation coefficients are the solution of the integral equation

$$\rho_{ij} = \int_{-\infty}^{\infty}\int_{-\infty}^{\infty}\left(\frac{x_i-\mu_i}{\sigma_i}\right)\left(\frac{x_j-\mu_j}{\sigma_j}\right)\phi_2(z_i,z_j,\bar{\rho}_{ij})\mathrm{d}z_i\mathrm{d}z_j \tag{1.11}$$

where ϕ_2 is the standard, two-dimensional Normal density function. Finally, a set of independent Normal variables $\boldsymbol{u}$ can be obtained by the Choleski or spectral decomposition of matrix $\boldsymbol{R}_{\underline{\boldsymbol{z}}}$. Empirical formulas for estimating $\bar{\rho}_{ij}$ after ρ_{ij} have been derived by [22]. The empirical equations can be summarized in the following unified form:

$$F_{ij} = \alpha_1 + \alpha_2\eta_j + \alpha_3\eta_j^2 + \alpha_4\rho + \alpha_5\rho^2 + \alpha_6\rho\eta_j + \alpha_7\eta_i + \alpha_8\eta_i^2 + \alpha_9\rho\eta_i + \alpha_{10}\eta_i\eta_j \tag{1.12}$$

where $\rho = \rho_{ij}$. The values of the coefficients can be found in [22]. The maximum error reported by the authors with respect to the exact values of the ratio is 4.5%. However, most errors are less than one percent.

1.4 FORM and SORM

1.4.1 Basic equations

The First and Second-Order Reliability Methods (FORM and SORM) consist in finding the design point $\boldsymbol{u}^*$ in a suitable standard space $\boldsymbol{u}$ and substituting the actual performance function by its first- or second-order Taylor expansion around that point. Notice that the transformation from $\boldsymbol{x}$ to $\boldsymbol{u}$ implies that a performance function $g(\boldsymbol{u})$ substitutes $g(\boldsymbol{x})$. Its second-order Taylor expansion about a point $\boldsymbol{u}^+$is

$$g(\boldsymbol{u}) \doteq g(\boldsymbol{u}^+) + \boldsymbol{a}^{\mathrm{T}}(\boldsymbol{u} - \boldsymbol{u}^+) + \frac{1}{2}(\boldsymbol{u} - \boldsymbol{u}^+)^{\mathrm{T}}\boldsymbol{H}(\boldsymbol{u} - \boldsymbol{u}^+) \tag{1.13}$$

where $\boldsymbol{a}$ is the gradient vector evaluated at the expansion point

$$\boldsymbol{a} = \nabla g|_{\boldsymbol{u}^+} \tag{1.14}$$

and $\boldsymbol{H}$ the Hessian matrix

$$\boldsymbol{H}_{ij} = \frac{\partial^2 g}{\partial u_i \partial u_j}|_{\boldsymbol{u}^+} \tag{1.15}$$

In FORM the last term in Eq. (1.13) is disregarded and the design point $\boldsymbol{u}^*$ is the solution of the optimization problem

$$\begin{aligned} \text{minimize} \quad & \beta = \left(\boldsymbol{u}^{\mathrm{T}}\boldsymbol{u}\right)^{\frac{1}{2}} \\ \text{subject to} \quad & g(\boldsymbol{u}) = 0 \end{aligned} \tag{1.16}$$

The solution of this optimization problem is carried out by mean of iterative techniques ([18]). This problem corresponds to finding the shortest distance from the

origin to the limit-state function in the transformed space $\boldsymbol{u}$ so that $g(\boldsymbol{u}^\star) = 0$. The result is

$$\beta = \boldsymbol{w}^{\mathrm{T}}\boldsymbol{u}^\star \tag{1.17}$$

where

$$\boldsymbol{w} = \frac{\boldsymbol{a}^\star}{|\boldsymbol{a}^\star|} = \frac{\nabla g(\boldsymbol{u}^\star)}{|\nabla g(\boldsymbol{u}^\star)|} \tag{1.18}$$

is the vector normal to the tangent hyperplane at the design point. Hence the equation of the hyperplane becomes

$$\begin{aligned} g(\boldsymbol{u}) &= \boldsymbol{w}^{\mathrm{T}}(\boldsymbol{u} - \boldsymbol{u}^\star) \\ &= \boldsymbol{w}^{\mathrm{T}}\boldsymbol{u} - \beta \end{aligned} \tag{1.19}$$

which, for comparison with some Statistical Learning equations presented later on, can be put in the form

$$g(\boldsymbol{u}) = \langle \boldsymbol{w}, \boldsymbol{u} \rangle - \beta \tag{1.20}$$

where $\langle \cdot, \cdot \rangle$ denotes Euclidean inner product.

SORM techniques are based on the above first-order solution. The approximation of the limit state function (1.13) can be presented in terms of β and $\boldsymbol{u}^\star$ as follows:

$$g(\boldsymbol{u}) \doteq \langle \boldsymbol{w}, \boldsymbol{u} \rangle - \beta + \frac{1}{2}(\boldsymbol{u} - \boldsymbol{u}^\star)^{\mathrm{T}}\boldsymbol{B}(\boldsymbol{u} - \boldsymbol{u}^\star) = 0 \tag{1.21}$$

where

$$\boldsymbol{B}_{ij} = \frac{1}{|\nabla g(\boldsymbol{u}^\star)|}\boldsymbol{H}_{ij}|\boldsymbol{u}^\star \tag{1.22}$$

Some approximations to Eq. (1.21) in terms of principal curvatures have been suggested ([24]; [25]). They are quoted here as they provide useful insight into the reliability problem. By a rotation of the $\boldsymbol{u}$ space to space $\boldsymbol{v}$ such that the design point is located in v_d the axis, function (1.21) can be recast in the form [24]

$$-(v_d - \beta) + \frac{1}{2}\begin{pmatrix} \boldsymbol{v}_{d-1} \\ v_d - \beta \end{pmatrix}^{\mathrm{T}} \boldsymbol{A} \begin{pmatrix} \boldsymbol{v}_{d-1} \\ v_d - \beta \end{pmatrix} = 0 \tag{1.23}$$

where $\boldsymbol{v}_{d-1} = [v_1 v_2 \dots v_{d-1}]^{\mathrm{T}}$ and $\boldsymbol{A} = \boldsymbol{R}\boldsymbol{B}\boldsymbol{R}^{\mathrm{T}}$, in which $\boldsymbol{R}$ is an orthonormal matrix with $-\boldsymbol{w}$ as its d^{th} row. Solving the above equation for v_d an retaining only the first two order terms yields

$$v_d = \beta + \frac{1}{2}\boldsymbol{v}_{d-1}^{\mathrm{T}}\boldsymbol{A}_{d-1}\boldsymbol{v}_{d-1} \tag{1.24}$$

where $\boldsymbol{A}_{d-1}$ is formed with the first $d-1$ rows and columns of $\boldsymbol{A}$. By solving the eigenvalue problem of matrix $\boldsymbol{A}_{d-1}$, i.e. $\boldsymbol{A}_{d-1}\boldsymbol{u} = \boldsymbol{\kappa}\boldsymbol{u}$ one obtains the approximation

$$u_d = \beta + \frac{1}{2}\sum_{i=1}^{d-1}\kappa_i u_i^2 \tag{1.25}$$

where the eigenvalues are called principal curvatures. This definition is disputed by [25] who support their approximation in the concept of principal curvature of differential geometry. Their approximation reads

$$u_d = \beta + \frac{1}{2R}\sum_{i=1}^{d-1} u_i^2 \tag{1.26}$$

where

$$R = \frac{d-1}{K}$$
$$K = \sum_{i=1}^{d}\boldsymbol{B}_{jj} - \boldsymbol{w}^{\mathrm{T}}\boldsymbol{B}\boldsymbol{w} \tag{1.27}$$

In these equations K is the sum of principal curvatures (according to differential geometry) and R is the average principal curvature radius.

1.4.2 Discussion

The calculation of the FORM hyperplane requires the computation of the gradients of the performance function with respect to all basic variables. This is due to the fact that the problem is formulated as a constrained optimization task. Since the performance function is normally not given in closed-form, the gradient calculation can only be performed by finite-difference strategies, which requires a minimum of $d+1$ finite element solver calls per iteration point [26]. Since the number of

iterations is of the order of ten, it is evident that the calculation of FORM solutions via finite-difference strategies is limited to low dimensionality problems. The situation is more severe in the case of SORM because it is necessary to calculate the elements of the Hessian matrix, which due to symmetry are $d(d-1)/2+d$. Such a involved computation is needed even for applying the approximate SORM techniques, as Eqs. (1.25) and (1.26) clearly indicate.

For these reason some approaches have been developed for simplifying this task, especially that of FORM. The main trend is the calculation of the gradients at the finite-element level, by means of the so-called *perturbation approach* (see e.g. [27]). This implies for instance the calculation of the derivatives of the stiffness matrices with respect to the basic variables or transformations thereof. This task, however, is also affected by the increase of the dimensionality, because the derivative of a $N \times N$ matrix with respect to a $d \times 1$ vector is a $Nd \times Nd$ matrix. Of course, the situation is more severe for using SORM with such low-level derivatives. Similar dimensionality explosions also occur in using other analytical approaches such as those based on polynomial chaoses ([28]; [29]).

Another aspect that should be considered is the accuracy and stability of these approaches. The limitations of FORM in this regard were pointed out by [30]. With respect to SORM [31] argues that there are several instances in which there is an infinite number of SORM quadratic approximations, for a given set of design point and principal curvatures, that have associated probabilities running from 0 to 1. In words, the SORM results are unstable. Mitteau [31] supports this statement on a single two-dimensional example but a rigorous derivation of its domain of validity is presently lacking. By the same time of Mitteau's paper, an ample study on both FORM and SORM was published by [32]. According to the authors the applicability of FORM is limited to curvatures

$$|K| \leq \frac{1}{10\beta} \tag{1.28}$$

and that of SORM to

$$-0.1\left((2+0.6\beta)\sqrt{d-1}+3\right) \leq |K| \leq 0.4\left(\sqrt{d-1}+3\beta\right) \tag{1.29}$$

This means that FORM is restricted to cases having very large curvature radius, irrespective to the number of basic variables, and its applicability reduces with the increase of the reliability as measured by β . On the other hand, SORM shows a different trend. Its applicability increases with the dimensionality and with the first-order reliability. However, a previous paper by the authors [25] shows that

SORM approximate equations are adequate only if the principal curvatures have all the same sign. If this condition is not met, as in the generalized approximation

$$u_d = \beta + \frac{1}{2R}\sum_{i=1}^{d-1} a^i u_i^2, \;\; a < 0, \tag{1.30}$$

all SORM formulas fail to give the exact results with a large error. This is but an effect of the rigidity of the SORM model in the sense defined in a next section.

In addition, despite [32] show that SORM has much wider applicability than FORM, they do not discuss the dimensionality scaling of the number of solver calls. In fact, it is important to note that in the study it is assumed that the gradients and curvatures have been calculated and, therefore, that the FORM problem has been solved. Hence, the dimensionality effects on the number of solver calls for rendering explicit the limit-state function, that were mentioned above, should anyhow be considered. As a conclusion, it can be said that besides the restrictions for applying FORM and SORM in terms of accuracy, both methods are applicable only in low-dimensional problems. For a large number of dimensions (a common situation in structural dynamics and stochastic finite element analysis, for instance) these approaches are highly expensive from the computational point of view.

Given the superiority of SORM over FORM some alternatives to alleviate its computational cost have been devised. They consist basically in approximating the gradients and curvatures by fitting a quadratic polynomial using an experimental plan which in the Response Surface Methodology is called saturated design ([24]; [33]). These applications of the Response Surface Method is called point-fitting in the context of SORM analysis. It is illustrated in Fig. 1.3 after the first of the quoted references. However, better approximations can be obtained with some Statistical Learning methods as shown in the sequel.

1.5 Monte Carlo methods

In order to review variance reduction Monte Carlo methods, which are the most commonly applied in structural reliability, let us first summarize the basic (or crude) Monte Carlo simulation technique. For estimating the integral

$$P_{\mathrm{f}} = \int_{\mathcal{F}} p_{\underline{x}}(\boldsymbol{x})\mathrm{d}\boldsymbol{x} \tag{1.31}$$

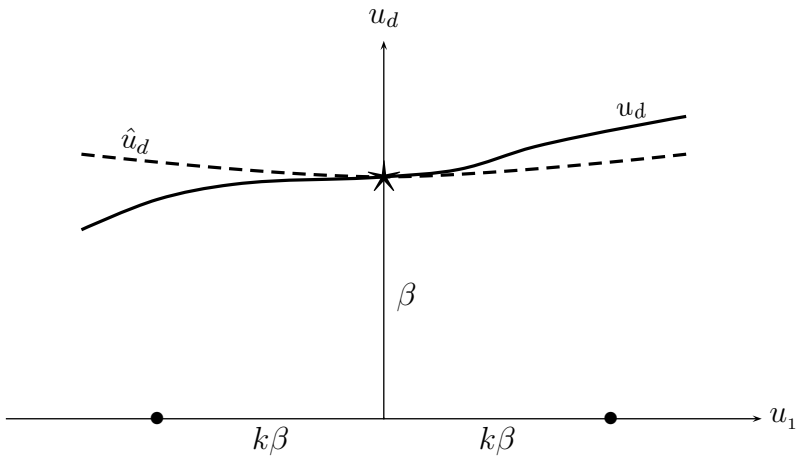

Figure 1.3: Point-fitting method for SORM approximation (Adapted from [24]).

the domain of integration can be changed to the entire real space using the indicator function

$$\Upsilon_{\mathcal{F}}(\boldsymbol{x}) = \begin{cases} 1, & \text{if } g(\boldsymbol{x}) \leq 0 \\ 0, & \text{if } g(\boldsymbol{x}) > 0 \end{cases} \tag{1.32}$$

In such case Eq. (1.31) takes the form

$$P_{\mathrm{f}} = \int \Upsilon_{\mathcal{F}}(\boldsymbol{x}) p_{\underline{\boldsymbol{x}}}(\boldsymbol{x}) \mathrm{d}\boldsymbol{x} \tag{1.33}$$

Therefore, the failure probability is the expected value

$$P_{\mathrm{f}} = \mathrm{E}\left(\Upsilon_{\mathcal{F}}(\boldsymbol{x})\right) \tag{1.34}$$

and, consequently, it can be estimated as

$$\hat{P}_{\mathrm{f}} = \frac{1}{n} \sum_{i=1}^{n} \Upsilon_{\mathcal{F}}(\boldsymbol{x}_i) \tag{1.35}$$

using n i.i.d samples $\boldsymbol{x}_i, i = 1, \ldots, n$. This basic Monte Carlo method is known to be excessively costly for reliability analysis because in order to produce one sample in the failure domain it is necessary to obtain a large number of them lying in the safe one. Hence, it is more efficient to modify Eq. (1.31) in order to work with a different expected value requiring less samples. Two techniques have been found useful for achieving this goal, namely Importance Sampling and Directional Simulation. In addition, they form the kernel of numerous advanced Monte Carlo methods for structural reliability, some which are mentioned in the next paragraph.

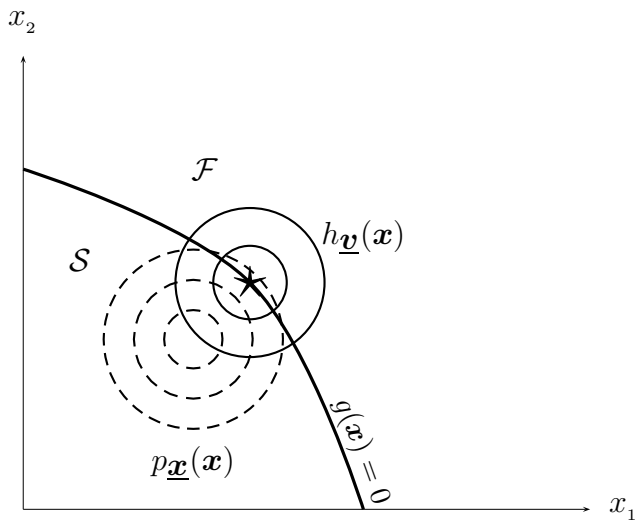

Figure 1.4: Importance Sampling method.

1.5.1 Importance Sampling

In the Importance Sampling (IS) technique (see e.g. [34]) the integral (1.31) is transformed to:

$$P_{\mathrm{f}} = \int_{\mathcal{F}} \frac{p_{\underline{\boldsymbol{x}}}(\boldsymbol{x})}{h_{\underline{\boldsymbol{y}}}(\boldsymbol{x})} h_{\underline{\boldsymbol{y}}}(\boldsymbol{x}) \mathrm{d}\boldsymbol{x} \tag{1.36}$$

or equivalently

$$P_{\mathrm{f}} = \int \Upsilon_{\mathcal{F}}(\boldsymbol{x}) \frac{p_{\underline{\boldsymbol{x}}}(\boldsymbol{x})}{h_{\underline{\boldsymbol{y}}}(\boldsymbol{x})} h_{\underline{\boldsymbol{y}}}(\boldsymbol{x}) \mathrm{d}\boldsymbol{x} \tag{1.37}$$

where $h_{\underline{\boldsymbol{y}}}(\boldsymbol{x}$ is an auxiliary density function intended to produce samples in the region that contributes most to the integral (1.31). This transformation implies that the estimate of the failure probability becomes:

$$\hat{P}_{\mathrm{f}} = \frac{1}{n} \sum_{i=1}^{n} \Upsilon_{\mathcal{F}}(\boldsymbol{v}_i) \frac{p_{\underline{\boldsymbol{x}}}(\boldsymbol{v}_i)}{h_{\underline{\boldsymbol{y}}}(\boldsymbol{v}_i)} \tag{1.38}$$

where the samples $\boldsymbol{v}_i, i = 1, \ldots, n$ are now generated from $h_{\underline{\boldsymbol{y}}}(\boldsymbol{x})$ instead of $p_{\underline{\boldsymbol{x}}}(\boldsymbol{x})$ as before. It is easy to demonstrate that the optimal IS density equals (see e.g. [35]):

$$h_{\underline{\boldsymbol{y}}}(\boldsymbol{x}) = \frac{\Upsilon_{\mathcal{F}}(\boldsymbol{x}) p_{\underline{\boldsymbol{x}}}(\boldsymbol{x})}{P_{\mathrm{f}}} \tag{1.39}$$

which in practice is ineffective, as it depends on the target of the calculation, i.e. P_{f}.

At this point, Importance Sampling methods that have been proposed in the literature can be grouped into two categories:

1. *Importance Sampling with design points.* Early applications of the Importance Sampling concept in structural reliability used a density $h_{\underline{\boldsymbol{y}}}(\boldsymbol{x})$ on the design point ([5]; [30]; [36]) (See Fig. 1.4). The point is approximately identified by a preliminary Monte Carlo simulation with a few samples. A similar procedure was proposed for the case of multiple design points ([37]; [35]). In these approaches use is normally made of a single multivariate Normal density (for one design point) or of a linear combination of Gaussians (for several points, such as those arising in system safety analysis).

   The use of a design point as a location for a sampling density is, however, not a good choice in some cases. This can be illustrated by having resort to SORM simplified models, which are useful for testing reliability analysis techniques with simple but realistic examples. If the principal curvatures in

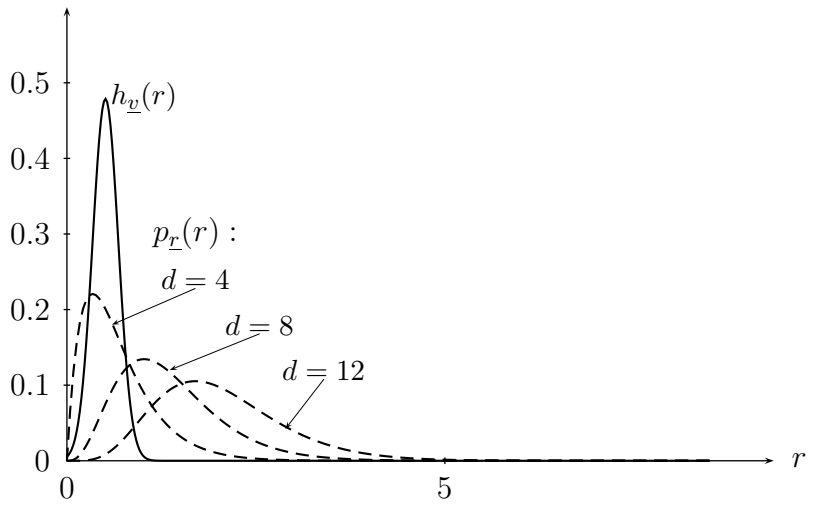

Figure 1.5: On the inadequacy of Importance Sampling with design points for problems with curvatures of the same sign. If $g(\boldsymbol{u}) = \beta - u_d + \sum_{i=1}^{d-1} u_i^2 = 0$ the variable $r = \sum_{i=1}^{d-1} u_i^2$ is χ^2_{d-1} distributed. An Importance Sampling standard Normal density placed on $u_d = \beta = 3$ does not capture the probability flow of this variable as the dimensionality grows.

Eq. (1.25) are all negative, an increasing probability mass flows to the failure domain as the number of dimensions increase, so that a density function placed on the design point will not capture the important region as intended. The opposite situation occurs for positive curvatures. This phenomenon is illustrated by Fig. 1.5 in which a standard Normal model is used as the IS density. The same phenomenon happens in case of the cylindrical safe region

$$g(\boldsymbol{u}) = \eta^2 - \sum_{i=1}^{d} u_i^2 = 0 \tag{1.40}$$

having the probability of failure

$$P_{\mathrm{f}} = 1 - P[\chi_d^2 \leq \eta^2] \tag{1.41}$$

For this domain some reliability indices become negative for a moderate number of dimensions. All this means that in using direct Monte Carlo simulation methods (i.e. without a solver surrogate as indicated by Fig. 1.1) it would be more efficient to locate the *most likely failure point*, defined as that having the highest probability density ordinate in the failure domain, as opposed to the *design point*, defined as that closest to the origin in the standard space.

It can be argued that the Normal density could be made adaptive according to problem dimensionality by increasing the diagonal elements of the covariance matrix. However, according to a recent research by [10], deviations from the standard model are not recommended for a large number of dimensions, since this leads to large deviations of the IS density from its optimal value (1.39). In fact, in the quoted paper the authors conclude that the IS method is applicable with single or multiple design points in the standard $\boldsymbol{u}$ space with many dimensions if the covariance matrix of the Gaussian IS density does not deviate from the identity matrix. However, the authors do not discuss the problem posed by principal curvatures of equal sign, which makes the IS method with design points altogether ineffective as the dimensionality grows.

2. *Adaptive Importance Sampling strategies.* In this group we have several techniques aimed at establishing an IS density as close as possible to the optimal value given by Eq. (1.39) ([38]; [39]; [40]). This option is also disputable for large dimensions. In order to show this it is important to compare the estimates of the failure probability given by the basic Monte Carlo method and Importance Sampling (Eqs. 1.35 and 1.38, respectively). Note that while the latter requires the estimation of a density function that approaches the optimal one, the former does not. The problem of generating samples after the optimal IS density without the knowledge of P_{f} can be circumvented by means of simulation algorithms of the Metropolis family (see e.g. [41]), because they operate with a probability ratio in which P_{f} cancels out. This technique has been applied in [40]. However, it remains the problem that an accurate estimation of a density function is seriously affected by the curse of dimensionality, as illustrated by [42]. Let us quote an example conveyed

by this author. A direct measure of the accuracy of a density estimate from a given set of samples is the so-called *equivalent sample size* $n_d(\epsilon)$, which is the number of samples in d dimensions necessary to attain an equivalent amount of accuracy ϵ in using conventional kernel or finite-mixture density estimates ([42]; [43]) such as those use by [38] and [40]. The crucial point is that the equivalent sample size grows exponentially with problem's dimension. [42] exposes an example in which $n_d(\epsilon) = 50$ in $\mathbb{R}^1$, $n_d(\epsilon) = 258$ in $\mathbb{R}^2$, $n_d(\epsilon) = 1126$ in $\mathbb{R}^3$, etc, using the so-called Epanechnikov criterion for density estimation accuracy. Therefore, if use is made of a low number of samples in Eq. (1.38), the errors in estimating $h_{\underline{\boldsymbol{v}}}(\boldsymbol{v})$ will be large. Taking into account that this factor enters in the denominator of the equation, while in the numerator there is a density given beforehand, it is easily concluded that the introduction of a density estimation problem in the way of calculating a single probability is equivalent to solve a more complicated problem than the target one as an intermediate step.

1.5.2 Directional Simulation

Directional Simulation is based on the concept of conditional probability. It also exploits the symmetry of the standard space $\boldsymbol{u}$ [44]. Referring to Fig. 1.6, the probability of failure can be expressed as

$$P_{\mathrm{f}} = \int_{\boldsymbol{a} \in \Omega_d} P[g(r\underline{\boldsymbol{a}}) \leq 0 | \underline{\boldsymbol{a}} = \boldsymbol{a}] p_{\underline{\boldsymbol{a}}}(\boldsymbol{a}) \mathrm{d}\boldsymbol{a} \tag{1.42}$$

where Ω_d is a unit sphere centered at the origin of the $d-$dimensional space, $\underline{\boldsymbol{a}}$ is a random unit vector in the sphere sampled with a uniform density $p_{\underline{\boldsymbol{a}}}(\boldsymbol{a})$ and r is the solution of $g(r\boldsymbol{a}) = 0$. In this simple directional simulation approach, the probability of failure is estimated as

$$\hat{P}_{\mathrm{f}} = \frac{1}{n} \sum_{i=1}^{n} P[g(r\boldsymbol{a}_i) \leq 0] \tag{1.43}$$

with n samples of $\underline{\boldsymbol{a}}$. If there is only one root r then the probability $P[g(r\boldsymbol{a}_i) \leq 0]$ is equivalent to $P[\underline{r} > r]$ and hence the probability of failure for each sample is given by Eq. (1.41). Therefore, Eq. (1.43) becomes

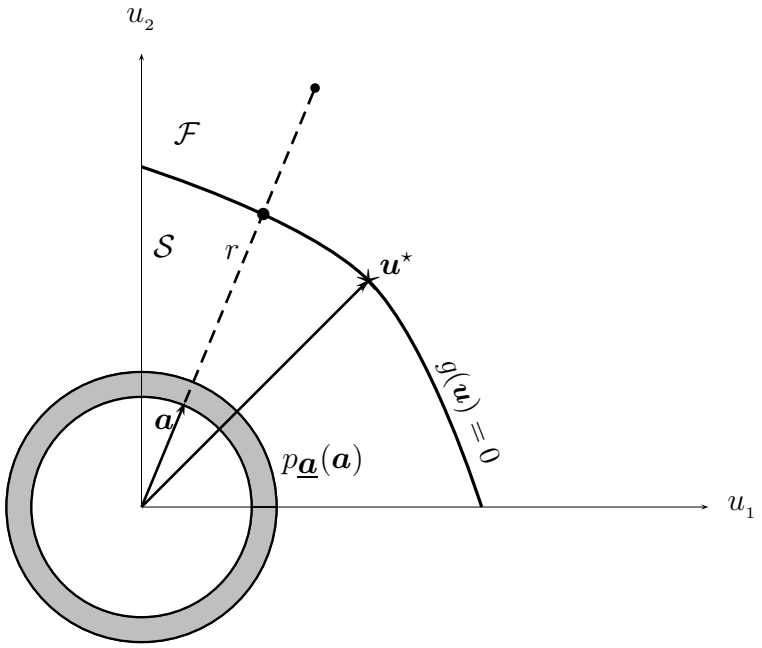

Figure 1.6: Directional Simulation method.

$$\hat{P}_{\mathrm{f}} = \frac{1}{n}\sum_{i=1}^{n}\left(1 - P[\chi_d^2 \leq r^2]\right) \tag{1.44}$$

Notice that in this approach the problem of curvatures with the same sign is explicitly incorporated in the formulation by having resort to the unit sphere. More sophisticated alternatives involve the use of an IS density posed on top of the unit sphere and focused to the design point $\boldsymbol{u}^\star$ [7]. In these alternatives the solution of the equation $g(r\boldsymbol{a}) = 0$, which is difficult in case of implicit performance functions, is substituted by the calculation of a one-dimensional integral. Since the IS density used in them is not placed on the design point but merely oriented towards it, and no optimal IS density is built, the problems of the IS method in high dimensions mentioned above are not present. For this reason, the Directional Simulation method seems theoretically superior than Importance Sampling technique

for dealing with high dimensional problems.

1.5.3 General characteristics of simulation methods

After summarizing the most important simulation techniques in the previous paragraphs, it is important to state apart some general features of Monte Carlo methods in order to highlight the relevance of solver-substitution techniques that are briefly examined in the next section.

First of all it is important to recall the fundamental advantages of the basic (or crude) Monte Carlo integration method as applied to structural reliability :

- It makes no assumptions about the shape of the limit state function or the location of design points.
- It does not need transformations nor rotations of the basic variable space.
- It is not affected by the so-called curse of dimensionality. In fact, the error rate of crude Monte Carlo integration with n samples is $O(n^{-1/2})$ regardless of the dimensionality of the problem, while other numerical integration methods require $O(n^d)$ samples in order to reach an error rate of $O(n^{-1})$ [45].
- It is entirely general, in the sense that it can be equally applied to linear or nonlinear structural models of any size.
- It does not require the writing of special structural codes as it makes use of standard software employed by the analyst for doing deterministic calculations.

The particular features of advanced Monte Carlo methods have been remarked in the previous paragraphs. However, all Monte Carlo methods as a whole have the disadvantage of being highly expensive from the computational viewpoint. This is not only due to the fact that it requires the repeated call of the numerical solver for the assessment of any statistical quantity but also that these quantities become random variables, with the consequence that the entire simulation should be repeated several times in order to estimate the quantity through an average and derive some statistics of the failure probability. In the particular case of failure probabilities, the coefficient of variation of the estimates are, of course, lower when using variance reduction techniques but it tends to be inversely proportional to P_{f}. In other words, the lower the failure probability, the higher the spread of the

estimates ([46]; [47]; [48]; [8]). The coefficient of variation can reach values as high as 0.6 for $P_{\mathrm{f}} = 10^{-4}$, which is a common figure in applications, thus meaning that the one-sigma bounds for it are $[0.4 \times 10^{-4}, 1.6 \times 10^{-4}]$, which is a wide range indeed.

The high randomness of Monte Carlo estimates is usually not sufficiently stressed the literature, but it obviously contributes to the refusal of Monte Carlo methods, that is common in structural mechanics fields in which the solution of each deterministic sample takes a large amount of storage and time. In this regard, it is important recall that the advance in the computing capabilities has brought about a parallel increase in the number of degree of freedom used in finite element calculation and a sophistication of the constitutive models implemented into the structural solvers. Despite the important increase of storage and calculation speed of modern computers that have taken place in recent years, such parallel refinement of finite element models has a negative effect in the diffusion on Monte Carlo methods in actual engineering practice.

1.6 Relevance of solver-surrogate building

Summarizing the conclusions reached after the examination of the development of analytical and synthetic methods, the relevance of building solver surrogates for assisting the reliability analysis of a complex structure is based on the following facts:

- For the reliability analysis at the component or at the structural levels, the limit state function is actually implicit. This hinders the direct application of analytical methods requiring not only the value of the function but also of its gradient and, in the SORM case, the curvatures at the design point. Hence, in spite of FORM and SORM methods are in a sense solver-surrogate techniques, they require much information on the performance function, especially the latter. This information could be provided by a good functional approximation.

- Monte Carlo methods do not require such refined information on the function but need a large number of samples to produce an estimate of the failure probability. This number is much larger than normally stated because any quantity estimated with these techniques is a random variable and hence the simulation programme should be repeated several times in order to derive some statistics such as the mean and the standard deviation and to reduce

the confidence interval for the mean of the failure probability. This enormous task could be drastically reduced if use is made of a good approximation of the implicit functions given by a finite element code.

In addition, it must be said that solver-surrogate methods are not affected by problems of probability flow with dimensionality increase, such as that posed by principal curvatures having the same sign because they are simply approximations of deterministic functions. For this reason, the design point is in these methods more important than the most likely failure point.

The task of building solver surrogates has traditionally been pursued by means of the Response Surface Method (RSM) ([6];[49]; [50];[36]; [51]), which has been adopted by the structural reliability community after its development in the field of Design of Experiments (see e.g. [12]; [11]). As said above, some Statistical Learning techniques can be very useful to this purpose. In particular, Neural Networks or Support Vector Machines, which have the characteristic of being flexible and adaptive approaches which are in contrast to the rigidity and non-adaptive nature of the models used in RSM.

In the next section the RSM is briefly reviewed. It will be shown that some problems of the method that have been highlighted in recent years ([52]; [53]) are due to the rigid structure of the RSM model and its way of approaching the limit-state function. Next, it is shown why the flexibility and adaptivity of Statistical Learning techniques such as Neural Networks and support vector machines make them attractive to overcome these difficulties for the goal of building good approximations of the implicit functions needed in a structural reliability analysis.

1.7 Solver-surrogate methods

1.7.1 Response Surface Method

The Response Surface Method is purported to replace the structural model solver needed for computing the value of the performance function with a simple expression, which is usually of second-order polynomial form:

$$\hat{g}(\boldsymbol{x}) = \theta_0 + \sum_{i=1}^{d} \theta_i x_i + \sum_{i=1}^{d} \theta_{ii} x_i^2 \tag{1.45}$$

or

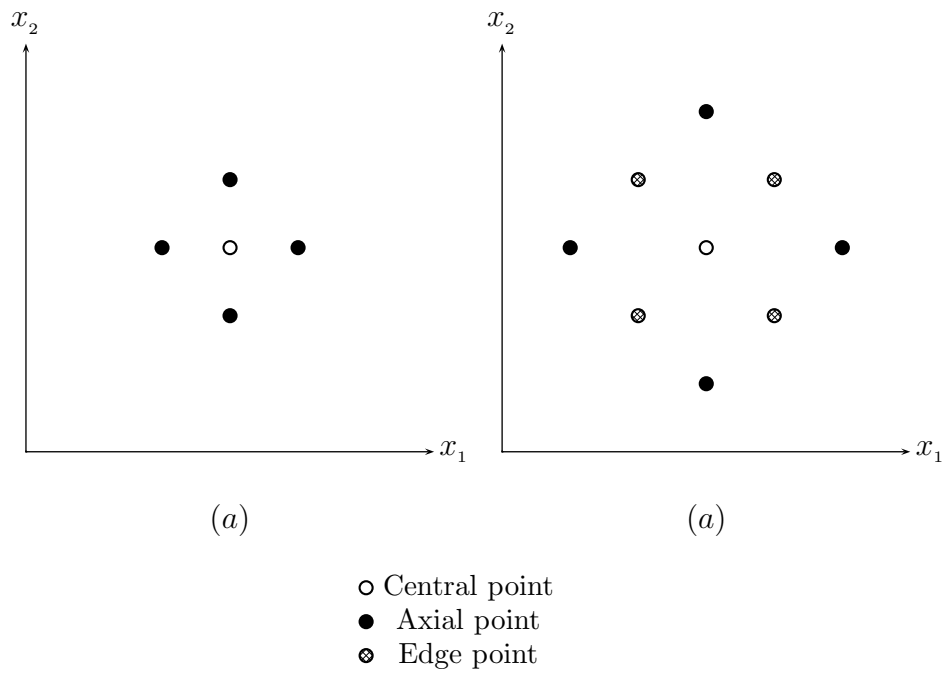

Figure 1.7: Experimental designs for the Response Surface Method. (a): Saturated Design (b): Central Composite Design.

$$\hat{g}(\boldsymbol{x}) = \theta_0 + \sum_{i=1}^{d} \theta_i x_i + \sum_{i=1}^{d} \sum_{j=1}^{d} \theta_{ij} x_i x_j \tag{1.46}$$

Here $\boldsymbol{x}$ is the vector of the d input values, $\hat{g}(\cdot)$ is an estimate of the performance function and the θ's are parameters. The difference between these equations is that the first includes cross terms while the second does not. This function is fitted to a non-random experimental plan by solving a simple algebraic problem. The number of solver calls and the way of finding the coefficients depend on the experimental plan adopted (see Fig. 1.7 and Table 1.1). The coordinates of the experimental vectors in the initial trial can be described by the formula $\mu_i \pm k\sigma_i$,

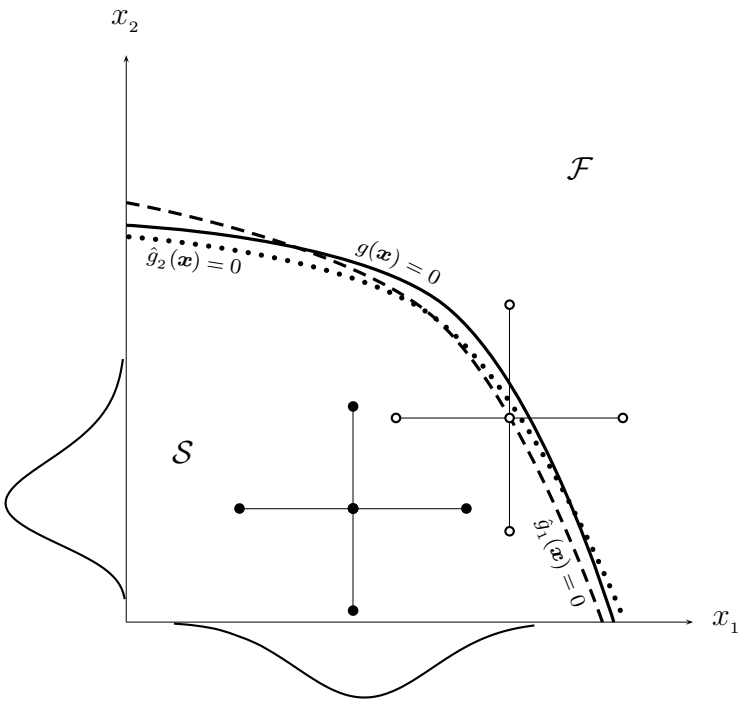

Figure 1.8: Response Surface Method fitting procedure using Saturated Design. A first experimental plan is placed around the mean vector in the $\boldsymbol{x}$-space. The design point corresponding to the first approximation $\hat{g}_1(\boldsymbol{x}) = 0$ is located, a new plan is placed about it and a new surface is calculated.

where μ_i, σ_i are respectively the mean and standard deviation of the i-th variable and k is a coefficient for the point type. Obviously, $k = 0$ for the central points and typically $k = 1$ for edge points and $k = 2$ to 3 for axial points. After a first trial function, the design point in the standard space can be easily found and successive improvements of the response surface are obtained by locating the center of the experimental plan on the current design point (Fig. 1.8). A total of R runs of the entire program is hence necessary.

The problems found in applying this technique will be reviewed after the introduction to the Statistical Learning techniques done in the next paragraph.

Table 1.1: Number of solver calls required by the Response Surface Method

Design	Cross terms	Number of calls
Saturated Design	No	$R(2d+1)$
Central Composite Design	Yes	$R(2^d+2d+1)$

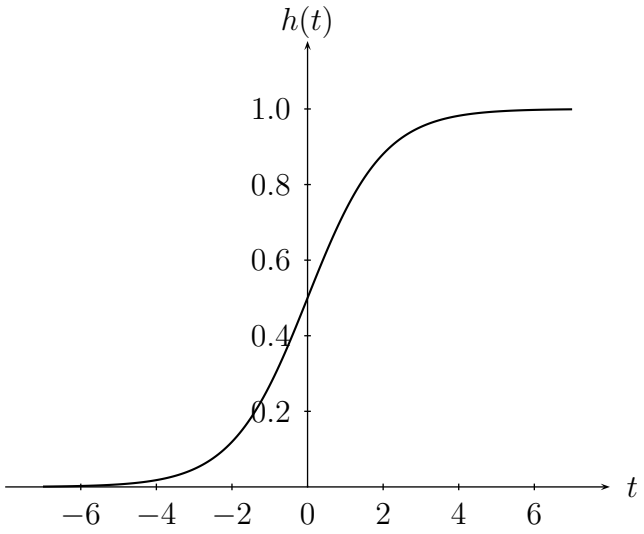

Figure 1.9: Logistic sigmoid function used in Multi-Layer Perceptrons.

1.7.2 Neural Networks and Support Vector Machines

Two classes of Neural Networks have been found to be very useful for building the solver-surrogates [54]: Multi-Layer Perceptrons (MLP) and Radial Basis Function Networks (RBFN). The former implement a function of the form (see e.g. [55])

$$\hat{g}(\boldsymbol{x}) = \tilde{h}\left(\sum_{k=0}^{m} w_k \; h\left(\sum_{i=0}^{d} w_{ki} x_i\right)\right) \tag{1.47}$$

where w_k, w_{ki} are weights. The inner sum runs over the number of dimensions d, so that x_i denotes the $i-$th coordinate of vector $\boldsymbol{x}$. On the other hand, $h(\cdot), \tilde{h}(\cdot)$ are nonlinear functions in general. A widely used function h in the inner sum is the logistic sigmoid

$$h(t) = \frac{1}{1 + \exp(-t)} \tag{1.48}$$

depicted in Fig. 1.9. This function is also used for $\tilde{h}(\cdot)$ in classification analyses while a linear function $\tilde{h}(t) = t$ is commonly applied for regression purposes.

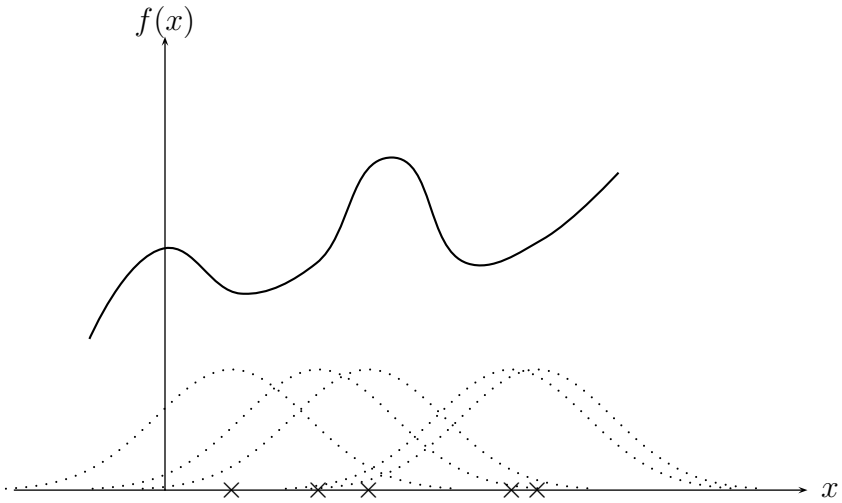

Figure 1.10: Radial Basis Functions. The crosses indicate the centers at which the radial functions such as the Gaussian are located.

Radial Basis Function Networks are based on a different concept. Instead of working with the coordinates of vector $\boldsymbol{x}$ they use some samples $\boldsymbol{x}_i, i = 1, 2, \ldots, m$ as centers of a symmetrical function in a $d-$dimensional space and build a model of the form

$$\hat{g}(\boldsymbol{x}) = \sum_{i}^{m} w_i h(\boldsymbol{x}, \boldsymbol{x}_i) \tag{1.49}$$

where w_i are weights. A common model for the radial function $h(\boldsymbol{x}, \boldsymbol{x}_i)$ is the Gaussian

$$h(\boldsymbol{x}, \boldsymbol{x}_i) = \exp\left(-\frac{||\boldsymbol{x} - \boldsymbol{x}_i||^2}{2\omega^2}\right) \tag{1.50}$$

where the constant ω defines the width of the so-called receptive field of the function. On the other hand, another technique known as Support Vector Machines (SVM) implements a function similar to Eq. (1.49) but the weights and number of basis functions are calculated rather differently [56]. The corresponding model is

$$\hat{g}(\boldsymbol{x}) = \sum_{i}^{m} w_i K(\boldsymbol{x}, \boldsymbol{x}_i) - b \tag{1.51}$$

where $K(\boldsymbol{x}, \boldsymbol{x}_i)$ is a kernel function and b is a parameter.

The following are the main characteristics of these statistical learning models:

1. *Adaptivity.* By this expression it is meant that the model is composed by a weighted sum of functions whose parameters are determined by the given samples. This is rather evident in the case of RBFN and SVM. In the case of MLP this is achieved indirectly, as the weights which enter as arguments of the functions are determined by the given samples through an optimization algorithm.

2. *Flexibility.* This means that the active region of the basis functions is limited. For instance in the radial basis function (1.50) an input $\boldsymbol{x}$ far from a given center $\boldsymbol{x}_i$ does not cause a meaningful result, whereas other inputs closer to it determine higher outputs. See Fig. 1.10.

The main consequence of these properties considered together is that the model adapts to the given set of samples, so that if these are correctly selected they will

have an active participation in the determination of the output. In particular, an important consequence of the adaptivity is that the samples used to fit the model determine both the functions and the weights, thus distributing the effects of incorrect sample selection into a large number of arguments and in a nonlinear form in some of them. On the other hand, the flexibility property implies that a training sample has a limited radius of effect, so that an error in its selection would not have serious consequences in the entire range of the output.

1.7.3 Characteristics of the Response Surface Method

In contrast to the above SL devices, the RSM works with a model of the form

$$\hat{g}(\boldsymbol{x}) = \sum_{i}^{m} w_i h_i(\boldsymbol{x}) \tag{1.52}$$

in which $h_i(\boldsymbol{x})$ are power functions of the coordinates, such as x_j, x_j^2 or $x_j x_k$, with $j, k = 1, 2, \ldots, d$. The RSM model has the following characteristics:

1. Functions $h_i(\boldsymbol{x})$ are non-adaptive. In fact, they are not indexed by the given samples of the experimental plan. As a consequence, the effect of this latter is exerted only on the weights w_i, which bear the entire responsibility for the errors. This makes the model highly sensitive to the sample selection.

2. Functions $h_i(\boldsymbol{x})$ are non-flexible. This is due to the fact that they have infinite active support, in contrast to the radial basis functions or to the derivative of the sigmoid function, which have a bell shape.

In order to illustrate the effects of such rigidity and non-adaptivity, let us consider Figures 1.11 and 1.12, which show two RSM approximations to a nonlinear limit state function

$$g(x_1, x_2) = 4 - 0.001x^8 - 2 \tag{1.53}$$

discussed by [30] for illustrating the limitations of FORM and by [53] in a paper containing a systematic study on the Response Surface Method. The approximations were obtained by the RSM using the central composite designs shown in the figures and a second order complete polynomial. Notice the important differences in the response surfaces between the two figures. It is evident that the rigidity of the RSM renders difficult the adaptation to an arbitrary, though simple and

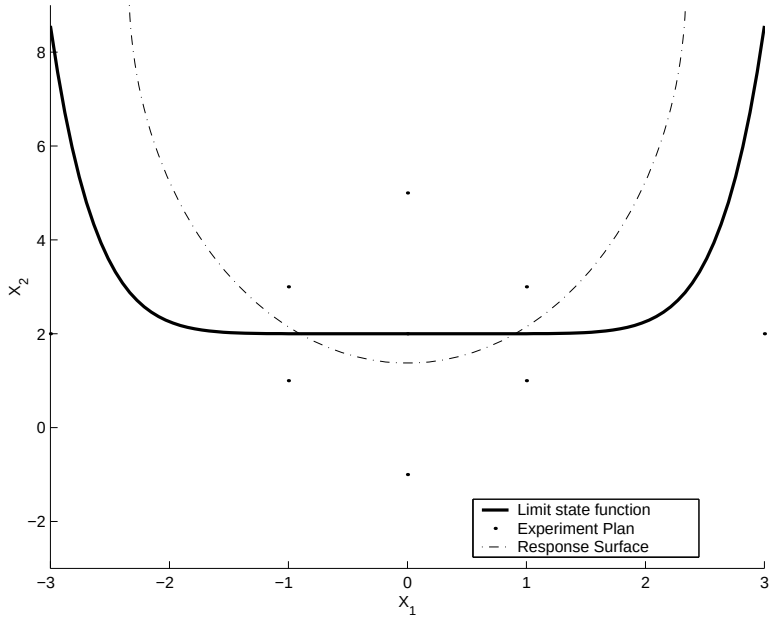

Figure 1.11: Deficiencies of the RSM for approximating limit state functions. Central composite design with $k = 1$ for the edge points and $k = 3$ for the axial points.

smooth target function, in spite of the amplitude of the experimental plan. Also, that the resulting surface and hence the estimates of the failure probability and the reliability index are strongly dependent on the experimental plan, as observed in the paper by [53], whose more important conclusions are the following:

- Since the postulated surface depends on the experimental plan (as determined by the parameter k), the assessment of the design point (onto which the plan is moved after the first run) will also change. Therefore, the value of the reliability coefficient β and hence the failure probability will also be sensitive to the plan. These values can vary very wildly for small changes of k, as illustrated by Fig. 1.13 for an example of a three bay-five story frame with a dimensionality equal to 21.

- Such wild fluctuations of the reliability measures are also a consequence of

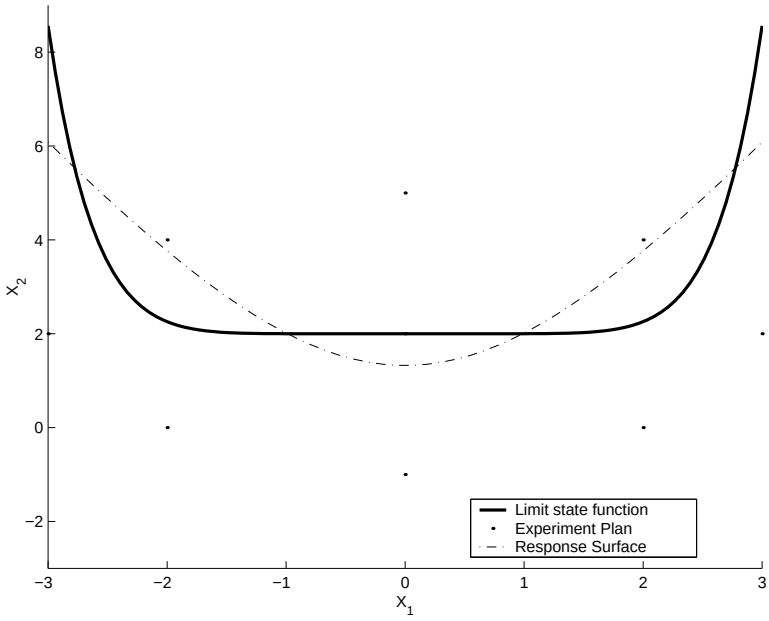

Figure 1.12: Deficiencies of the RSM for approximating limit state functions. Central composite design with $k = 2$ for the edge points and $k = 3$ for the axial points.

the transformation of the basic variables to a standard Normal space required by some reliability methods.

These problems of the RSM can be attributed to the rigidity of the model. In fact, since the constituent functions are not indexed by the samples, the coefficients of the estimated surface, the trial design point and other quantities are the result of a trade-off (i.e. least square) solution which balances the global errors and assigns all the responsibility to the model weights. Besides, the infinite support of the basis functions causes that the fitting errors affect the entire domain of the basis functions, as is evident from Fig. (1.8). On the contrary, with adaptive-flexible methods using locally active functions (such as neural networks, kernel functions, support vector machines, etc) the coefficients of the function are balanced with respect to the local errors of the particular function being active in the whereabouts of a certain sample or sample group. To illustrate this, Fig. 1.14

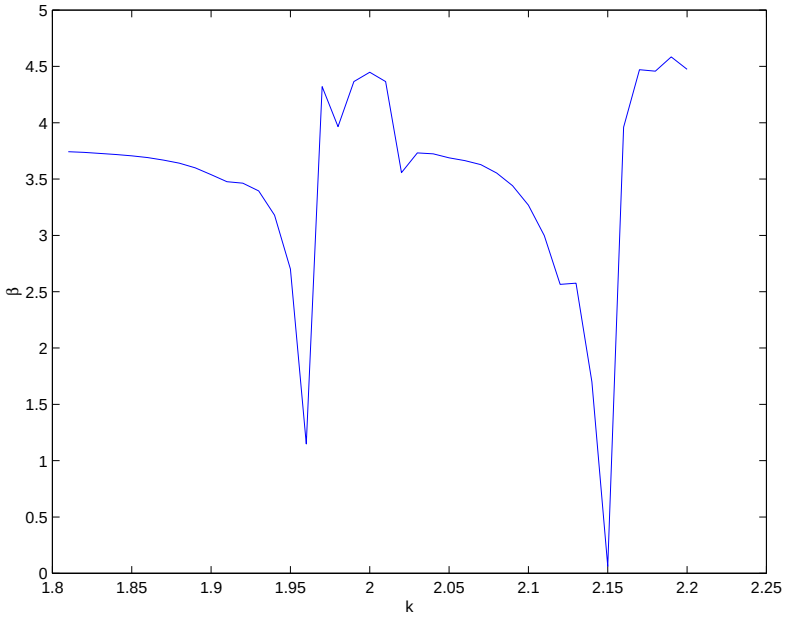

Figure 1.13: Instability of the RSM estimates of the reliability index for a three bay-five story frame (After [53]).

shows the approximation to the function (1.53) used above with a support vector machine trained with the algorithm exposed in [14], which uses a random search procedure. Although the SVM approximation required more training samples than the RSM in this case, it is also true that by no means a quadratic polynomial can approximate one of the eighth order with reasonable accuracy. However, a fitting over an ample domain such as that in the figure is necessary when the probability density in the failure region is very flat. For such situations rigid methods like RSM are only adequate if the actual limit state can be well fitted by the imposed model in the entire region; otherwise there is a large risk of error. This discussion illustrates the limitations of rigid models, which at first seem to be more suited for local approximations, i.e. for highly concentrated probability masses such as those arising in problems with highly correlated basic variables. However, the frame example of [53], in which there are some variables highly correlated, shows that

there is little hope in that the RSM would be generally applicable even for search domains reduced by high correlation. This is perhaps due to the wrong estimation of the trial design points caused by the rigidity of the basis functions of the model.

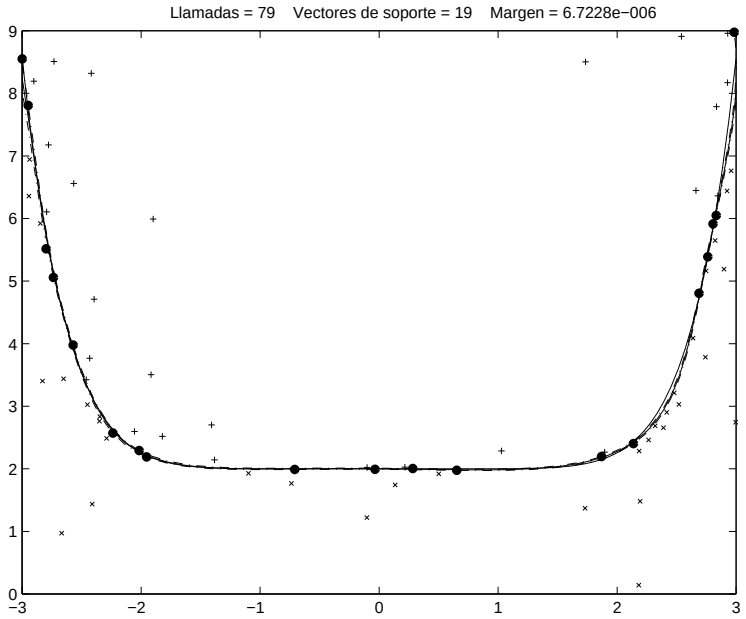

Figure 1.14: On the advantages of flexible methods for approximating limit state functions. Support Vector approximation of function in Fig. 1.11.

A situation in which the advantages of flexible over rigid models is more evident is in case of multiple limit state functions, which is common case in reliability analysis. In this case the intersections of the functions are often non smooth. Since the rigid RSM model imposes a continuous smooth function, it obviously leads to large errors in the estimation of the failure probability in this case. To cope with that situation, it would be preferable to fit one response surface for each state, a procedure that increases the computational cost. On the contrary, a single approximating function suffices when using flexible models. This is illustrated by Fig. 1.15 which corresponds to the parallel problem $\{\boldsymbol{x} \,|\, \underline{x}_1 > 3 \cap \underline{x}_2 > 3\}$, where $\underline{x}_i, i = 1, 2$ are standard Normal variables. Again, the algorithm reported in [14] for

training support vector machines was used. It is observed that the flexible model adapts well to the right angle so that the error in estimating the failure probability in this case is expected to be low. The dots appearing in the figure correspond to an underlying data bank of random samples needed by the algorithm only for picking up a few of them in the sequential training process.

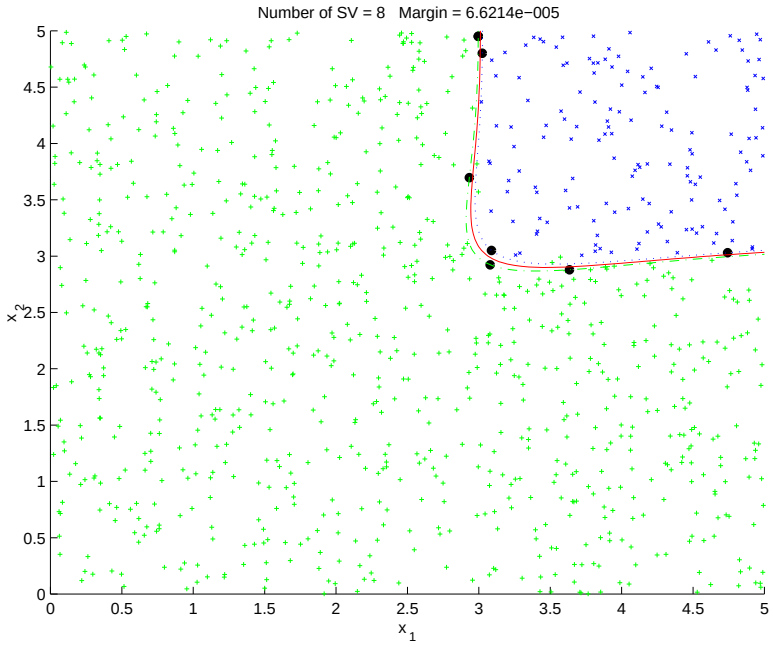

Figure 1.15: On the advantages of flexible methods for approximating limit state functions. Support Vector approximation for a parallel system problem.

An analogous contrast between adaptive and flexible models on the one hand and non-adaptive and rigid modes on the other is also exemplified by wavelet and Fourier decompositions of time functions. In fact, whereas wavelet decomposition is made with basis functions with finite support located on specific time positions, the basis functions used by Fourier analysis have infinite support and have no dependence on specific times.

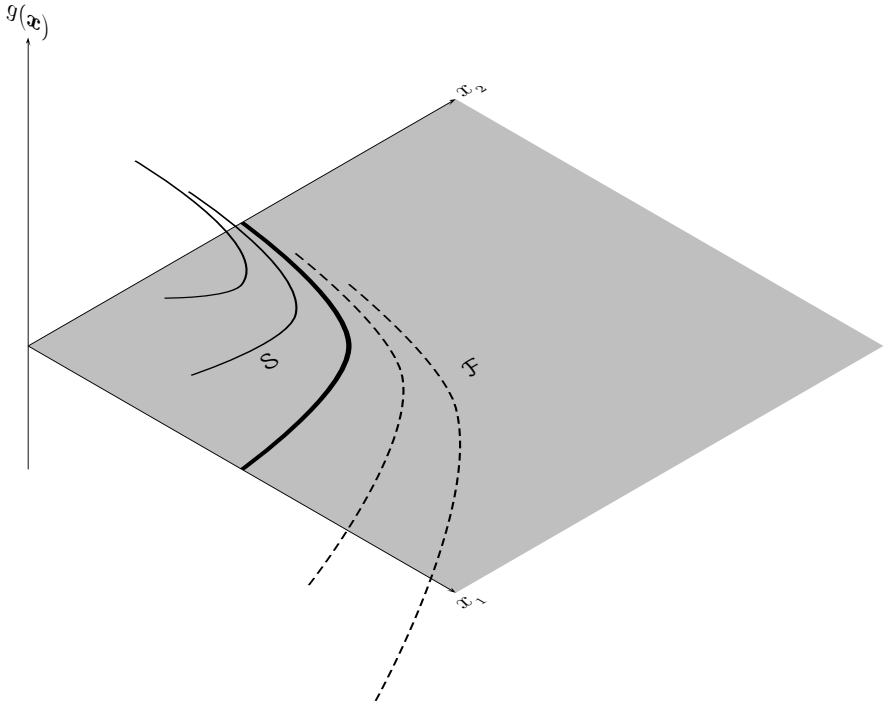

Figure 1.16: Regression approach for implicit functions.

1.8 Regression and Classification

As said in the preceding, the building of a solver surrogate for the performance function has been traditionally been carried out by means of the RSM. Recently, this goal has been pursued by means of Neural Networks, mainly of the MLP type ([57]; [54]; [58]; [59]). However, the author has called the attention to the fact that the radial basis function networks are also useful to this purpose ([13]; [60]).

All these approaches (RSM, MLP and RBFN) are intended to a functional approximation of the performance function, which upon adopting the statistical jargon can be labeled as a *regression approach* (See Fig. 1.16), in spite of this name has a very particular origin with no mathematical meaning at all [61]. However, little attention has been paid by the structural reliability research community to

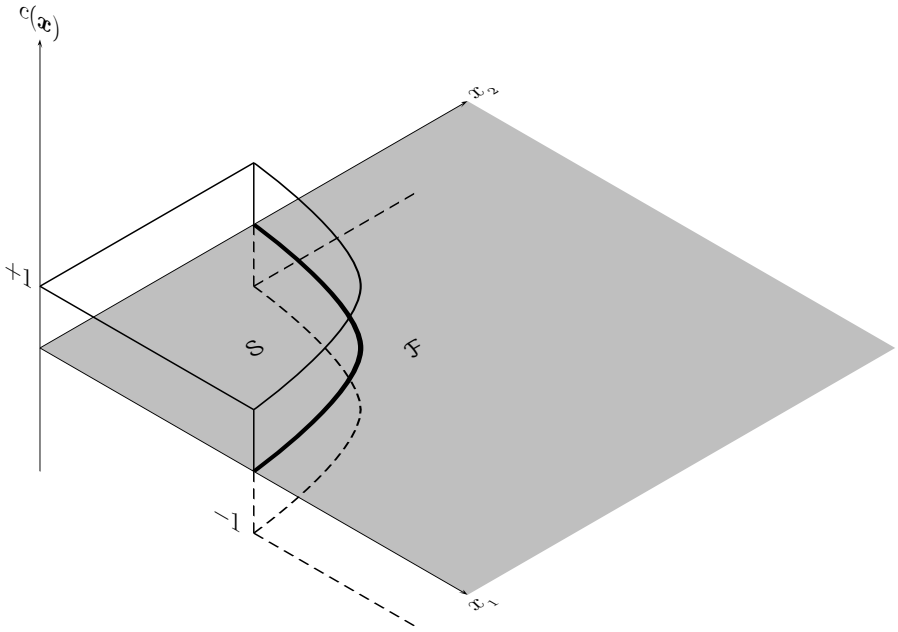

Figure 1.17: Classification approach for implicit functions.

the fact that the problem of rendering explicit the limit-state function and hence estimating the probability of failure can be solved by a *classification approach*, inasmuch as the function separates two well-defined domains, namely the safe and the failure ones (See Fig. 1.17). On the basis of some given samples, of which the sign of the performance function is known, the problem becomes that of *pattern recognition* (e.g. [62]), i.e. assigning new incoming samples to one or the other class.

The classification paradigm has the following advantages:

1. There is no need of requiring high accuracy in the estimation of the performance function values, as only the sign of the function for an specific sample $\boldsymbol{x}$ determines the class to which the sample belongs.

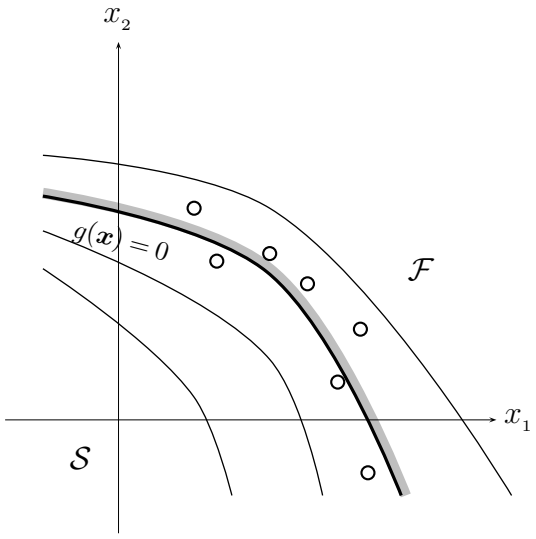

Figure 1.18: Sampling for limit-state function approximation in the classification approach.

2. The sampling for solver-surrogate building can be concentrated in the vicinity of the limit-state function as this is the actual boundary between the two classes. In other words, while regression approaches require a sampling over an ample domain of the performance function like that shown in Fig. 1.8, classification methods are able to construct a classifier with a concentrated sampling like that shown in Fig. 1.18. The geometry of the standard space $\boldsymbol{u}$ can be used to facilitate the generation of such a population as shown later on.

In this regard, it is important to call the reader's attention to the fact that a concentrated sampling such as that shown in Fig. 1.18 was proposed by [52] for building a Response Surface, in a paper that can be considered to be in the direction of overcoming the problems of the RSM by adopting a classification paradigm.

1.9 FORM and SORM approximations with Statistical Learning devices

As shown in the preceding, the FORM and SORM approximations to the limit-state function require information on the derivatives of the performance function at the design point. This information, and especially that required by SORM, is difficult to obtain in case of implicit limit-state functions. However, this task can be facilitated by the approximation of the limit-state function with linear flexible models such as RBFN and SVM that implement models (1.49) and (1.51), which are very similar. Consider for instance the second of them, with the following particular choice of the kernel function

$$K(\boldsymbol{x}, \boldsymbol{y}) = (\langle \boldsymbol{x}, \boldsymbol{y} \rangle + \theta)^p \tag{1.54}$$

where $\langle \cdot, \cdot \rangle$ stands for Euclidean inner product. This is known as the Inhomogeneous Polynomial Kernel in Pattern Recognition literature [63]. Expanding this function for the particular case of $p = 2$ yields

$$K(\boldsymbol{x}, \boldsymbol{y}) = \sum_{n=1}^{d} \sum_{j=1}^{d} x_n x_j y_n y_j + 2\theta \sum_{n=1}^{d} x_n y_n + \theta^2 \tag{1.55}$$

The derivative of the estimate with respect to a coordinate x_k is, therefore,

$$\begin{aligned} \frac{\partial \hat{g}(\boldsymbol{x})}{\partial x_k} &= \sum_{i}^{m} w_i \frac{\partial K(\boldsymbol{x}, \boldsymbol{x}_i)}{\partial x_k} \\ &= \sum_{i}^{m} w_i \left(\left[\sum_{\substack{n=1 \\ n \neq k}}^{d} x_n x_{kn} x_{in} \right] + 2 x_k x_{ik}^2 + 2\theta x_{ik} \right) \end{aligned} \tag{1.56}$$

In addition,

$$\begin{aligned} \frac{\partial^2 \hat{g}(\boldsymbol{x})}{\partial x_k^2} &= 2 \sum_{i}^{m} w_i x_{ik}^2 \\ \frac{\partial^2 \hat{g}(\boldsymbol{x})}{\partial x_k \partial x_j} &= \sum_{i}^{m} w_i x_{kj} x_{ij}, \quad j \neq k \end{aligned} \tag{1.57}$$

Similar derivations can be easily carried out for other basis functions. The case of Multi-Layer Perceptrons is, however, more involved, as is evident upon considering Eq. (1.47), especially if function $\tilde{h}(\cdot)$ applied at the output layer is nonlinear. However, the Jacobian and Hessian matrices can be easily evaluated by numerical procedures in which use is made of the very network. This is explained at length in [55], to which the interested reader is referred.

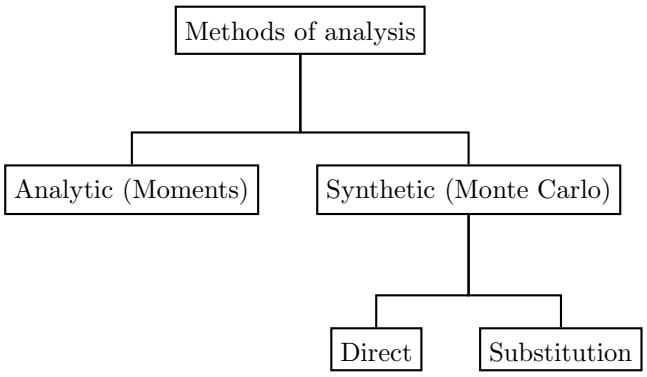

Figure 1.19: Methods based on the performance function.

1.10 Methods based on the performance function

Most methods based on the performance function that have been published thus far are based on the estimation of the density function using moments of the structural response (Fig. 1.19). The moments and/or the density function are obtained either on the basis of the principle of maximum entropy ([64]; [65]; [66]), polynomial chaos expansion of the random variables [28], polynomial approximation of the densities ([67]; [68]; [69]) or kernel density estimation [70]. Also in this group there are methods aimed at the direct estimation of the reliability with Eq. (1.4) via Monte Carlo simulation [71], statistical approximation techniques ([72]) or Pearson distribution ([73]; see, though, [74]).

The Statistical Learning methods briefly introduced in this chapter (MLP, RBFN, SVM) can also be used for this kind of approach acting as solver-surrogates. To this end they are employed as regression functions for substituting the finite-element code in the calculation of the observed responses that make the performance functions.

Chapter 2

Information characteristics of Monte Carlo simulation

2.1 Introduction

As said in the previous chapter, the basic problem of structural reliability can be defined as the estimation of the probability mass of a failure domain $\mathcal{F}$ defined by a limit state function $g(\boldsymbol{x})$ of the set of basic random variables $\underline{\boldsymbol{x}}$:

$$P_{\mathrm{f}} = \int_{\mathcal{F}} p_{\underline{\boldsymbol{x}}}(\boldsymbol{x}) \mathrm{d}\boldsymbol{x} \tag{2.1}$$

where $p_{\underline{\boldsymbol{x}}}(\boldsymbol{x})$ is the joint probability density function of the basic variables. A common characteristic of the simulation techniques is the aim of reducing the computational cost of the Simple Monte Carlo Simulation (SMCS), consisting in generating a large population from density $p_{\underline{\boldsymbol{x}}}(\boldsymbol{x})$, calculating the value of $y = g(\boldsymbol{x})$ for each sample and, finally, estimating the failure probability as the fraction of cases for which $y = g(\boldsymbol{x})$ is less than or equal to zero. According to the classification regard to structural reliability problem [54], using the results of such repeated computations of the limit state function, the probability of failure can be computed as

$$\hat{P}_{\mathrm{f}} = \frac{1}{N}\sum_{i=1}^{N} z(\boldsymbol{x}_i) \tag{2.2}$$

where $z(\boldsymbol{x})$ is the transformation

$$z(\boldsymbol{x}) = \frac{1}{2}\left[1 - \mathrm{sgn}(y)\right] \tag{2.3}$$

of the sign function, defined as

$$\mathrm{sgn}(y) = \begin{cases} -1 & \text{if } y \leq 0 \\ +1 & \text{if } y > 0 \end{cases} \tag{2.4}$$

In practice, a widely used technique for performing Monte Carlo simulation in structural reliability analysis is to stop the simulation when the estimate of the binomial coefficient of variation of the failure probability, given by [35, 75, 76]:

$$\hat{\nu}_{\mathrm{b}} = \sqrt{\frac{1 - \hat{P}_{\mathrm{f}}}{N\hat{P}_{\mathrm{f}}}} \tag{2.5}$$

becomes lower than or equal to 0.1. Here N is the actual number of samples for which the limit state functions is actually computed. This criterion stems from the assimilation of Monte Carlo simulation to a sequence of Bernoulli trials, so that the number of trials reaching the failure domain obey a binomial distribution.

As an illustration, consider the limit state function

$$g(x_1, x_2) = 0.1(x_1 - x_2)^2 - \frac{1}{\sqrt{2}}(x_1 + x_2) + 2.5$$

where the random variables $\underline{x}_1, \underline{x}_2$ are both standard Normal. The probability of failure was computed with 500 populations of $N = 25,000$ samples and making use of the stopping criterion mentioned above. This was possible in 382 out of the 500 cases. Figure 2.1 shows the relationship between the failure probability and the actual number of samples. The concentration at $N = 25,000$ corresponds to 128 cases in which the coefficient of variation estimated according to Eq. (2.5) remained higher than 0.1. For the rest of cases, in which it was possible to stop the simulation at a lower number of the limit state function evaluations, it is evident that, the lower the number of samples, the higher the failure probability. On the other hand, the histogram of the failure probability exhibits a wide range of variation, given exactly by [0.0032 0.0060], whereas the mean value computed

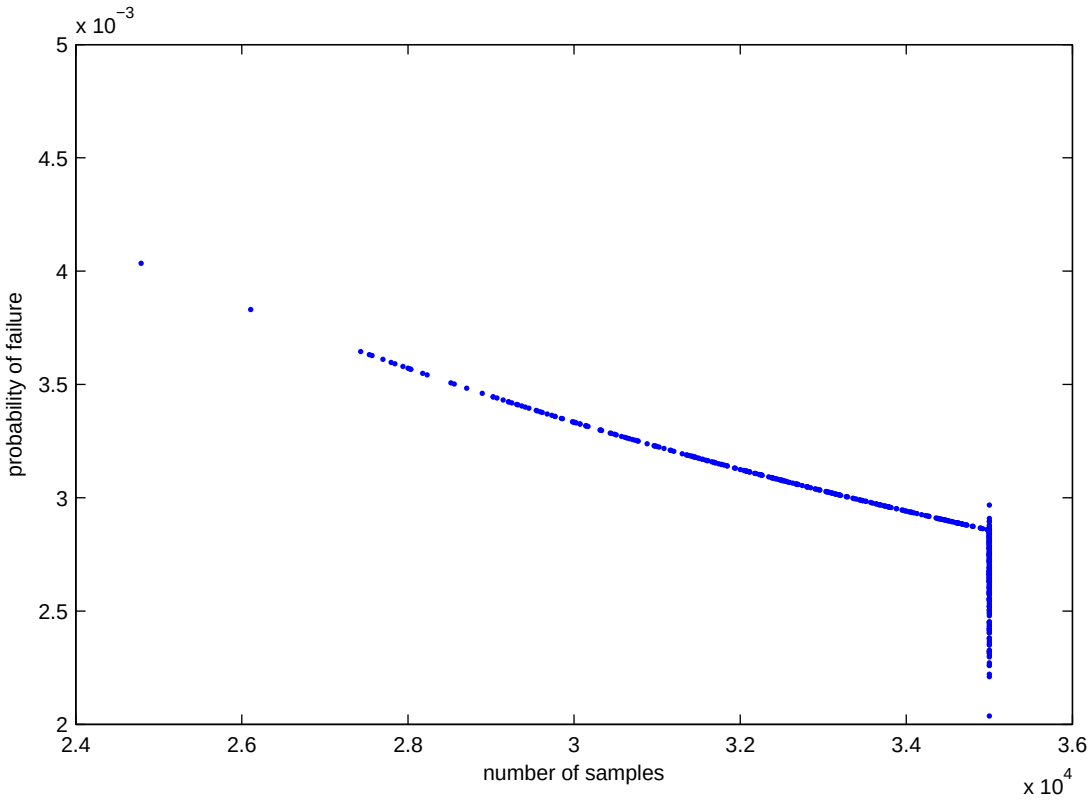

Figure 2.1: Relationship between the number of samples and the failure probability when the stopping criterion is applied.

over the 500 populations is 0.0043. Accordingly, the maximum error with respect to this average is 39%, which can be considered very high.

The sample estimate of the coefficient of variation of the failure probability (i.e. the ratio between the standard deviation and the mean) was found to be 0.0987. A similar value (0.0936) was obtained without applying the stopping criterion supplied by Eq. (2.5), thus indicating that the determining factor for the accuracy of the failure probability estimation is the number of samples and not the application of the stopping criterion $\hat{\nu}_{\mathrm{b}} < 0.1$. In fact, the above values raise respectively to 0.157 and 0.150 for $N = 10,000$ samples, using also 500 populations.

On the other hand, notice in Figure 1 that the application of the stopping criterion occasions the largest departures from the mean value instead of approaching to it, as it could naively be expected. This is due to the dependence of the binomial estimate of the coefficient of variation on the estimate of the probability, according to which the larger $\hat{P}_{\mathrm{f}}$ the lower $\hat{\nu}_{\mathrm{b}}$, so that it suffices that the current estimate of the probability be large to stop the simulation. This fact, which has been observed in all the analysis reported later in this chapter, clearly indicates that the simulation stopping criterion based on the binomial estimate given by Eq. (2.5) can be seriously misleading. According to these observations, the criterion is found to be more relevant for computational savings than for accuracy benefits.

The use of the basic Monte Carlo method in standard practice of structural reliability analysis is examined in this chapter, having especially in focus the randomness of the estimate (2.2) and the effects of using Eq. (2.5) for stopping the simulation programme. It is demonstrated that the use of Information Theory concepts allows a selection of the population to be used in a Monte Carlo simulation in order to obtain a good estimate of the mean value of the failure probability, thus avoiding random estimates which can lie very far from it, and whose separation from such a mean remains unknown. To be specific, the proposal consists in generating a large number of populations of the input random variables and selecting that having the average entropy because it leads to an estimate close to the actual mean value of the probability of failure. Therefore, the entropy provides a preprocessing criterion for selecting the optimal population for the simulation, thus avoiding reliance on $\hat{\nu}_{\mathrm{b}}$ for yielding the probability estimate and using it only for reducing the number of samples. By means of a theoretical derivation and several examples the validity of this proposal is demonstrated.

The next section of the chapter is devoted to a brief exposition of some concepts of Information Theory which constitute a basis for the proposal presented herein. This is followed by the theoretical and empirical demonstration of the soundness of the proposal. The chapter ends with some conclusions and directions for future research.

2.2 Some concepts of Information Theory

In this section the essential concepts of Information Theory (IT) that are relevant for the purposes of the chapter are summarized after [77, 78, 79].

The degree of information offered by a sample regarded as a realization of a random variable depends on the degree of surprise it provokes in its arising.

Thus we can build an information function $I(P)$ with the simple rule that non surprising events, i.e. those having a probability of occurrence $P = 1$, afford no information, while those of little probability are very informative. No, consider two independent events A and B with probabilities P_A and P_B. Since the events are independent, their joint probability is the product $P_{AB} = P_A P_B$. Similarly, the joint information given by the events can be denoted as $I(P_A P_B)$. In terms of their individual information contents, this joint information can be defined by mean of the following rule:

$$I(P_A P_B) - I(P_A) = I(P_B) \tag{2.6}$$

This means that the residual information on the joint occurrence of the events, after receiving the information that A has occurred, is not different from the information that B has occurred, because the events are independent. Presenting the above equation as

$$I(P_A P_B) = I(P_A) + I(P_B) \tag{2.7}$$

indicates that for independent events the joint information is additive, while the joint probability is multiplicative. From these equations it results that for the same event

$$I(P^2) = 2I(P) \tag{2.8}$$

and hence

$$I(P^q) = qI(P) \tag{2.9}$$

Let $r \equiv -\ln(P)$. Then, $P = (1/e)^r$ and applying the previous equation one obtains

$$I(P) = I\left[(1/e)^r\right] = rI(1/e) = -I(1/e)\ln(P) \tag{2.10}$$

Defining the scale term $I(1/e) \equiv 1$, one finally obtains

$$I(P) = -\ln(P) \tag{2.11}$$

This is the so-called self-information of a random event of probability P and it defines the information content of a certain region of the space. Notice that $I(P) \to \infty$ as $P \to 0$ and $I(P) \to 0$ as $P \to 1$. In words, the information grows as the event becomes more rare and diminishes as it becomes more certain, as expected.

From the above definition of self-information and for the general case of multiple events, it results that the information content depends on the definition of the regions of the space on which the random occurrences are observed, i.e. on the partition of the samples space. In practice, for computing the empirical entropy use is made of the regular partition used for computing histograms. In general, for N samples generated from the distribution function of a vector random variable $\underline{\boldsymbol{x}}$, grouped in the bins defined by a partition $\mathcal{X} = \{\bar{x}_1, \bar{x}_2, \ldots\}$, one can associate the bin probability estimates $\hat{P}_j = n_j/N, j = 1, 2, \ldots, n$, where n_j is the number of samples in each bin. The expected value of the information on the variable yielded by the population is the weighted average of the self-information values:

$$H(\underline{\boldsymbol{x}}, \mathcal{X}) = -\sum_{j=1}^{L} P_j \ln P_j \tag{2.12}$$

where L is the total number of bins. As is well known, this average is called entropy. For a given population of samples, the corresponding estimate of the entropy is

$$\hat{H}_k(\underline{\boldsymbol{x}}, \mathcal{X}) = -\sum_{j=1}^{L} \frac{n_j}{N} \ln \frac{n_j}{N} \tag{2.13}$$

for $k = 1, 2, \ldots, M$, where M is the number of such populations. For a large number of populations M, the estimate of the average entropy is

$$\hat{\bar{H}}(\underline{\boldsymbol{x}}, \mathcal{X}) = \frac{1}{M} \sum_{k=1}^{M} \hat{H}_k(\underline{\boldsymbol{x}}, \mathcal{X}) \tag{2.14}$$

For the ensuing developments it is important to recall two further statements of Information Theory. First, that if a partition $\mathcal{X}'$ is obtained by refining a partition $\mathcal{X}$, then

$$H(\underline{\boldsymbol{x}}, \mathcal{X}) \leq H(\underline{\boldsymbol{x}}, \mathcal{X}') \tag{2.15}$$

Second, that for a transformation of a discrete random variable $\underline{\boldsymbol{x}}$ into $\underline{y} = g(\underline{\boldsymbol{x}})$ the following equation holds [79]:

$$H(\underline{y}, \mathcal{X}) \leq H(\underline{\boldsymbol{x}}, \mathcal{X}) \tag{2.16}$$

The equality sign holds when the transformation is one-to-one.

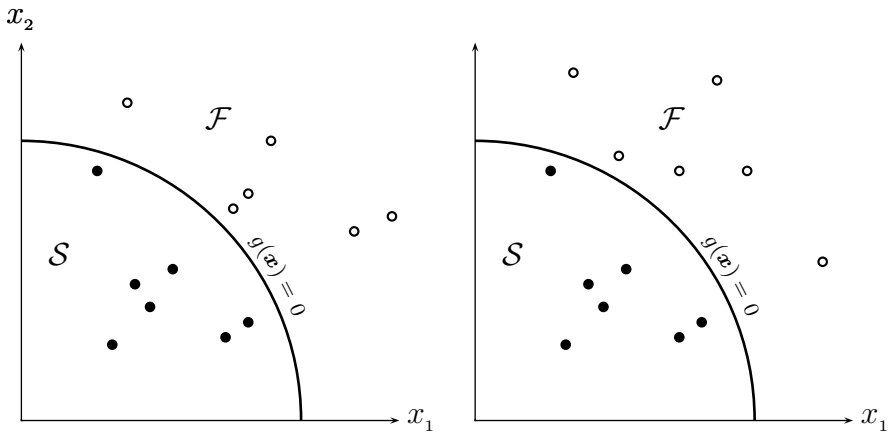

Figure 2.2: Two realizations of a contrived experiment used for establishing an approximate relationship between the entropy and the probability of failure.

2.3 Information characterization of Monte Carlo simulation

According to Eqs. (2.2) to (2.4), each experiment in a Monte Carlo simulation can be regarded as the transformation of a sample $\boldsymbol{x}$ through a system yielding a realization y of random variable $\underline{y} = g(\underline{\boldsymbol{x}})$ which in turn is transformed by another system yielding the realization z of the random variable $\underline{z}$.

In order to examine the relationship between the failure probability and the sample entropy, let us contrive a particular numerical experiment (see Figure 2.2). In it, a global partition is determined by the limit state function and for computing the empirical entropy (2.13) each domain is partitioned in a certain number of bins each. The populations are generated with the same number of samples. The main condition of the experiment is that the quantity of the samples in the safe region $\mathcal{S}$ is kept constant. This restriction is justified because the contribution of the samples in the safe domain to the failure probability estimate given by Eq. (2.1) is null. In contrast, the position of the samples in the failure domain $\mathcal{F}$ is allowed

to vary randomly, so that the empirical entropy given by Eq. (2.13) also becomes random, as is evident. Notice that for all the populations k, $k = 1, 2, \ldots, M$ of this experiment, the estimates of the failure probability $\hat{P}_{\mathrm{f},k}$ will be equal to each other and to the mean computed over all populations thus generated, $\bar{P}_{\mathrm{f}}$.

Under such conditions, Eq. (2.12) takes the form

$$\underline{H}(\underline{\boldsymbol{x}}, \mathcal{X}) = -\sum_{i=1}^{L_{\mathrm{f}}} \underline{P_i} \ln \underline{P_i} - \sum_{j=1}^{L_{\mathrm{s}}} P_j \ln P_j \tag{2.17}$$

where L_{f} is the total number of bins in the failure domain and L_{s} that of the safe domain. Notice that according to the above exposition the empirical probabilities in the failure domain and, accordingly, the empirical entropy, become random variables, as indicated by the underlined variables in the preceding equation. It can be put in the form

$$S + \underline{H}(\underline{\boldsymbol{x}}, \mathcal{X}) = -\sum_{i=1}^{L_{\mathrm{f}}} \ln \underline{P_i}^{\underline{P_i}} \tag{2.18}$$

where

$$S = \sum_{j=1}^{L_{\mathrm{s}}} P_j \ln P_j \tag{2.19}$$

is a constant term according to the definition of the experiment. Equation (2.18) can re rewritten as

$$-\prod_{i=1}^{L_{\mathrm{f}}} \underline{P_i}^{\underline{P_i}} = \exp(S) \exp(\underline{H}(\underline{\boldsymbol{x}}, \mathcal{X})) \tag{2.20}$$

Let us now apply the expectation operator to both sides of the preceding equation:

$$-\mathrm{E}\left[\prod_{i=1}^{L_{\mathrm{f}}} \underline{P_i}^{\underline{P_i}}\right] = \mathrm{E}\left[\exp(S) \exp(\underline{H}(\underline{\boldsymbol{x}}, \mathcal{X}))\right] \tag{2.21}$$

For the left-hand side it is evident that

$$-\mathrm{E}\left[\prod_{i=1}^{L_{\mathrm{f}}} \underline{P_i}^{\underline{P_i}}\right] = -\prod_{i=1}^{L_{\mathrm{f}}} \mathrm{E}\left[\underline{P_i}^{\underline{P_i}}\right] \tag{2.22}$$

because of the independence of Monte Carlo trials. Applying a first order approximation, the above product can be estimated as

$$-\prod_{i=1}^{L_\mathrm{f}} \mathrm{E}\left[\underline{P_i}^{P_i}\right] \doteq -\prod_{i=1}^{L_\mathrm{f}} \bar{P}_i^{\bar{P}_i} \tag{2.23}$$

where $\bar{P}_i$ is the expected value of the probability in i-th bin of the failure domain. It is evident that it is given by

$$\bar{P}_i = \frac{\bar{P}_\mathrm{f}}{N_\mathrm{f}} \tag{2.24}$$

where N_f is the number of samples in the failure domain. Therefore, the right-hand side of Eq. (2.21) becomes

$$-\mathrm{E}\left[\prod_{i=1}^{L_\mathrm{f}} \underline{P_i}^{P_i}\right] = -\left[\frac{\bar{P}_\mathrm{f}}{N_\mathrm{f}}\right]^{\left(\frac{\bar{P}_\mathrm{f} L_\mathrm{f}}{N_\mathrm{f}}\right)} \tag{2.25}$$

Noticing that

$$\bar{P}_\mathrm{f} = \frac{N_\mathrm{f}}{N} \tag{2.26}$$

where N is the total number of samples, Equation (2.25) can be finally put in the form

$$-\mathrm{E}\left[\prod_{i=1}^{L_\mathrm{f}} \underline{P_i}^{P_i}\right] = -\left[\frac{1}{N}\right]^{\left(\frac{\bar{P}_\mathrm{f} L_\mathrm{f}}{N_\mathrm{f}}\right)} \tag{2.27}$$

On the other hand, for the right-hand side of Eq. (2.21), a first order approximation yields

$$\exp(S)\mathrm{E}\left[\exp(\underline{H}(\underline{\boldsymbol{x}}, \mathcal{X}))\right] \doteq \exp(S)\exp(\bar{H}(\underline{\boldsymbol{x}}, \mathcal{X})) \tag{2.28}$$

where $\bar{H}(\underline{\boldsymbol{x}}, \mathcal{X})$ is the mean entropy. Therefore, reuniting Eqs. (2.27) and (2.28), corresponding to the two sides of Eq. (2.21) and taking logarithms yields

$$-\frac{\bar{P}_\mathrm{f} L_\mathrm{f}}{N_\mathrm{f}} \ln \frac{1}{N} = S + \bar{H}(\underline{\boldsymbol{x}}, \mathcal{X}) \tag{2.29}$$

which finally renders the following relationship between the mean entropy and the mean probability of failure:

$$\bar{P}_{\mathrm{f}} = \frac{N_{\mathrm{f}}}{L_{\mathrm{f}} \ln N} \left(S + \bar{H}(\underline{\boldsymbol{x}}, \mathcal{X}) \right) \tag{2.30}$$

The meaning of this equation is that there is a linear relationship between the mean values of the entropy and the failure probability, for the contrived experiment at least. In the general case, in which the positions and number of the samples in both domains are allowed to vary in a random fashion, a general relationship is difficult to establish. However, since the samples in the safe domain, which are the vast majority, do not contribute at all to the expected value of the failure probability, the above experiment is close to the actual situation and, therefore, the result given by Eq. (2.30) gives a practical support to the main hypothesis of the present chapter, i.e. that the mean failure probability, considered as a random variable, can be estimated with a population having a mean entropy among a large set of candidate ones. Therefore, the failure probability estimate can be obtained with the population of $\boldsymbol{x}$ having the closest entropy $\hat{\bar{H}}(\underline{\boldsymbol{x}}, \mathcal{X})$ to that of the empirical mean of the entropies, computed over all populations using Eq. (2.14):

$$\hat{\bar{P}}_{\mathrm{f},1} \Leftarrow \hat{\bar{H}}(\underline{\boldsymbol{x}}, \mathcal{X}) \tag{2.31}$$

For the sake of completeness, notice that for the simple binary partition $\mathcal{B}$ of the variable space into two bins, one corresponding to the safe domain and the other to the failure one, the entropy is

$$H(\underline{\boldsymbol{x}}, \mathcal{B}) = -P_{\mathrm{f}} \ln P_{\mathrm{f}} - (1 - P_{\mathrm{f}}) \ln(1 - P_{\mathrm{f}}) \tag{2.32}$$

This function is illustrated in Figure 2.3 for a failure probability fluctuating in the common range $[1 \times 10^{-4} \quad 1 \times 10^{-3}]$. Despite this simple theoretical result is of little use in practice, because the entropy-based selection of the population would directly depend on the target of the calculation, notice anyhow that it confirms the close-to-linear relationship between failure probability and entropy, as in Eq. (2.30) which corresponds to a rather different partition. In fact, making use of Eq. (2.15), $H(\underline{\boldsymbol{x}}, \mathcal{B}) < H(\underline{\boldsymbol{x}}, \mathcal{X})$.

In addition, it is important to mention that, due to the randomness of the failure probability estimate, in the actual practice of Monte Carlo simulation in structural reliability analysis the entire simulation is run several times, normally three, and the average is delivered as the final result, when the computational effort thus implied is not severely high. For such cases, besides $\hat{\bar{P}}_{\mathrm{f},1}$, it seems

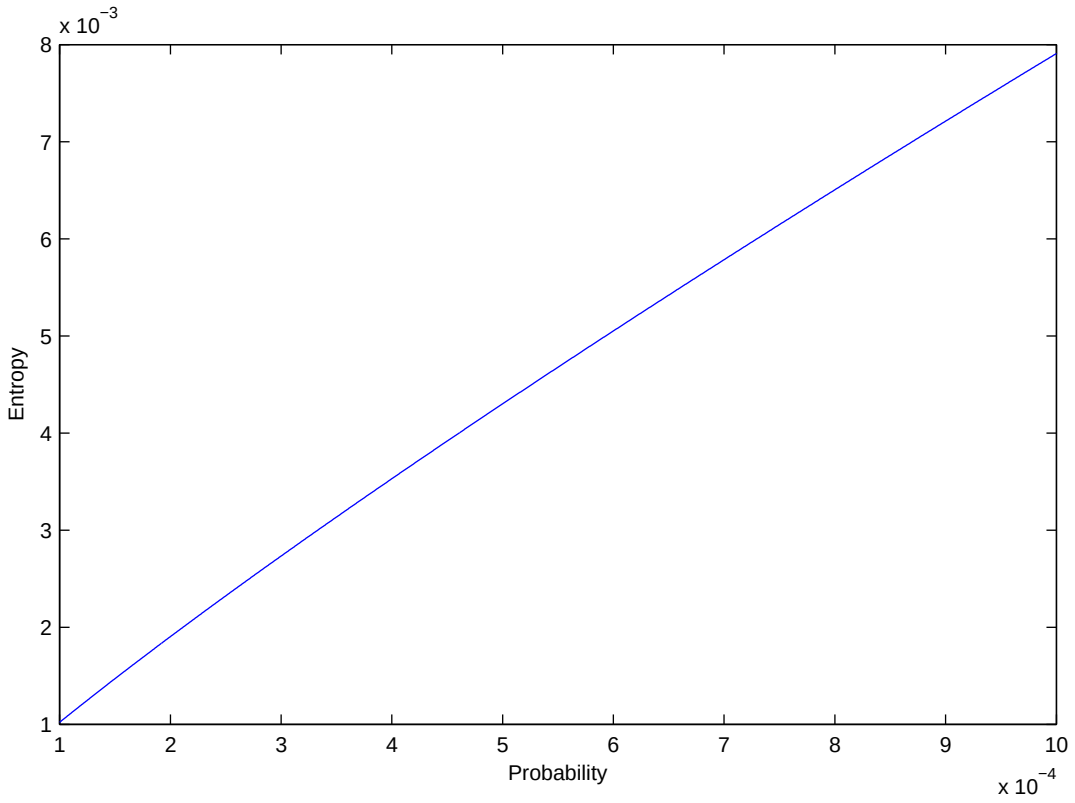

Figure 2.3: Relationship between the entropy of the Bernoulli mass density function and the failure probability.

preferable to deliver the following two additional estimates instead of two random ones obtained by simply repeating the simulation:

1. The failure probability estimate obtained as the average of those corresponding to the populations showing the minimum, the average and the maximum entropies, amongst a large set of candidates:

$$\hat{\bar{P}}_{\mathrm{f},2} = \frac{1}{3}\left(\hat{P}_{\mathrm{f,min}} + \hat{\bar{P}}_{\mathrm{f},1} + \hat{P}_{\mathrm{f,max}}\right) \tag{2.33}$$

where

$$\begin{aligned} \hat{P}_{\mathrm{f,min}} &\Leftarrow \hat{H}_{\min}(\underline{\boldsymbol{x}}, \mathcal{X}) \\ \hat{P}_{\mathrm{f,max}} &\Leftarrow \hat{H}_{\max}(\underline{\boldsymbol{x}}, \mathcal{X}) \end{aligned}$$

2. The failure probability estimate obtained as the entropy-weighted average of those corresponding to the populations showing the minimum, the average and the maximum entropies:

$$\hat{\tilde{P}}_{\mathrm{f},2} = \frac{\hat{H}_{\min}\hat{P}_{\mathrm{f,min}} + \hat{\tilde{H}}\hat{\tilde{P}}_{\mathrm{f},1} + \hat{H}_{\max}\hat{P}_{\mathrm{f,max}}}{\hat{H}_{\min} + \hat{\tilde{H}} + \hat{H}_{\max}} \tag{2.34}$$

where the arguments of the entropy terms have been omitted for the sake of clarity.

2.4 Application examples

In this section the application of the proposal of selecting the Monte Carlo population according to information criteria is illustrated with several benchmark examples taken from [80]. In all cases the variables are standard independent Normal, unless stated otherwise. The number of populations used for all the cases was $M = 500$.

1. A convex two-dimensional limit state with a combined term:

$$g(\boldsymbol{x}) = 0.1(x_1 - x_2)^2 - \frac{1}{\sqrt{2}}(x_1 + x_2) + 2.5$$

This function has been used in the introduction, but it is incorporated herein for comparison purposes.

2. A concave two-dimensional function with combined term:

$$g(\boldsymbol{x}) = -0.5(x_1 - x_2)^2 - \frac{1}{\sqrt{2}}(x_1 + x_2) + 3$$

3. A two-dimensional function with a saddle point:

$$g(\boldsymbol{x}) = 2 - x_2 - 0.1x_1^2 + 0.06x_1^3$$

4. A highly convex function:

$$g(\boldsymbol{x}) = 2.5 - 0.2357(x_1 - x_2) + 0.00463(x_1 + x_2 - 20)^4$$

   In this case, both variables have mean equal to 10 and standard deviation equal to 3.

5. Another highly concave function:

$$g(\boldsymbol{x}) = 3 - x_2 + (4x_1)^4$$

6. A five dimensional parallel system:

$$\begin{aligned} g_1(\boldsymbol{x}) &= 2.677 - x_1 - x_2 \\ g_2(\boldsymbol{x}) &= 2.5 - x_2 - x_3 \\ g_3(\boldsymbol{x}) &= 2.323 - x_3 - x_4 \\ g_4(\boldsymbol{x}) &= 2.25 - x_4 - x_5 \\ g(\boldsymbol{x}) &= \max(g_1, g_2, g_3, g_4) \end{aligned}$$

7. A three dimensional series system:

$$\begin{aligned} g_1(\boldsymbol{x}) &= -x_1 - x_2 - x_3 + 3\sqrt{3} \\ g_2(\boldsymbol{x}) &= 3 - x_3 \\ g(\boldsymbol{x}) &= \min(g_1, g_2) \end{aligned}$$

8. A three dimensional parallel system:

$$\begin{aligned} g_1(\boldsymbol{x}) &= -x_1 - x_2 - x_3 + 3\sqrt{3} \\ g_2(\boldsymbol{x}) &= 3 - x_3 \\ g(\boldsymbol{x}) &= \max(g_1, g_2) \end{aligned}$$

9. A two-dimensional series system with multiple failure points:

$$\begin{aligned} g_1(\boldsymbol{x}) &= 2 - x_2 + \exp(-0.1x_1^2) + (0.2x_1)^4 \\ g_2(\boldsymbol{x}) &= 4.5 - x_1 x_2 \\ g(\boldsymbol{x}) &= \min(g_1, g_2) \end{aligned}$$

10. A two-dimensional parallel system with multiple failure points:

$$\begin{aligned} g_1(\boldsymbol{x}) &= 2 - x_2 + \exp(-0.1x_1^2) + (0.2x_1)^4 \\ g_2(\boldsymbol{x}) &= 4.5 - x_1 x_2 \\ g(\boldsymbol{x}) &= \max(g_1, g_2) \end{aligned}$$

11. A two-dimensional series system with multiple failure points:

$$\begin{aligned} g_1(\boldsymbol{x}) &= 0.1(x_1 - x_2)^2 - \frac{1}{\sqrt{2}}(x_1 + x_2) + 2.5 \\ g_2(\boldsymbol{x}) &= 0.1(x_1 - x_2)^2 + \frac{1}{\sqrt{2}}(x_1 + x_2) + 2.5 \\ g_3(\boldsymbol{x}) &= x_1 - x_2 + 3.5\sqrt{2} \\ g_4(\boldsymbol{x}) &= -x_1 + x_2 + 3.5\sqrt{2} \\ g(\boldsymbol{x}) &= \min(g_1, g_2, g_3, g_4) \end{aligned}$$

The results are summarized in Tables 2.1 and 2. In both tables, the percent error with respect to the overall average $\bar{P}_{\rm f}$ computed over all populations and which can be taken as a reference for the exact value for obvious reasons, was calculated as

$$\epsilon = \frac{|P - \bar{P}_{\rm f}|}{\bar{P}_{\rm f}} \times 100 \tag{2.35}$$

where P is any probability. The following comments are in order:

(a) It is noticed first that all estimates $\hat{\bar{P}}_{\rm f,1}$, $\hat{\bar{P}}_{\rm f,2}$ and $\hat{\bar{P}}_{\rm f,3}$ yield small errors. In the average, the errors are lower for estimates $\hat{\bar{P}}_{\rm f,2}$ and $\hat{\bar{P}}_{\rm f,3}$ which, however, employ three populations instead of one.

Table 2.1: Entropy-based estimates

No.	N	$\bar{P}_{\rm f}$	$\hat{\bar{P}}_{\rm f,1}$	ϵ (%)	$\hat{\bar{P}}_{\rm f,2}$	ϵ (%)	$\hat{\bar{P}}_{\rm f,3}$	ϵ (%)
1	25,000	0.00429	0.00476	11.1	0.00433	1.04	0.00433	1.04
2	1,000	0.106	0.103	2.5	0.106	0.0	0.106	0.0
3	3,000	0.0352	0.0394	11.8	0.0339	3.8	0.0339	3.8
4	35,000	0.00290	0.00288	0.9	0.00282	2.8	0.00283	2.8
5	600,000	0.000181	0.000169	6.8	0.000171	5.3	0.000171	5.3
6	500,000	0.000215	0.000211	2.0	0.000205	4.4	0.000206	4.4
7	40,000	0.00260	0.00250	3.9	0.00261	0.5	0.00261	0.5
8	850,000	0.000126	0.000113	10.0	0.000128	1.8	0.000128	1.8
9	30,000	0.00352	0.00371	5.4	0.00367	4.4	0.00367	4.4
10	400,000	0.000244	0.000223	8.9	0.000228	6.4	0.000228	6.4
11	50,000	0.00225	0.00245	9.1	0.00234	4.2	0.00235	4.2

Table 2.2: Ranges of fluctuation of probability estimates

No.	$\min P_{\rm f}$	ϵ (%)	N	$\max P_{\rm f}$	ϵ (%)	N
1	0.00316	26.2	25,000	0.00596	39.0	16,676
2	0.077	27.0	1,000	0.149	40.9	578
3	0.0254	27.7	3,000	0.0489	40.0	1,962
4	0.00204	29.9	35,000	0.00403	38.9	24,789
5	0.000137	24.5	600,000	0.000261	44.5	38,243
6	0.000155	27.9	500,000	0.000299	39.3	333,837
7	0.00197	23.9	40,000	0.00361	38.8	27,705
8	0.000093	25.8	850,000	0.000169	34.0	592,703
9	0.00263	25.0	30,000	0.00474	34.9	21,175
10	0.000183	25.1	400,000	0.000336	37.8	297,225
11	0.00151	33.0	50,000	0.00323	43.8	30,927

(b) Secondly, it can be seen that the errors associated to the minimum and maximum probabilities are much larger than those corresponding to the entropy-based selected populations. The magnitude of this errors indicates that the application of simple Monte Carlo simulation without a selection preprocess may occasion to incur in errors up to 40%.

(c) Third, it is noticed that the errors corresponding to the maximum probability are systematically higher than those of the minimum probability. This is due to the fact that, in applying the stopping criterion based on the binomial estimate of the failure probability $\hat{\nu}_{\mathrm{b}}$, it suffices that the probability being currently estimated by the simulation be large (i.e. that the number of samples found in the failure domain be large) for the simulation to stop when a $\hat{\nu}_{\mathrm{b}} < 0.1$ is reached. In fact, the number of samples actually used for computing the maximum probability was smaller than the scheduled number of samples, which for all the cases was required by 30% of the populations in the average. This result demonstrates the inadequacy of $\hat{\nu}_{\mathrm{b}} < 0.1$ as the simulation stopping criterion in terms of accuracy, and that it is a good method for computational savings only.

Chapter 3

Seismic random variables

3.1 Introduction

In a paper reviewing the criticism addressed to standard methods of seismic design practice and contemporary proposals for their improvement [81], the authors propose several strategies for obtaining safer designs, one of which is the probabilistic analysis of the structural system, in recognition of the large uncertainties posed by the seismic action. In fact, while the coefficient of variation (COV) of random variables present in the design for gravity loads are normally lower than 0.25, variables such as the peak ground acceleration for a return period of 475 years, which determines the entire design according to current practices, is estimated to have a COV in the range from 0.56 to 1.38, according to the same authors. In addition, there is the randomness associated to the seismic acceleration history as such, which have been modeled as a realization of a random process of even a random field, implying thousands of random variables in an adequate modeling.

A serious criticism that may be addressed to standard seismic design practice is that probabilistic considerations in design codes are normally limited to the definition of the probability of exceeding a critical value by the peak ground acceleration in the estimated life of the structure, while no probabilistic verifications of the structural responses are required. Since evidently design codes condition the design software and even the average amount of knowledge commonly regarded as sufficient for design practice, the paradoxical result is that probabilistic concepts

and methods find little application in the field of structural engineering in which the uncertainties are the largest.

It may be objected that a full and accurate probabilistic analysis implies large computational efforts posed by the general technique known as Monte Carlo simulation. To this objection it may be replied that the same criticism has rarely, if at all, been addressed to a deterministic technique requiring huge hardware capabilities, which is the Finite Element method, and, on the contrary, its users routinely demand increasing amounts of computer resources and significant research is devoted to the subject of parallelization.

Such a bias in this regard to computer technology exploitation betrays a problem of engineering education [82]. In fact, engineering emerged from the paradigm of exactness and accuracy, a label assumed by physics and other sciences, which has its roots in the mathematical interpretation of nature. With such an origin, engineering education favors the deterministic regard over the probabilistic one because the randomness arising in natural phenomena is regarded simplistically as a deficiency in the mathematical model, a drawback that is expected to be remedied in the near or distant future. Meanwhile, current deterministic models for dealing with random environments are used with caution. These naive thoughts are behind the well-known safety factors, which hardly relate to elementary probabilistic measures of safety, according to a recent research [83]. While a satisfactory deterministic model is perhaps possible in some simple cases, in others such an ideal is largely impractical or even impossible. This is specifically the case of Seismology and Earthquake Engineering, for obvious reasons. This renders illusory the ideal of a complete deterministic earthquake-resistant design and sheds light on the need of developing practical methods for incorporating probabilistic computation in the design practice in order to have adequate measures of the risk involved in each design, thus making better use of computer technology in seismic design.

This chapter is intended to contribute to such desirable goals. Two main probabilistic design approaches, namely the Robust Design Optimization (RDO) and the Reliability-based Design Optimization (RBDO), are focused. While the former operates on estimates of first- and second-order statistical moments of the structural responses, in the latter decisions are based on probabilities of exceeding critical response thresholds (probabilities of failure). The chapter is organized as follows. First, after a brief exposition of RDO and RBDO, some well established stochastic models of the seismic action are exposed. The fundamentals of random vibration analysis of linear and nonlinear structures, which yields satisfactory estimates of the low order moments, is next summarized. Then the problem of an accurate computation of the structural robustness for earthquake demands

is addressed. It is shown that the combination of analytical random vibration techniques with the method of Point Estimates is sufficient for practical robust design. The important problem of a practical computation of the probabilities of failure for seismic actions is finally addressed. This is a case in which analytical methods of random vibration are far from satisfactory and resort has to be made to the synthetic approach, i.e. Monte Carlo simulation. In order to reduce the large computational effort implied by a full Monte Carlo calculation, a mixed analytic-synthetic approach is proposed. It consists in a treatment of a small set of responses computed by both techniques using the Total Probability Theorem (TPT) and a new sampling method named Backward Stratified Sampling (BSS. By means of an example concerning a base isolated building, it is shown that the method offers an economical as well as elegant solution to this important step of reliability-based seismic design.

Considering the specialization of the field of stochastic dynamics and, at the same time, the practical orientation of present book, the chapter is as self-contained as possible.

3.2 Robust and Reliability-based design options

Proposals for the consideration of uncertainties in seismic design can be grouped into two main categories: (a) Robust Design Optimization (RDO), which is oriented to minimizing the structural cost as well as the spread of the structural responses, as measured by low-order statistical moments [84, 85]; (b) Reliability-Based Design Optimization (RBDO), which minimizes the cost function with probabilistic constraints [86, 87, 88, 89].

A common formulation of RBDO can be formally presented as follows:

$$
\begin{aligned}
&\textit{Reliability}-\textit{based optimization}: \\
&\qquad\qquad \text{find}: \quad \boldsymbol{y} \\
&\qquad\qquad \text{minimizing}: \quad C(\boldsymbol{y}) \\
&\qquad\qquad \text{subject to}: \quad \mathrm{P}[f_i(\underline{\boldsymbol{x}}, \boldsymbol{y}) > F_i] \leq Q_i, \quad i = 1, 2, \ldots \\
&\qquad\qquad\qquad\qquad\qquad\quad \boldsymbol{y}^- \leq \boldsymbol{y} \leq \boldsymbol{y}^+
\end{aligned}
\tag{3.1}
$$

where $C(\boldsymbol{y})$ is the cost function depending on the design variables collected in vector $\boldsymbol{y}$, $\underline{\boldsymbol{x}}$ is a set of random variables, $\mathrm{P}[A]$ the probability of the random event A and Q_i its limiting value. Function $g_i(\underline{\boldsymbol{x}}, \boldsymbol{y}) = F_i - f_i(\underline{\boldsymbol{x}}, \boldsymbol{y})$ is the function

known in structural reliability as the limit state function. On the other hand $\boldsymbol{y}^-$ and $\boldsymbol{y}^+$ are bounds imposed to the design variables, normally constituting geometric constraints. For seismic design it has been suggested that the target probabilities correspond to a reliability index $\beta = 1.75$, so that $Q_i = 0.0401$ [90].

Some researchers and designers, however, favor the design guided by the concept of robustness, understood as safety against unpredictable variations of the design parameters. Mathematically speaking, robustness can be defined in several forms, depending on whether use is made of the clustering [91] or conventional, frequentist interpretation of uncertainty. In this chapter the second interpretation is adopted. A possible formulation of this task is

$$\begin{aligned} &\textit{Robust optimization}: \\ &\text{find}: && \boldsymbol{y} \\ &\text{minimizing}: && C(\boldsymbol{y}) \\ &\text{subject to}: && f_i\left(\boldsymbol{\mu}_{\boldsymbol{z}}(\underline{\boldsymbol{x}}, \boldsymbol{y}), \boldsymbol{\sigma}_{\boldsymbol{z}}(\boldsymbol{x}, \boldsymbol{y})\right) \leq 0, \quad i = 1, 2, \ldots \\ & && \boldsymbol{y}^- \leq \boldsymbol{y} \leq \boldsymbol{y}^+ \end{aligned} \tag{3.2}$$

where $\boldsymbol{\mu}_{\boldsymbol{z}}(\underline{\boldsymbol{x}}, \boldsymbol{y}), \boldsymbol{\sigma}_{\boldsymbol{z}}(\boldsymbol{x}, \boldsymbol{y})$ are respectively the mean and standard deviation vectors of structural responses collected in vector $\boldsymbol{z}$, and $f_i(\cdot, \cdot)$ are functions thereof.

The nature of these two alternative methods can be explained with the help of Fig. 1, which shows two alternative probability density functions of a structural response. While RDO aims to reduce the spread, RBDO is intended to bound the probability of surpassing the critical threshold. Notice that in applying RDO the effect pursued by RBDO is indirectly obtained, because the reduction of the spread implies a reduction of the failure probability. The reliability (or its complement, the failure probability) refers to the occurrence of extreme events, whereas the robustness refers to the spread of the structural responses under large variation of the input parameters. This is assumed to assure a narrow response density function, which in turn assures a low failure probability, if it is unimodal, as is common case. However, this is not necessarily true: to a significant spread of the structural response may correspond a low failure probability because the definition of the limit state can be such that the possibility of surpassing it is very rare, as the situation it describes is rather extreme (See Fig. 1).

In this chapter no discussion is made on whether the robust or the reliability approaches is more suitable for the specific problem of seismic design under uncertainties; nor a specific numerical method for solving either RDO nor RDBO is proposed, for which the reader is referred to specialized references [84, 92, 93, 94,

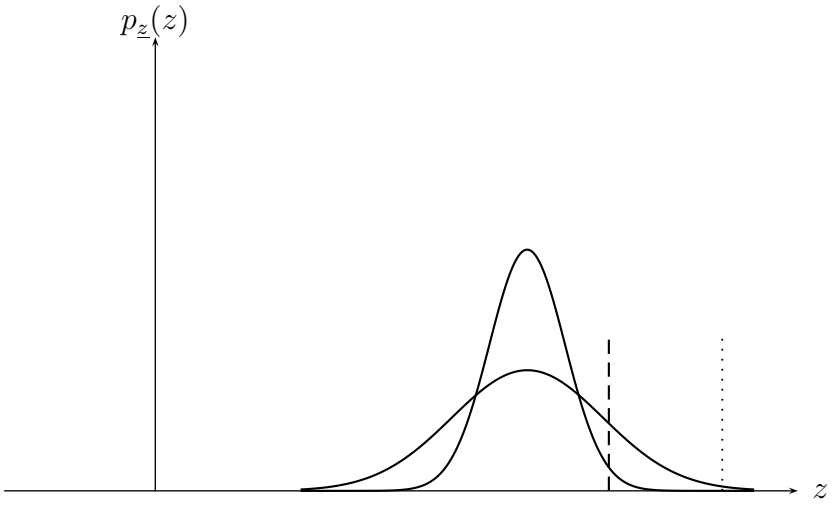

Figure 3.1: Robust and reliability-based design options. While the first aims at reducing the spread of the response function, the second attempts to control the probability of surpassing a critical threshold (dashed line). However, low failure probabilities may correspond to large spreads (dotted line).

95, 96, 97, 85]. Instead, the chapter is oriented to propose practical techniques for calculating the stochastic quantities implicit in these methods, namely low order response moments and failure probabilities under earthquake ground motion excitations.

3.3 Stochastic models of seismic action

In this section some useful equations for a stochastic modeling of the seismic action in design practice are recalled. First, convenient way of modeling the ground motion acceleration is the response of one or more linear filters excited by a white noise. Two models have found extensive application in practice, namely the Kanai-

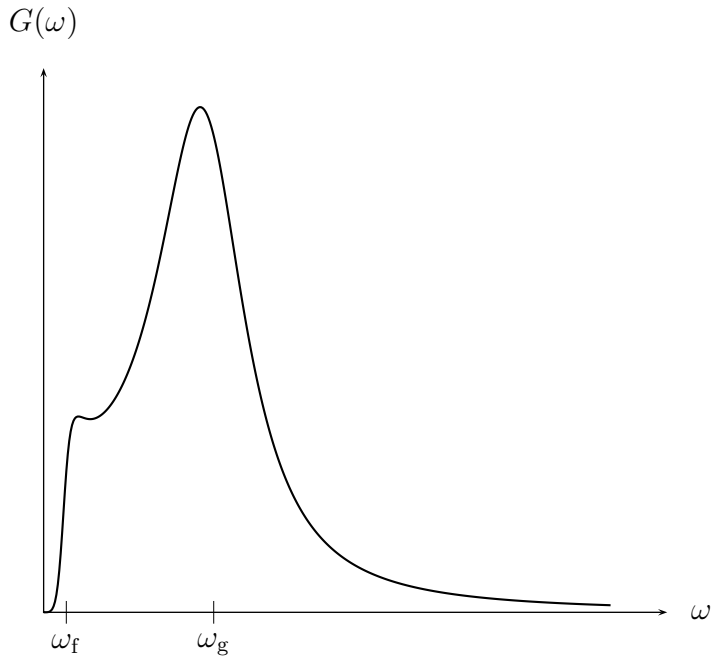

Figure 3.2: Clough-Penzien seismic spectral model.

Tajimi and the Clough-Penzien filters. In the former case, a linear system is

$$\ddot{\underline{u}}_{\mathrm{g}} + 2\,\nu_{\mathrm{g}}\omega_{\mathrm{g}}\dot{\underline{u}}_{\mathrm{g}} + \omega_{\mathrm{g}}^2\underline{u}_{\mathrm{g}} = -\underline{w}(t) \tag{3.3}$$

where $\underline{w}(t)$ is a white noise. The other parameters appearing in this equation have already been explained. In the latter case, it is necessary to append, in addition, the equation

$$\ddot{\underline{u}}_{\mathrm{f}} + 2\,\nu_{\mathrm{f}}\omega_{\mathrm{f}}\dot{\underline{u}}_{\mathrm{f}} + \omega_{\mathrm{f}}^2\underline{u}_{\mathrm{f}} = -\left(2\,\nu_{\mathrm{g}}\omega_{\mathrm{g}}\dot{\underline{u}}_{\mathrm{g}} + \omega_{\mathrm{g}}^2\underline{u}_{\mathrm{g}}\right) \tag{3.4}$$

meaning that the Clough-Penzien filter is driven by a compound excitation given by the sum of the velocity and displacement responses of the Kanai-Tajimi filter. The Clough-Penzien better represents the actual power spectrum of earthquakes,

as this features a decreasing energy as $\omega \to 0$. For the Clough-Penzien model the power spectrum is given by [98]

$$G(\omega) = \frac{\omega_{\mathrm{g}}^4 + 4\nu_{\mathrm{g}}^2\omega_{\mathrm{g}}^2\omega^2}{(\omega_{\mathrm{g}}^2 - \omega^2)^2 + 4\nu_{\mathrm{g}}^2\omega_{\mathrm{g}}^2\omega^2} \cdot \frac{\omega^4}{(\omega_{\mathrm{f}}^2 - \omega^2)^2 + 4\nu_{\mathrm{f}}^2\omega_{\mathrm{f}}^2\omega^2}\, G_0 \tag{3.5}$$

where ω_{g} and ν_{g} are parameters associated to the dominant soil frequency and damping, respectively, ω_{f} and ν_{f} give the spectrum a necessary decreasing shape in the low frequency region, and G_0 is the constant power spectral density of the underlying white noise $\underline{w}(t)$. The Clough-Penzien spectral density is shown in Fig. 3.2.

In practice, the intensity of the white noise can be related to the peak ground acceleration A_{g} by [99, 100]

$$G_0 = 2\left(\frac{A_{\mathrm{g}}}{28.4}\right)^2 \tag{3.6}$$

On the basis of random vibration theory it is possible to derive other analytical equations for estimating response quantities of linear and, in some case, nonlinear systems [101, 102, 103]. For instance, a useful equation for estimating the spectral displacement of a linear SDOF system is [104]

$$S_{\mathrm{d}}(\omega, \nu) = \lambda(s, R)\, \sigma_u \tag{3.7}$$

where σ_u is the standard deviation of the displacement response and $\lambda(s, R)$ the so-called peak factor, which is a function of the duration of the motion in its stationary phase s_0 and R the probability of the system to remain below the level $S_{\mathrm{d}}(\omega, \nu)$. In other words, R is the reliability that the designer intends to confer to the system and thus it is given by $R = 1 - Q$, where Q is the limiting failure probability in the optimization (see Eq. 3.1). The standard deviation of the displacement can be obtained from the following expression:

$$\sigma_u^2 = \frac{1}{\omega^4}\left[\omega G(\omega)\left(\frac{\pi}{4\nu_{\mathrm{s}}} - 1\right) + \int_0^{\omega} G(\Omega)\mathrm{d}\Omega\right] \tag{3.8}$$

On the other hand, the peak factor is approximately given by

$$\lambda(s, R) \approx \sqrt{2\ln\left(-\frac{\omega s}{\pi \ln R}\left[1 - \exp\left\{-\sqrt{4\nu_{\mathrm{s}}\ln\left(-\frac{\omega s}{\pi \ln R}\right)}\right\}\right]\right)} \tag{3.9}$$

where

$$\nu_{\mathrm{s}} = \frac{\nu}{1 - \exp(-2\nu\omega s_0)} \tag{3.10}$$

where s_0 is the duration of the strong motion phase. A useful regression equation for this parameter is [105, 106]:

$$s_0 = 30 \exp\left(-3.254\ A_{\mathrm{g}}^{0.35}\right) \tag{3.11}$$

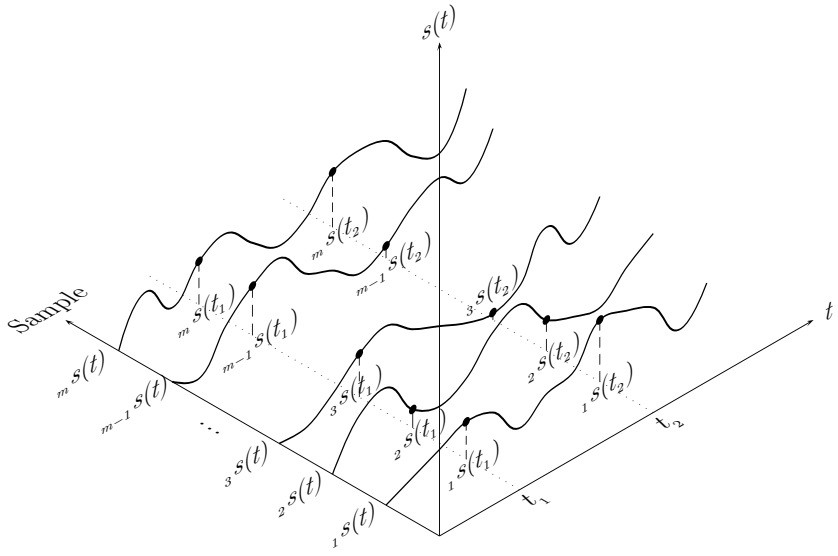

Figure 3.3: Realizations of a random process.

On the basis of the power spectral density function it is possible to generate artificial accelerograms. A first step is the generation of realizations of the stationary random process, such as those shown in Fig. 3.3. To this end a practical algorithm is [107]:

$$s(t) = \sum_{j=1}^{J} \sqrt{2G(\omega_j)\Delta\omega}\cos(\omega_j t + \zeta_j) \tag{3.12}$$

where J is a large number (of the order of one or two thousands), ζ_j is a random number having uniform distribution in the range $[0, 2\pi]$, $\Delta\omega$ is the resulting interval

in the discretization of the $\omega-$axis into J frequencies. This equation indicates that the signals $s(t)$ are the result of a large sum of harmonics with random phases having an amplitude depending on their value in the power spectrum. In order to obtain a realistic accelerogram it is necessary to give a non-stationary shape to the signal. This is achieved using

$$\ddot{u}_{\mathrm{g}}(t) = \xi(t)s(t) \tag{3.13}$$

where $\xi(t)$ is a function characterized by three phases: an ascendent one, corresponding to the first trains of seismic waves, a flat one associated to the strong ground motion and a descending one. There are several proposals for this function. Among them, the Amin-Ang modulating function [108] fits well in the modeling of the seismic action dealt with in this chapter, as it can be made dependent on the duration of the strong motion phase, given by Eq. (3.11). It is given by

$$\xi(t) = \begin{cases} \left(\frac{t}{t_1}\right)^2 & \text{if } t \leq t_1 \\ 1 & \text{if } t_1 \leq t \leq t_2 \\ \exp\left(-c(t-t_{_2})\right) & \text{if } t_2 < t \end{cases} \tag{3.14}$$

with parameters $t_{_1}$ corresponding to the start of the strong motion phase, $t_{_2} = t_{_1} + s_0$ and c, a parameter used for modeling the waning phase of the acceleration history.

For the purposes of present chapter it is important to remark that all parameters referred hereto are highly random. This means that in addition to the randomness of the acceleration history as such, the uncertainty about the underlying stochastic model must be considered for an adequate computation of structural robustness and reliability. Among the parameters defining the model, those having the largest impact into the uncertainty spread are

$$\boldsymbol{x} = \{\omega_{\mathrm{g}},\, \nu_{\mathrm{g}},\, A_{\mathrm{g}}\} \tag{3.15}$$

The peak ground acceleration, normally defined as that having a 10% probability of being exceeded in 50 years, can be modeled as a Lognormal variable with a coefficient of variation equal to 0.6, according to the research reported in [109] (The mean value of A_{g} depends on the seismicity of the region under consideration). It must be noted, however, that the randomness of the peak ground acceleration may be larger, since according to a study quoted in [81] its coefficient of variation lies in the range from 0.56 to 1.38. For the other two parameters the statistical analyses reported in [105, 106] yield the values appearing in Table 3.1. Note that

the uncertainty of all these variables is very large. According to the information given in [106], the correlation among all these variables is close to zero, so that the covariance matrix can be taken as diagonal. In addition, there are two dependent random variables, namely the strong motion duration and the white noise power spectral intensity, given respectively by Eqs. (3.11) and (3.6).

Table 3.1: Probabilistic definition of spectral random variables

Parameter	Distribution	Mean	c.o.v.
ω_{g}	Gamma	20.3 rad/s	0.448
ν_{g}	Lognormal	0.32	0.421
A_{g}	Lognormal	—	0.6

For the ensuing analyses with this modeling, the rest of parameters are assumed with the following fixed values: $t_{_1} = 2$s, $c = 0.18$, $\omega_{\mathrm{f}} = 2$rad/s and $\nu_{\mathrm{f}} = 0.6$.

3.4 Fundamentals of random vibration analysis

As is well known, the dynamics of a linear structure with mass, viscous damping and stiffness matrices denoted by $\boldsymbol{M}$, $\boldsymbol{C}$ and $\boldsymbol{K}$, respectively, is given by [98]

$$\boldsymbol{M}\ddot{\boldsymbol{u}}(t) + \boldsymbol{C}\dot{\boldsymbol{u}}(t) + \boldsymbol{K}\boldsymbol{u}(t) = \boldsymbol{p}(t) \tag{3.16}$$

where $\boldsymbol{u}, \dot{\boldsymbol{u}}$ and $\ddot{\boldsymbol{u}}$ are the displacement, velocity and acceleration vectors, respectively. With the aim of calculating the statistical second order response of the structure, it is convenient to express the above system of equations in state space form. That is, by collecting the displacement and velocity responses in the state vector $\boldsymbol{q}^{\mathrm{T}}(t) = [\boldsymbol{u}^{\mathrm{T}}(t), \dot{\boldsymbol{u}}^{\mathrm{T}}(t)]$, the original system of l second order differential equations is transformed into the following system of $2l$ first order differential equations:

$$\dot{\boldsymbol{q}}(t) = \boldsymbol{A}\boldsymbol{q}(t) + \boldsymbol{f}(t) \tag{3.17}$$

Here $\boldsymbol{A}$ is the so-called system matrix given by

$$\boldsymbol{A} = \begin{pmatrix} \boldsymbol{0} & \boldsymbol{I} \\ -\boldsymbol{M}^{-1}\boldsymbol{K} & -\boldsymbol{M}^{-1}\boldsymbol{C} \end{pmatrix} \tag{3.18}$$

and the vector of external loads is then

$$\boldsymbol{f}(t) = \begin{pmatrix} \mathbf{0} \\ -\boldsymbol{M}^{-1}\boldsymbol{p}(t) \end{pmatrix} \tag{3.19}$$

Let us now derive the differential equations governing the evolution of the first and second order moments of the random response of a linear structure, when excited by an external load defined as a stochastic process $\boldsymbol{p}(t)$. Under this stochastic point of view Eq. (3.17) is written as

$$\dot{\underline{\boldsymbol{q}}}(t) = \boldsymbol{A}\underline{\boldsymbol{q}}(t) + \underline{\boldsymbol{f}}(t) \tag{3.20}$$

The application of the expected value operator $\mathrm{E}[\cdot]$ to this equation gives the evolution of the vector of mean responses

$$\dot{\boldsymbol{\mu}}(t) = \boldsymbol{A}\boldsymbol{\mu}(t) + \boldsymbol{\mu}_{\boldsymbol{f}}(t) \tag{3.21}$$

For the sake of simplicity in the derivation of the covariance evolution, let us assume that the excitation and, consequently, the response have zero mean. The covariance matrix is defined as

$$\boldsymbol{\Sigma}(t) = \mathrm{E}[\underline{\boldsymbol{q}}(t)\underline{\boldsymbol{q}}(t)^{\mathrm{T}}] \tag{3.22}$$

For instance, in the case of a SDOF system, its entries are

$$\boldsymbol{\Sigma}(t) = \begin{pmatrix} \sigma^2_{\underline{u}}(t) & \sigma_{\underline{u}\dot{\underline{u}}}(t) \\ \sigma_{\underline{u}\dot{\underline{u}}}(t) & \sigma^2_{\dot{\underline{u}}}(t) \end{pmatrix} \tag{3.23}$$

where $\sigma_{\underline{u}}(t), \sigma_{\dot{\underline{u}}}(t)$ are the standard deviations of the displacement and velocity, respectively, and $\sigma_{\underline{u}\dot{\underline{u}}}(t)$ their covariance. The time derivative of the covariance matrix is given by

$$\dot{\boldsymbol{\Sigma}}(t) = \frac{\mathrm{d}}{\mathrm{d}t}\mathrm{E}[\underline{\boldsymbol{q}}(t)\underline{\boldsymbol{q}}^{\mathrm{T}}(t)] \tag{3.24}$$

with the result

$$\dot{\boldsymbol{\Sigma}}(t) = \mathrm{E}[\{\boldsymbol{A}\underline{\boldsymbol{q}}(t) + \underline{\boldsymbol{f}}(t)\}\underline{\boldsymbol{q}}^{\mathrm{T}}(t)] + \mathrm{E}[\underline{\boldsymbol{q}}(t)\{\boldsymbol{A}\underline{\boldsymbol{q}}(t) + \underline{\boldsymbol{f}}(t)\}^{\mathrm{T}}] \tag{3.25}$$

which leads to

$$\dot{\boldsymbol{\Sigma}}(t) = \boldsymbol{A}\mathrm{E}[\boldsymbol{q}(t)\boldsymbol{q}^{\mathrm{T}}(t)] + \mathrm{E}[\boldsymbol{q}(t)\boldsymbol{q}^{\mathrm{T}}(t)]\boldsymbol{A}^{\mathrm{T}} + \mathrm{E}[\boldsymbol{f}(t)\boldsymbol{q}^{\mathrm{T}}(t) + \boldsymbol{q}(t)\boldsymbol{f}^{\mathrm{T}}(t)] \tag{3.26}$$

that is,

$$\dot{\boldsymbol{\Sigma}}(t) = \boldsymbol{A}\boldsymbol{\Sigma}(t) + \boldsymbol{\Sigma}(t)\boldsymbol{A}^{\mathrm{T}} + \mathrm{E}[\boldsymbol{f}(t)\boldsymbol{q}^{\mathrm{T}}(t) + \boldsymbol{q}(t)\boldsymbol{f}^{\mathrm{T}}(t)] \tag{3.27}$$

For seismic ground motions, the system of equations of motion (Eq.3.16) must be enlarged to include the filter equations (3.3) and (3.4). Accordingly, the vector of external forces in Eq. 3.16 excited by the filter acceleration $\underline{\ddot{u}}_{\mathrm{f}}$ takes the form

$$\underline{\boldsymbol{p}}(t) = -\boldsymbol{M}\boldsymbol{r}\xi(t)\underline{\ddot{u}}_{\mathrm{f}}(t) \tag{3.28}$$

where $\boldsymbol{r}$ is a vector of static structural displacements caused by a unit static ground motion [98]. Thus, the leading underlying excitation is a single white noise (see Eq. 3.3). It can be shown that under such an excitation the last term of the above equation becomes

$$\mathrm{E}[\boldsymbol{f}(t)\boldsymbol{q}^{\mathrm{T}}(t) + \boldsymbol{q}(t)\boldsymbol{f}^{\mathrm{T}}(t)] = \pi \begin{pmatrix} \boldsymbol{0} & \boldsymbol{0} \\ \boldsymbol{0} & \boldsymbol{b} \end{pmatrix} \tag{3.29}$$

with

$$\boldsymbol{b} = \boldsymbol{M}^{-1}\boldsymbol{r}\boldsymbol{r}^{\mathrm{T}}\boldsymbol{M}^{-1}\xi^2(t)G_0 \tag{3.30}$$

The differential equation for the evolution of the covariance matrix finally becomes

$$\dot{\boldsymbol{\Sigma}}(t) = \boldsymbol{A}\boldsymbol{\Sigma}(t) + \boldsymbol{\Sigma}(t)\boldsymbol{A}^{\mathrm{T}} + \pi\boldsymbol{S}_{\boldsymbol{f}}(t) \tag{3.31}$$

where

$$\boldsymbol{S}_{\boldsymbol{f}}(t) = \pi \begin{pmatrix} \boldsymbol{0} & \boldsymbol{0} \\ \boldsymbol{0} & \boldsymbol{b} \end{pmatrix} \tag{3.32}$$

For nonlinear structures, the method of equivalent linearization [110, 111, 112] is perhaps the only non-Monte Carlo approach that can be readily applied to large systems [113]. For the common case displacement and velocity dependent nonlinear restoring forces,

$$\boldsymbol{M}\ddot{\boldsymbol{u}}(t) + \boldsymbol{C}\dot{\boldsymbol{u}}(t) + \boldsymbol{H}(\boldsymbol{u}, \dot{\boldsymbol{u}})(t) = \boldsymbol{p}(t) \tag{3.33}$$

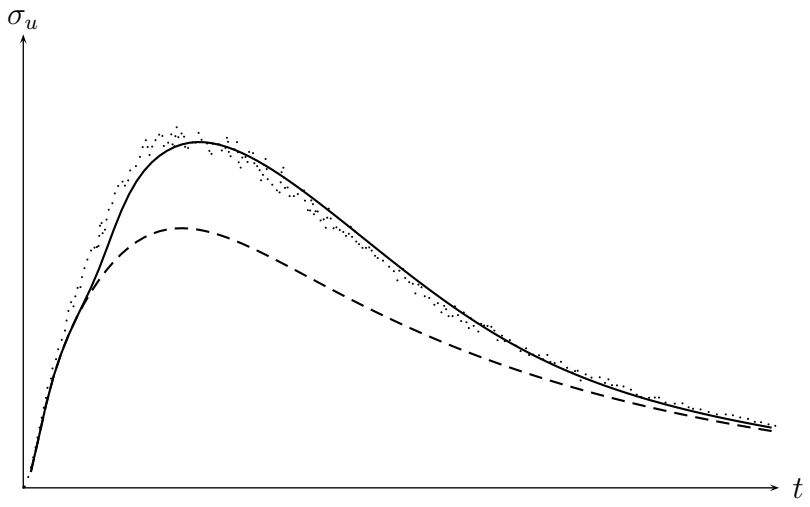

Figure 3.4: Comparison of Gaussian (dashed line) and non-Gaussian stochastic equivalent linearization (solid line) for an hysteretic oscillator using Monte Carlo results (dotted line)

the method consists in first finding equivalent matrices $\boldsymbol{C}_{\mathrm{e}}$ and $\boldsymbol{K}_{\mathrm{e}}$ for building a system of equations of the form

$$\boldsymbol{M}\ddot{\boldsymbol{u}}(t) + \boldsymbol{C}_{\mathrm{e}}\dot{\boldsymbol{u}}(t) + \boldsymbol{K}_{\mathrm{e}}\boldsymbol{u}(t) = \boldsymbol{p}(t) \tag{3.34}$$

and then applying the above procedures for finding the covariance evolution. The equivalent matrices are found through the minimization of the expected value of the squared difference between Eqs. (3.33) and (3.34). As a result, the entries of these matrices become dependent on the covariance responses at each time step, i.e. they are time-varying. If it is assumed that the responses are Gaussian the computations for some hysteretic systems, such as the Bouc-Wen model [114] are greatly facilitated [115]. Despite this assumption yields satisfactory results for stationary analysis (in which $\dot{\boldsymbol{\Sigma}}(t) = 0$) [110], the results may be far from satisfactory for the nonstationary case [116]. For this reason other, non-Gaussian approaches have been proposed [36, 117, 116]. As an illustration, Fig. 3.4 shows the results

for the standard deviation of the displacement of a Bouc-Wen hysteretic system driven Clough-Penzien seismic excitation, calculated with Monte Carlo simulation, equivalent linearization with Gaussian assumption and the non-Gaussian method of reference [116].

3.5 Practical computation of seismic robustness

In this section the problem of computing measures of the structural robustness under the input of earthquake loads is addressed. As said in the preceding, such measures are the statistical response moments of the first two orders. Except in cases of severe nonlinear behavior (such as the liquefaction of soils), it can be assumed that the responses to earthquakes have zero mean. Accordingly, for responses such as displacements, velocities and restoring forces it is sufficient to solve the equation of the evolution of the covariance matrix (3.31). However, if robustness is specified in terms of maximum responses in the absolute sense, the mean value will be different from zero. To this end the following procedure yields good estimations [118].

3.5.1 Moments of maximum response

Let $\underline{z}_{\mathrm{m}}$ denote the maximum of a random variable $\underline{z}$. In [118] it is postulated the following Gumbel-type distribution function for a maximum occurring between time instants t_1 and t_2 :

$$F(z_{\mathrm{m}}, t_1, t_2) = \exp\left[-\exp\left\{-K^{\eta-1}\left(\frac{z_{\mathrm{m}}}{\epsilon} - K\right)\right\}\right] \tag{3.35}$$

where the parameters η and ϵ depend on the time instants t_1 and t_2 and the first two moments of the peaks occurring in that interval. The latter are given by

$$\mu_{\mathrm{P}}(t_1, t_2) = \frac{\sqrt{\pi}}{2}\frac{1}{t_2 - t_1}\int_{t_1}^{t_2} \sigma_{\underline{z}}(t)\mathrm{d}t \tag{3.36}$$

$$\sigma_{\mathrm{P}}^2(t_1, t_2) = \frac{2}{t_2 - t_1}\int_{t_1}^{t_2} \sigma_{\underline{z}}^2(t)\mathrm{d}t \tag{3.37}$$

where $\sigma_{\underline{z}}(t)$ is the standard deviation of $\underline{z}$. On the other hand, η and ϵ can be obtained by solving the following system of nonlinear equations:

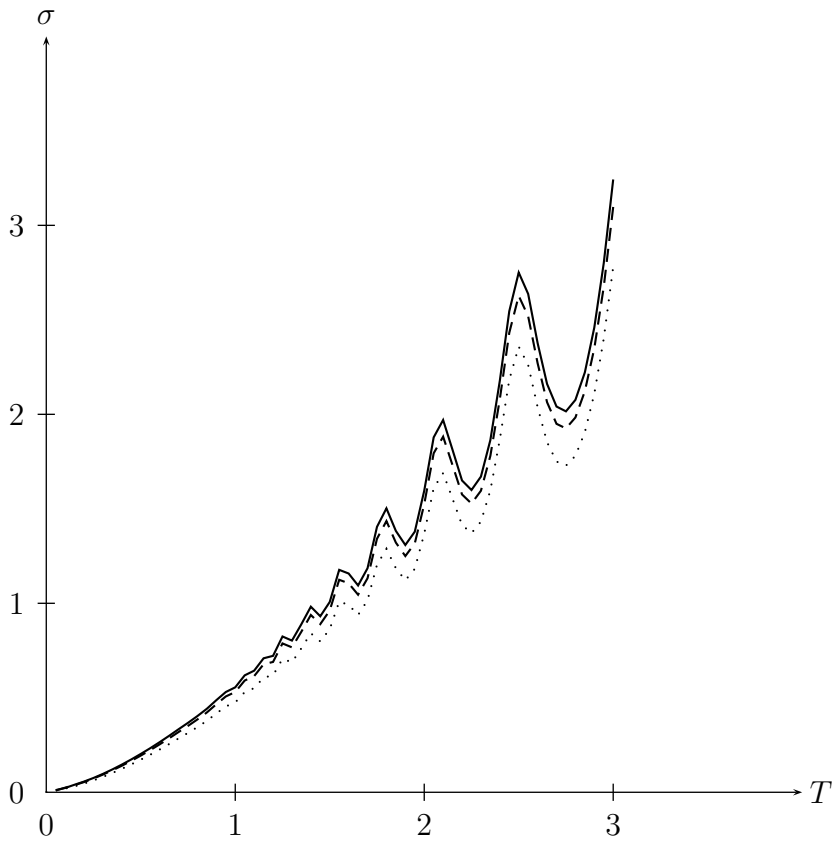

Figure 3.5: On the accuracy of the Point Estimate technique for calculating the spectrum of the unconditional standard deviation of SDOF displacement. Solid line: Point Estimate method. Dashed line: Monte Carlo simulation (1,000 samples). The dotted line corresponds to the standard deviation without considering uncertainties in the Kanai-Tajimi model and using the mean values of the parameters.

$$\frac{\sigma_{\mathrm{P}}(t_1,t_2)}{\mu_{\mathrm{P}}(t_1,t_2)} = \frac{\left[\Gamma\left(\frac{2}{\eta}+1\right) - \Gamma^2\left(\frac{1}{\eta}+1\right)\right]^{\frac{1}{2}}}{\Gamma\left(\frac{1}{\eta}+1\right)} \tag{3.38}$$

$$\mu_{\mathrm{P}}(t_1,t_2) = \epsilon\eta^{\frac{1}{\eta}}\Gamma\left(\frac{1}{\eta}+1\right) \tag{3.39}$$

where $\Gamma(\cdot)$ is the Gamma function. The value of K is expressed in terms of the time-varying zero upcrossing rate of the process $\lambda^{\uparrow}(t)$, i.e. the mean rate at which the process crosses the time axis with positive slope:

$$K = \left[\eta \ln \int_{t_1}^{t_2} 2\lambda^{\uparrow}(t)\mathrm{d}t\right]^{\frac{1}{\eta}} \tag{3.40}$$

It has been reported that the use of the zero upcrossing rate of Gaussian processes gives satisfactory results. This is given by

$$\lambda^{\uparrow}(t) = \frac{\sigma_{\underline{\dot{z}}}(t)\sqrt{1-\rho^2_{\underline{z}\underline{\dot{z}}}(t)}}{2\pi\sigma_{\underline{z}}(t)} \tag{3.41}$$

where $\sigma_{\underline{\dot{z}}}(t)$ is the standard deviation of the time derivative of $\underline{z}$ and $\rho_{\underline{z}\underline{\dot{z}}} = \sigma_{\underline{z}\underline{\dot{z}}}/(\sigma_{\underline{z}}\sigma_{\underline{\dot{z}}})$ the correlation coefficient of $\underline{z}$ and $\underline{\dot{z}}$, as given by the second order analysis (3.31). Note that since the postulated distribution of the maximum is of the Gumbel type, the mean and standard deviation of the maximum are

$$\mu_{z_{\mathrm{m}}}(t) = (K + 0.577K^{1-\eta})\epsilon \tag{3.42}$$

$$\sigma_{z_{\mathrm{m}}}(t) = \frac{\pi\epsilon}{\sqrt{6}K^{1-\eta}} \tag{3.43}$$

3.5.2 Unconditional moments

In order to assure the robustness of the structural system under the action of earthquake loads it is not sufficient to use a stochastic model of the ground motion exposed in the preceding. This is due to the fact that some of the parameters defining the model are highly random. Therefore, a correct estimations of the statistical moments of the response requires the consideration of such a randomness in a satisfactory manner. In this paragraph the main methods for accomplishing this task are discussed, with special emphasis on the Point Estimate technique, which to this purpose has been found accurate and simple to apply.

Perturbation methods, based on the Taylor expansion of the response vector $\boldsymbol{q}$, have been proposed to the purpose of computing the sensitivity of the statistical moments to variations of the random variables $\underline{\boldsymbol{x}}$ [100, 119, 120]. Considering $\boldsymbol{q}$ a function of the vector of parameters $\underline{\boldsymbol{x}}$, the first order expansion for the covariance response yields

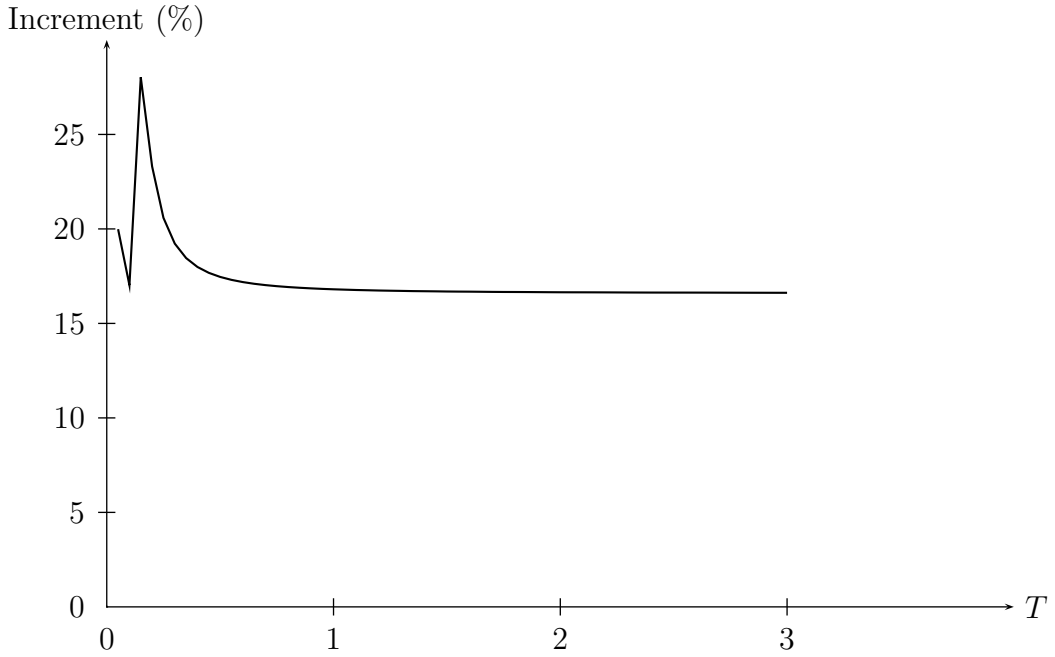

Figure 3.6: Spectrum of the increment of the standard deviation of the SDOF displacement when considering the uncertainties of the Kanai-Tajimi model parameters.

$$\frac{\partial \dot{\boldsymbol{\Sigma}}(t)}{\partial \boldsymbol{x}} = \frac{\partial \boldsymbol{A}(t)}{\partial \boldsymbol{x}} \boldsymbol{\Sigma}(t) + \boldsymbol{A}(t) \frac{\partial \boldsymbol{\Sigma}(t)}{\partial \boldsymbol{x}} + \frac{\partial \boldsymbol{\Sigma}(t)}{\partial \boldsymbol{x}} \boldsymbol{A}^T(t) + \boldsymbol{\Sigma}(t) \frac{\partial \boldsymbol{A}^T(t)}{\partial \boldsymbol{x}} + \pi \frac{\partial \boldsymbol{S_f}(t)}{\partial \boldsymbol{x}} \tag{3.44}$$

The matrix $\partial \boldsymbol{\Sigma}(t)/\partial \boldsymbol{x}$ contains the sensitivities of the second order responses with respect to the seismic parameters. With these sensitivities the increase of the statistical moments due to the parameters' spread can be estimated. However, perturbation methods in general are accurate only for parameters having a coefficient of variation of, say, less than 0.1. Since all the seismic parameters considered herein have a much larger spread, this technique should be discarded for this application.

Let us consider now the application of Monte Carlo simulation, consisting in solving repeatedly Eq. (3.31) using a random realization of vector $\boldsymbol{x}$ in each analysis and then computing the average of the variances and covariances of the structural responses. To this end the use of techniques oriented to estimate low order statistical moments of the responses with a small number of samples, such as the Latin Hypercube sampling [2], is recommended. However, as shown next, the method of Point Estimates is perhaps the most practical solution.

The method of Point Estimates was originally proposed in [121] and has been applied in several areas of structural engineering research, including Earthquake Engineering [122, 123, 124]. Its main difference with respect to the perturbation approach is that it is intended to cancel the higher order terms in the Taylor expansion instead of disregarding them. There are several proposals for applying this concept [121, 125, 126, 127, 128]. The simplest variant of those proposed in [128] will be evaluated for its application in the seismic design context.

For uncorrelated parameters, which is the case considered herein, the method postulates a linear equation for the moments of the system response $h(x)$, regarded as a function of a random parameter $\underline{x}$, in the form

$$\mathrm{E}[h^j(x)] = \sum_{k=1}^{n}\sum_{i=1}^{m} w_{k,i} h(x_{k,i})^j \quad j = 1, 2, \ldots \tag{3.45}$$

in which n is the number of variables and m is the number of concentration points. The function $h(\cdot)$ is evaluated at points $x_{k,i} = \mu_x + \xi_{k,i}\sigma_x, i = 1, 2$, where μ_x and σ_x are respectively the mean and standard deviation of the random parameters. For each variable k the values of the weights w_i and the normalized evaluation coordinates ξ_i are [128]

$$\begin{aligned} \xi_i &= \frac{\gamma_3}{2} + (-1)^{3-i}\sqrt{n + \left(\frac{\gamma_3}{2}\right)^2} \\ w_i &= \frac{1}{n}(-1)^i \frac{\xi_{3-i}}{\zeta} \end{aligned} \tag{3.46}$$

with $\zeta = 2\sqrt{n + \gamma_3^2/4}$. Here γ_l is a normalized central moment defined as

$$\gamma_l = \frac{1}{\sigma^l}\int_{-\infty}^{\infty} (x-\mu)^l p(x)\mathrm{d}x \tag{3.47}$$

where $p(x)$, μ and σ are respectively the probability density function, the mean and the standard deviation of the variable x.

In order to evaluate the accuracy of this method, it has been applied to the estimation of the spectrum of the unconditional standard deviation of the displacement of a SDOF linear system with damping ratio $\xi = 0.05$. To this end use is made of the Total Probability Theorem, applied to estimate the unconditional variance of the structural displacement $u(\boldsymbol{x})$, considered as a function of the ground motion parameters $\boldsymbol{x} = \{\omega_{\mathrm{g}},\ \nu_{\mathrm{g}},\ A_{\mathrm{g}}\}$, as follows:

$$\mathrm{Var}(u) = \int \mathrm{Var}(u(\boldsymbol{x})|\boldsymbol{x}) p_{\underline{\boldsymbol{x}}}(\boldsymbol{x}) \mathrm{d}\boldsymbol{x} \tag{3.48}$$

where $\mathrm{Var}(u(\boldsymbol{x})|\boldsymbol{x})$ is obtained by means of the theory of random vibration as [98]

$$\mathrm{Var}(u(\boldsymbol{x})|\boldsymbol{x}) = \int \frac{1}{(\omega^2 - \Omega^2)^2 + 4\xi^2\Omega^2\omega^2} \cdot G(\Omega, x) \mathrm{d}\Omega \tag{3.49}$$

where $G(\Omega, \boldsymbol{x})$ is the power spectral density of the Kanai-Tajimi seismic model:

$$G(\Omega, \boldsymbol{x}) = \frac{\omega_{\mathrm{g}}^4 + 4\nu_{\mathrm{g}}^2\omega_{\mathrm{g}}^2\Omega^2}{(\omega_{\mathrm{g}}^2 - \Omega^2)^2 + 4\nu_{\mathrm{g}}^2\omega_{\mathrm{g}}^2\Omega^2}\ G_0 \tag{3.50}$$

Taking into account that the mean of the random displacement is zero, the unconditional variance of the response, given by Eq. (3.48), is estimated with the point estimate technique as

$$\mathrm{Var}(u) = \sum_{k=1}^{n}\sum_{i=1}^{m} w_{k,i} \mathrm{Var}\left(u(x_{k,i})\right) \tag{3.51}$$

using the probabilistic definition of the parameters $\boldsymbol{x}$ displayed in Table 3.1. For the parameter A_{g} a mean value equal to 0.25g has been employed. The concentration points and weights are as shown in Table 3.2.

Table 3.2: Values for the application of the Point Estimate method with stochastic Kanai-Tajimi spectrum

Parameter	x_1	w_1	x_2	w_2
ω_{g}	8.1852	0.2079	40.2275	0.1254
ν_{g}	0.1601	0.2266	0.6596	0.1067
A_{g}	0.1006 g	0.2505	0.7018 g	0.0828

The results are shown in Fig. 3.5. Notice that with only six calculations of the SDOF system per period, the results are in excellent agreement with the estimation yielded by Monte Carlo simulation obtained as the average of 1,000 calls of Eq. (3.49) for each period. The figure also displays the spectrum of the standard deviation without considering the uncertainties of the model parameters. The effect of such a consideration can be better appreciated in Fig. 3.6, which corresponds to the increment of the standard deviation using the uncertain stochastic model with respect to its use with mean values. It can be observed that the impact of the uncertainties is more important at lower periods than at larger ones, for which the increment stabilizes at about 17%. This result points out the relevance of using a full stochastic model for structural robustness computations under earthquake loads.

The above discussion suggests that the Point Estimate method in the version reported in [128] constitutes an excellent means to evaluate the unconditional structural robustness in Earthquake Engineering.

Chapter 4

Practical computation of seismic reliability

4.1 Introduction

A distinguishing feature of probabilistic mechanics is the availability of an entirely general and accurate method for evaluation of statistical characteristics of the structural responses, such as moments, distribution functions and probabilities, which is the Monte Carlo method. In fact, the method can be regarded as a sampling technique in the probability space yielding a large population of the structural responses. In its turn, this population can be regarded as the second best piece of information after the explicit knowledge of their joint probability distribution, which is normally unknown. On the other hand, the Monte Carlo method is general in the sense that it is not limited by the mechanical characteristics of the system under analysis, such as linearity or any kind of nonlinearity. However, as is well known, its basic restriction is that the number of samples necessary to yield meaningful results is large and, in some cases, prohibitively large. For this reason resort is commonly made to other, non-general and approximate methods based on simplifying assumptions, whose computational cost, however, is much lower.

In this chapter two practical procedures for the reliability assessment under

seismic loads are proposed. The first is a Monte Carlo technique consisting in applying a backward sampling procedure using an algorithm based on the Dealunay tessellation intended to reduced the number of solving calls. due to computational reasons the algorithm is restricted to cases with a reduced number of variables, which is just the case of the seismic problem when use is made of random vibration approaches, as explained in Chapter 2, since in this case the problem is dominated by the set of variables $\boldsymbol{x} = \{\omega_{\mathrm{g}}, \nu_{\mathrm{g}}, A_{\mathrm{g}}\}$. The second is a method for improving the accuracy of the estimates of the probability of failure given by such simplified probabilistic methods. It is based on the Total Probability Theorem applied to a small sample computed in parallel with both the simplified method and Monte Carlo simulations. The method is applied in connection with a sampling technique introduced herein, named Backward Stratified Sampling, intended to cause a further reduction of the number of deterministic solver calls.

4.2 Backward Sampling with Delaunay tessellation

In this section a practical procedure for computing the failure probability when using Monte Carlo simulation. For computational reasons it is restricted to the case of a reduced number of random variables.

Consider a Monte Carlo sample in $\boldsymbol{u}-$space that has been selected according to the entropy criterion exposed in Chapter 2. Taking into account that only a few samples lie in the failure region, an obvious method for reducing the number of structural solver calls is to avoid using the solver with samples lying in the safe region. To this end it is advisable to sort the samples according to the distance to the origin in the $\boldsymbol{u}-$space and to remove those lying inside a hyper-sphere of radius $\tilde{\beta}$, which corresponds to a rough estimate of the reliability index of the problem at hand. This is illustrated by figure 4.1 which corresponds to the limit state function

$$g(\boldsymbol{x}) = 2 - x_2 - 0.1x_1^2 + 0.06x_1^3$$

used in the discussions of Chapter 2. It can be seen that by this means an important reduction in the number of samples in comparison to the crude Monte Carlo method is achievable. However, a further reduction is possible by means of the Delaunay tessellation, which is defined as follows: given a set of data points, it is a set of lines connecting each point to its natural neighbors in such a way that

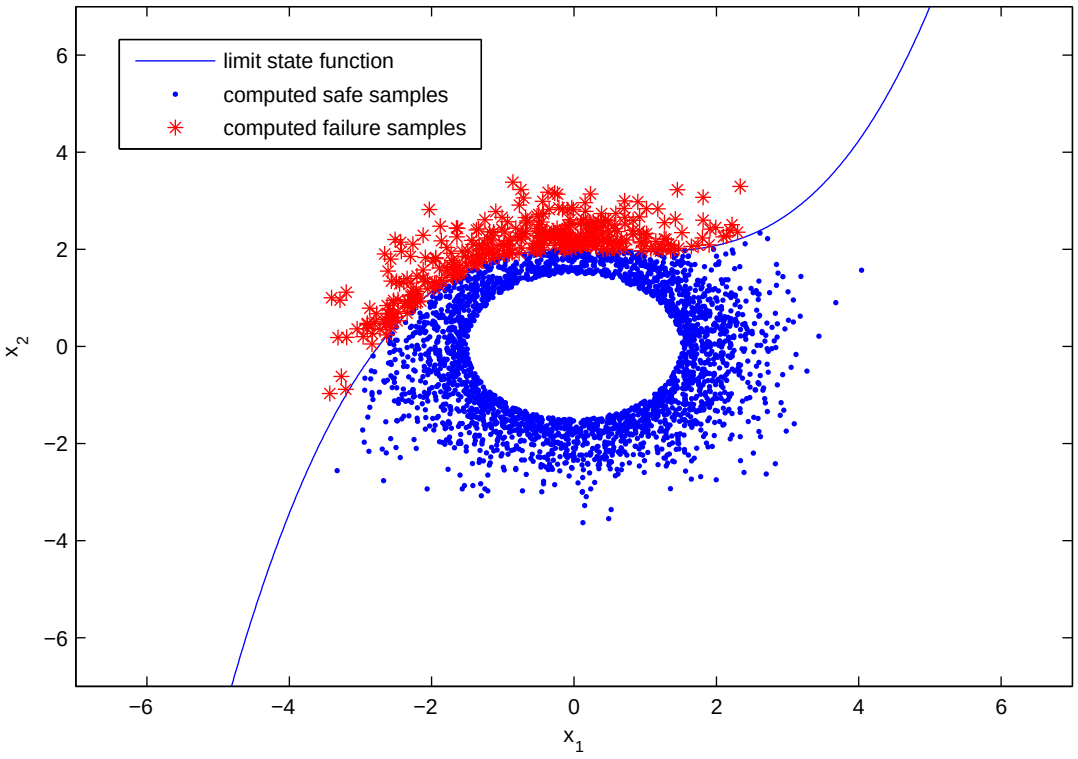

Figure 4.1: Backward sampling with removal of a hyper-sphere of samples.

no data points are contained in any hyper-triangle's circumcircle. The Delaunay triangulation is related to the Voronoi tessellation [129], because the circle circumscribed about a Delaunay hyper-triangle has its center at the vertex of a Voronoi polygon.

According to this definition, in two dimensions, the Delaunay tessellation produces a set of triangles joining samples in such a way that no line of any of them crosses any other line. The same applies to higher dimensional spaces. This property suggests that a method for processing the sorted Monte Carlo samples. Starting from a small subset of the farthest samples, one proceeds to the interior by processing all samples in a hyper-triangle, avoiding repetition. For each sample corresponding to a failure case, all samples of which it is a vertex are processed. This scanning procedure is followed until samples lying in the safe region are found.

In such a situation, the samples are not used for scanning new hyper-triangles.

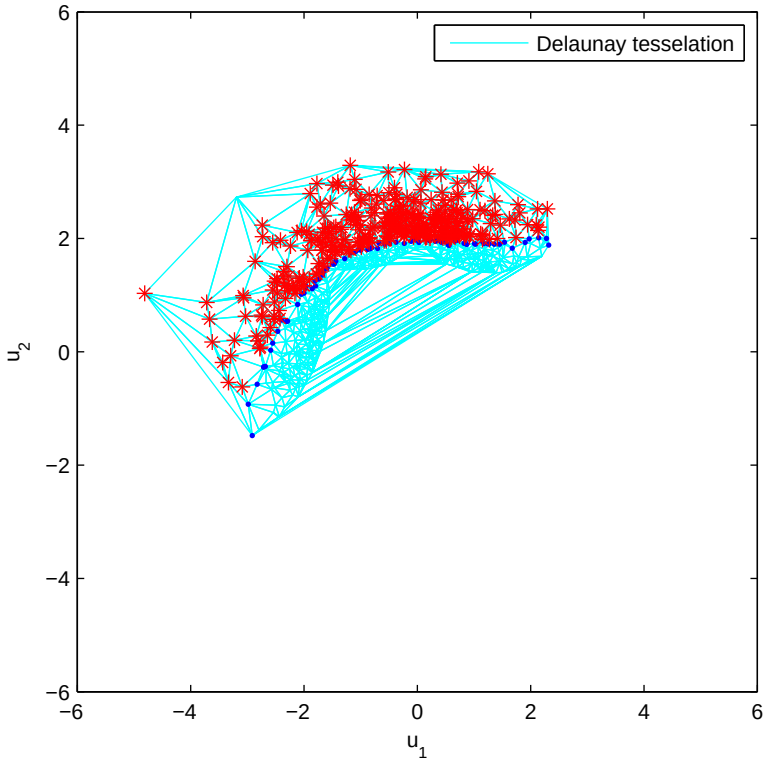

Figure 4.2: Delaunay tessellation procedure for Backward Sampling.

Algorithm: Backward Sampling with Delaunay tessellation:
- Generate N samples of $\boldsymbol{u}$.
- Sort the samples according to their distance to the origin.
- Remove samples within a distance $\tilde{\beta}$. Let the size of this set be $M < N$.
- Select a few starting failure samples lying far from the origin.
- Form the set $\boldsymbol{Q}$ with these starting samples.
- Perform Delaunay tessellation starting over the set.
- Set $STOP = 0, i = 0$.

while $STOP = 0$

- Scan the hyper-triangles of which each of the available failure samples

of set $\boldsymbol{Q}$ is a vertex.
• Increase the set $\boldsymbol{Q}$ with the new vertices and process them.
if failure condition is met **then**
• $i = i + \Delta i$, where Δi is the number of new failure samples in $\boldsymbol{Q}$.
else
• continue
end if
if no new failure samples enters into $\boldsymbol{Q}$ **then**
• Set $STOP = 1$
end if
end while
• Deliver the failure probability as the ratio i/N.

This procedure is illustrated by Figure 4.2. It can be seen that the sequences stop at safe samples so that the number of evaluated samples is slightly higher than those of the failure ones, which satisfies the criterion for the method stated at the beginning of this section. Notice also that the probability of failure computed by this procedure is exactly equal to that given by the standard Monte Carlo method.

4.3 Improving estimates with the Total Probability Theorem

As stated in the beginning of the present Chapter, a procedure is also presented for improving estimates of the failure probability when use is made of approximate models such as those corresponding to random vibration theories, using Monte Carlo simulation with nonlinear structural solvers as the reference of an exact calculation from both the viewpoints of structural mechanics and stochastic analysis.

Consider Fig. 4.4, in which events $B_1, B_2, \ldots, B_n$ are mutually exclusive and exhaustive (i.e., their union equals the total universal set U). For any event A the Total Probability Theorem states that [79]:

$$P[A] = \sum_j P[A|B_j]P[B_j] \tag{4.1}$$

This theorem follows from the definitions of conditional probability and mutual exclusion. In fact

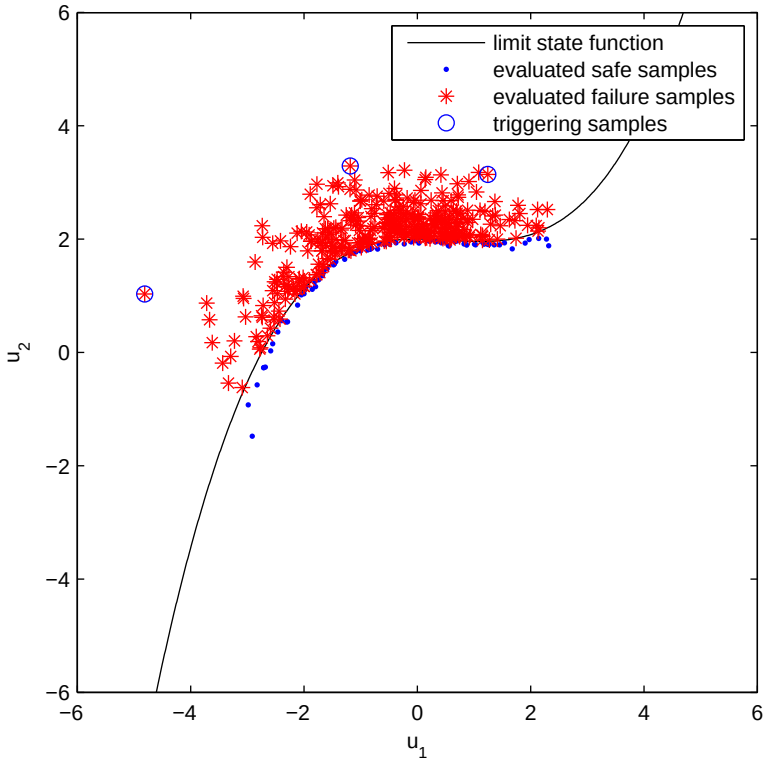

Figure 4.3: Computed samples used by the Delaunay tessellation procedure.

$$\begin{aligned} A = &\quad A \cap U = A \cap (B_1 + B_2 + \ldots + B_n) \\ = &\quad A \cap B_1 + A \cap B_2 + \ldots + A \cap B_n \end{aligned} \tag{4.2}$$

Since the events $A \cap B_j, j = 1, \ldots, n$ are mutually exclusive $P[A] = \sum P[A \cap B_j]$, Eq. (4.1) follows from the substitution of $P[A|B_j]P[B_j]$ for $P[A \cap B_j]$.

Consider now a stochastic response $\underline{z}(\underline{\boldsymbol{x}})$ which is a function of the random variables collected in vector $\underline{\boldsymbol{x}}$. The corresponding limit state function has typically the form

$$g(\underline{\boldsymbol{x}}) = \bar{z} - \underline{z}(\underline{\boldsymbol{x}}) \tag{4.3}$$

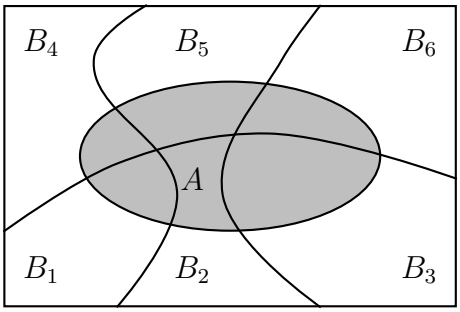

Figure 4.4: On the Total Probability Theorem

where $\bar{z}$ is a critical threshold for the response. The probability of failure is expressed as

$$P_{\mathrm{f}} = \mathrm{P}\left[g(\underline{\boldsymbol{x}}) \leq 0\right] \tag{4.4}$$

which is equivalent to

$$P_{\mathrm{f}} = \mathrm{P}\left[\underline{\boldsymbol{x}} \in \mathcal{F}\right] \tag{4.5}$$

where $\mathcal{F}$ is the failure domain. Suppose we have a small sample of responses $z(\boldsymbol{x})$ computed by both an approximate method (such as the analytical random vibration approach summarized above) and Monte Carlo simulation using realizations $\boldsymbol{x}$ of the random vector $\underline{\boldsymbol{x}}$. Let us denote these sets of responses as $z_1(\boldsymbol{x})$ and $z_2(\boldsymbol{x})$, respectively. Notice that for each realization $\boldsymbol{x}$ of the random vector the response is computed in two ways and the results will be obviously different. Figure 4.5 shows some results actually obtained in a structural dynamics application, in which the coordinates $z_2(\boldsymbol{x})$ correspond to Monte Carlo simulation, while the $z_1(\boldsymbol{x})$ were obtained with random vibration equations and the SRSS rule (square root of the sum of squares) for combining modal responses. In the figure the critical threshold is marked with solid thick lines. The dashed lines correspond to an arbitrary partition of the space alongside the $z_1(\boldsymbol{x})$ axis, thus defining a set of classes $\mathcal{C} = \{\mathcal{C}_1, \mathcal{C}_2, \ldots\}$. To this situation, the Total Probability Theorem (Eq. 4.1) is applied in the following form:

$$P[z_2 \in \mathcal{F}] = \sum_j P[z_2 \in \mathcal{F} | z_1 \in \mathcal{C}_j] P[z_1 \in \mathcal{C}_j] \tag{4.6}$$

in which the probabilities are estimated on the basis of the number of points in each subregion. As an illustration, consider the data plotted in Fig. 4.5, in which the total number of samples is 33. The Monte Carlo estimate of the probability of failure is, evidently,

$$P_{\mathrm{f}} \approx \frac{6}{33}$$

The application of Eq.(4.6) yields

$$P_{\mathrm{f}} \approx \frac{1}{21} \times \frac{21}{33} + \frac{2}{9} \times \frac{9}{33} + \frac{3}{4} \times \frac{4}{33} = \frac{6}{33}$$

Generalizing, Eq.(4.6) in practice assumes the form

$$P_{\mathrm{f}} \approx \sum_j \frac{N_k}{M_k} \times \frac{M_k}{N} \tag{4.7}$$

where the first ratio corresponds to the weight of Monte Carlo simulation inside each class and the second to the weight of the class in the total sum. Under this interpretation it is proposed to improve the estimation of the failure probability by refining the second ratio. This can be made by increasing both the numerator and denominator with additional calls of the approximate method only, while keeping the first ratio in its initial value, as it depends on Monte Carlo results. The new estimate then reads

$$P_{\mathrm{f}} \approx \sum_j \frac{N_k}{M_k} \times \frac{M'_k}{N'} \tag{4.8}$$

where $N' \gg N, M'_k \gg M'_k$.

Before illustrating the accuracy of this approach with an example, a method for further reduction of the computational cost implied by the preliminary exploration represented by Eq. (4.7) is introduced.

4.3.1 Backward stratified sampling

According to the above exposition on the application of the TPT, it is evident that the proposed method depends on the availability of a set of Monte Carlo results,

whose size should be as large as possible in order to give sufficient accuracy to the first ratios in Eq.(4.7), because they reappear in the refinement given by Eq.(4.8). In order to reduce the computational cost of such a calculation, consider again Fig.4.5 which shows that most of samples lie in the region in which both the analytical and synthetic approaches coincide to label as safe ones. This suggests devising a procedure for avoiding Monte Carlo computations in that zone. This can be done as follows.

Notice that since the first of the two ratios composing each summand is kept in Eq. (4.8), it is necessary to scan the $\underline{\boldsymbol{x}}-$variable space as exhaustively as possible with a low number of samples. For this goal the best available technique is the Stratified Sampling [34]. It consists in dividing the probability range $[0,1]$ into K intervals, thus yielding a total of $N = K^n$ divisions of the sample space $\underline{\boldsymbol{x}}$. A sample is generated randomly inside it using the inversion technique [34]. To this end, for each coordinate $\underline{x}_i, i = 1, 2, \ldots, n$ and for the interval $k, k = 1, 2, \ldots, K$, assign a probability

$$P_{i,k} = \frac{k - 1 + U}{K} \tag{4.9}$$

where U is a realization of a random number $\underline{U}$ having uniform distribution in $[0,1]$. The corresponding coordinate is found as

$$x_{i,k} = F^{-1}_{\underline{x}_i}(P_{i,k}) \tag{4.10}$$

where $F_{\underline{x}_i}(\underline{x}_i)$ is the distribution of variable $\underline{x}_i$. Evidently, this procedure implies a rapid explosion of the number of samples as the number of random variables becomes large. But, according to the discussion made in a previous section, in Earthquake Engineering applications using analytical random vibration analysis such a number is low and the set is dominated by the variables $\{\omega_{\mathrm{g}}, \nu_{\mathrm{g}}, A_{\mathrm{g}}\}$. Anyhow, advanced Stratified Sampling techniques oriented to the overcoming of such a curse of dimensionality are available [130] for cases in which the analyst desires to incorporate a significant number of random variables. Alternatively, stratification could be applied for the most important random variables $\{\omega_{\mathrm{g}}, \nu_{\mathrm{g}}, A_{\mathrm{g}}\}$ and simple Monte Carlo for the rest of them.

Figure 4.6 is a qualitative illustration of the traces of the limit state function of the type (4.3), in which $\underline{z}(\underline{\boldsymbol{x}})$ is a displacement response, on the planes $(\omega_{\mathrm{g}}, A_{\mathrm{g}}\}$ and $(\nu_{\mathrm{g}}, A_{\mathrm{g}}\}$. The traces are characterized by a flat zone for moderate and large values of ω_{g} and ν_{g} and a small depression towards the origin in both planes. The depression obeys to the following facts: (a) As shown by Fig. 3.2, the highest ordinates of

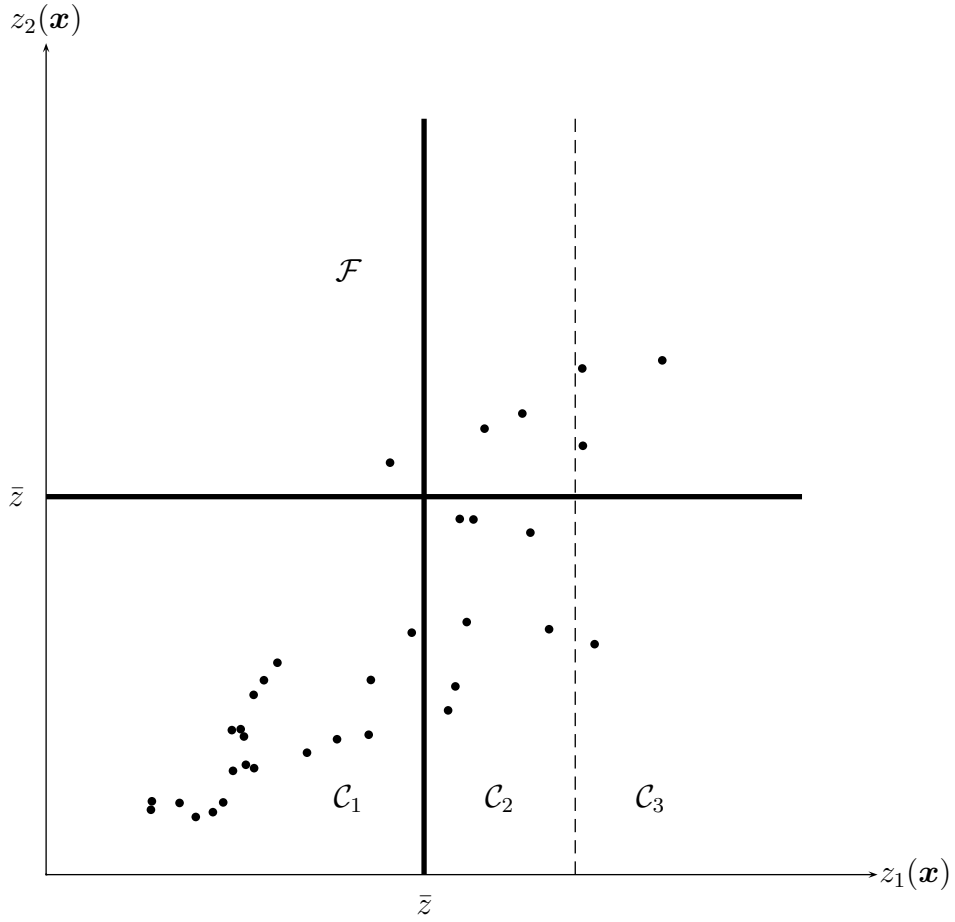

Figure 4.5: Illustrative example of the application of the Total Probability Theorem.

the power spectral density of the ground motion correspond to lower frequencies, thus determining an increase of failure cases in that zone; (b) This power spectral density acquires a more peaked shape as parameter ν_{g} diminishes, originating a higher input with low frequency content. Now, since the largest coefficient of variation among the three main variables $\underline{\boldsymbol{x}} = \{\omega_{\mathrm{g}}, \nu_{\mathrm{g}}, A_{\mathrm{g}}\}$ corresponds to the last of them, it is evident that by sorting the samples in descending order according to their coordinate A_{g}, the first analyses will correspond to the failure condition,

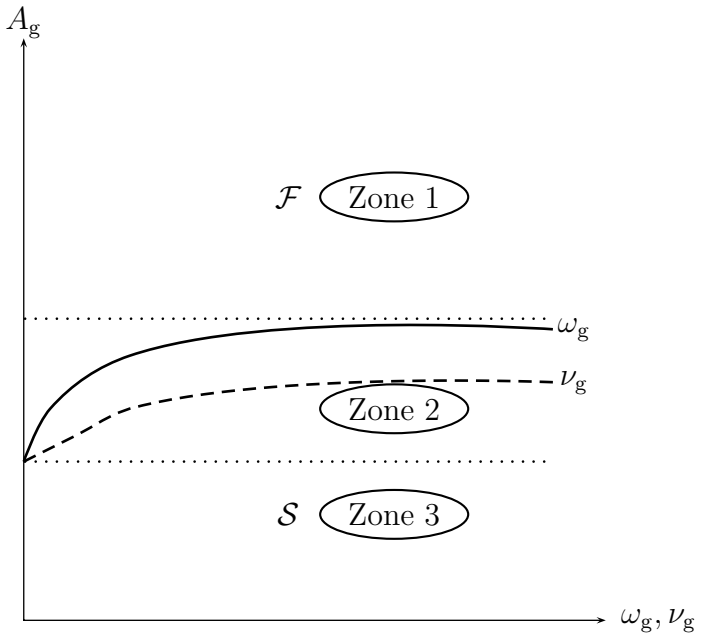

Figure 4.6: Typical traces of the limit state function in the planes (ω_g, A_g) and (ν_g, A_g).

then will appear an alternation of safe and failure samples, corresponding to the depression towards the origin, and, at the end, all samples will correspond to the safe condition (see Fig. 4.6). Taking into account that these latter constitute, by far, the vast majority of samples, the purpose is to avoid the computation of the actual response for this last group. The existence of the second group is recognized by introducing a counter for the safe samples found in this backward procedure with increasing frequency. According to practical experience, it is proposed that the algorithm stops when the counter reaches $N_{tol} \approx 0.1N$. The algorithm is, therefore, the following:

Algorithm: Backward Stratified Sampling applied to the estimation of failure probability under seismic action:

- Generate N samples of $\{\omega_g, \nu_g, A_g\}$
- Sort the samples according to their value of A_g in descending order.

• Set $N_{\text{tol}} \approx 0.1N$
• Set $i = 0$
• Set $STOP = 0$
while $STOP = 0$
    • Generate an artificial accelerogram.
    • Solve the equations of motion.
    if safety condition is met **then**
        • $i = i + 1$
        else
        • continue
    end if
    if $i \geq N_{\text{tol}}$ **then**
        • Set $STOP = 1$
    end if
end while

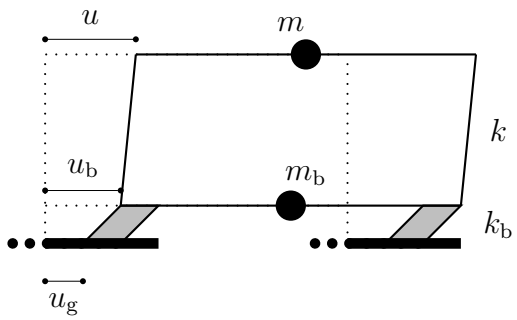

Figure 4.7: Base isolated building model.

4.3.2 Application to a base isolated building

The above method for improving the results of an approximate computation of the failure probability using a simplified approach will be illustrated with the case of a base isolated building. To this end consider the building model depicted in Figure 4.7. The bearings are of the steel-rubber type, so that a linear theory can be applied. The next exposition follows [131].

With respect to the ground, base and structural absolute displacements shown in the figure, let us define the relative ones

$$\begin{aligned} v_{\mathrm{s}} &= u - u_{\mathrm{b}} \\ v_{\mathrm{b}} &= u_{\mathrm{b}} - u_{\mathrm{g}} \end{aligned} \tag{4.11}$$

With respect to these degrees of freedom, the equations of motion are

$$\boldsymbol{M}\ddot{\boldsymbol{v}} + \boldsymbol{C}\dot{\boldsymbol{v}} + \boldsymbol{K}\boldsymbol{v} = -\boldsymbol{M}\boldsymbol{r}\ddot{u}_{\mathrm{g}} \tag{4.12}$$

with the matrices

$$\boldsymbol{M} = \begin{pmatrix} m + m_{\mathrm{b}} & m \\ m & m \end{pmatrix}, \quad \boldsymbol{C} = \begin{pmatrix} c_{\mathrm{b}} & 0 \\ 0 & c \end{pmatrix}, \quad \boldsymbol{K} = \begin{pmatrix} k_{\mathrm{b}} & 0 \\ 0 & k \end{pmatrix}, \quad \boldsymbol{v} = \begin{pmatrix} v_{\mathrm{b}} \\ v_{\mathrm{b}} \end{pmatrix} \quad \boldsymbol{r} = \begin{pmatrix} 1 \\ 0 \end{pmatrix}$$

In these equations m is the floor mass, $m_{\mathrm{b}}, c_{\mathrm{b}}, k_{\mathrm{b}}$ the mass, damping and stiffness constants of the base isolation subsystem and $\ddot{u}_{\mathrm{g}}$ is the horizontal ground acceleration. The damping coefficients and frequencies are

$$\omega_{\mathrm{s}}^2 = \frac{k}{m}, \quad \omega_{\mathrm{b}}^2 = \frac{k_{\mathrm{b}}}{m + m_{\mathrm{b}}}, \quad \nu_{\mathrm{s}} = \frac{c}{2m\omega_{\mathrm{s}}}, \quad \nu_{\mathrm{b}} = \frac{c}{2(m + m_{\mathrm{b}})\omega_{\mathrm{b}}} \tag{4.13}$$

The first order approximation for the mode shapes is

$$\boldsymbol{\phi}_1 = \begin{pmatrix} 1 \\ \epsilon \end{pmatrix}, \quad \boldsymbol{\phi}_2 = \begin{pmatrix} 1 \\ -\frac{1}{\gamma}\left(1 - \epsilon(1 - \gamma)\right) \end{pmatrix} \tag{4.14}$$

where

$$\epsilon = \frac{\omega_{\mathrm{b}}^2}{\omega_{\mathrm{s}}^2}, \quad \gamma = \frac{m}{m + m_{\mathrm{b}}} \tag{4.15}$$

Following the SRSS rule, the spectral estimates of the maximum displacements are

$$\begin{aligned} \max|v_{\mathrm{s}}| &= \sqrt{\phi_{1,\mathrm{s}}^2 b_1^2 + \phi_{2,\mathrm{s}}^2 b_2^2} \\ \max|v_{\mathrm{b}}| &= \sqrt{\phi_{1,\mathrm{b}}^2 b_1^2 + \phi_{2,\mathrm{b}}^2 b_2^2} \end{aligned} \tag{4.16}$$

where

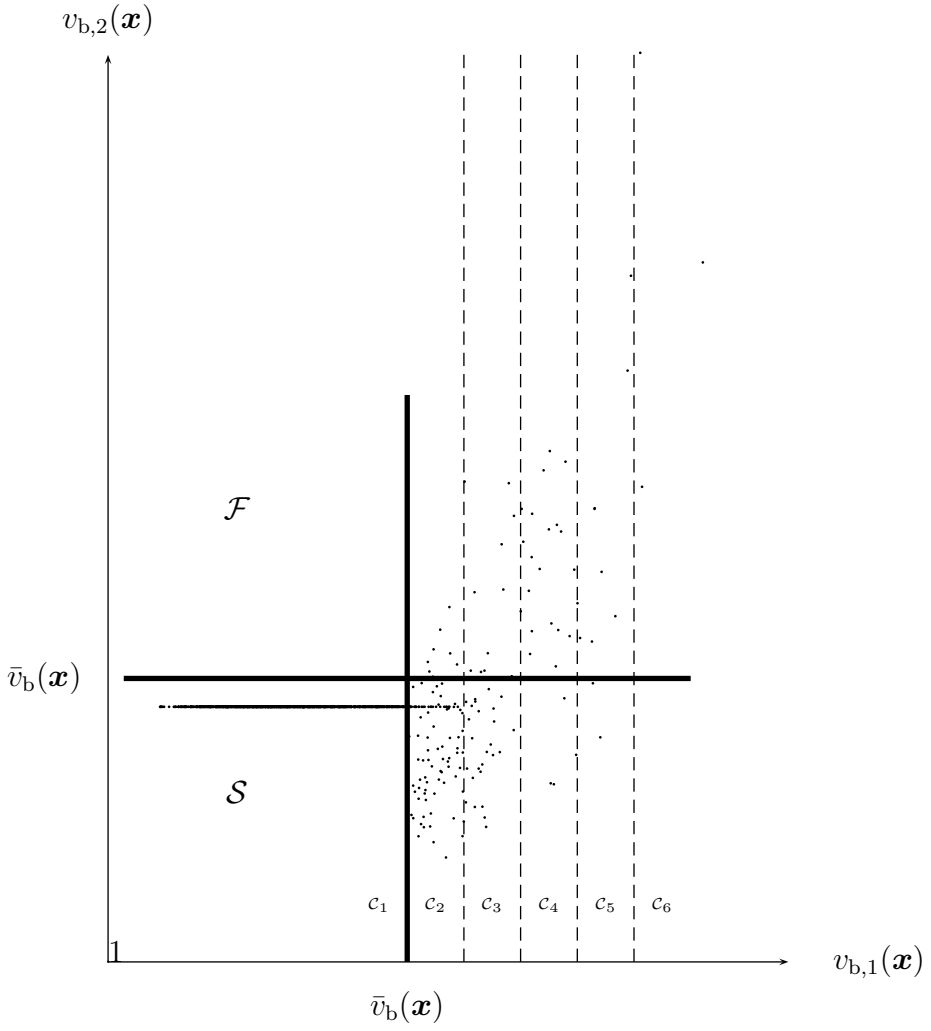

Figure 4.8: Results of the application of the proposed method to the base isolated building.

$$\begin{aligned} b_1 &= L_1\, S_{\mathrm{d}}(\omega'_{\mathrm{b}}, \nu'_{\mathrm{b}}) \\ b_2 &= L_2\, S_{\mathrm{d}}(\omega'_{\mathrm{s}}, \nu'_{\mathrm{s}}), \end{aligned} \tag{4.17}$$

in which the $L_i, i = 1, 2$ are the modal participation factors and $S_{\rm d}(\omega, \nu)$ is the displacement spectrum. Their expressions, together with those of the rest of parameters are as follows:

$$L_1 = 1 - \gamma\epsilon, \qquad L_2 = \gamma\epsilon$$

$$\omega'_{\rm b} = \omega_{\rm b}\sqrt{1-\gamma\epsilon}, \qquad \omega'_{\rm s} = \omega_{\rm s}\sqrt{\tfrac{1+\gamma\epsilon}{1-\gamma}} \tag{4.18}$$

$$\nu'_{\rm b} = \nu_{\rm b}\left(1 - 1.5\gamma\epsilon\right), \qquad \nu'_{\rm s} = \left(\tfrac{\nu_{\rm s}}{\sqrt{1-\gamma}} + \tfrac{\gamma\nu_{\rm b}\sqrt{\epsilon}}{\sqrt{1-\gamma}}\right)\left(1 - 1.5\gamma\epsilon\right) \tag{4.19}$$

Notice that this analytical approximate method implies the following assumptions and simplifications:

1. The assumption of Gaussianity of the stochastic process required to estimate the threshold level crossings implicit in Eq. (3.9), as well as other simplifications and empirical coefficients [104].

2. The SRSS rule for combining modal responses.

However, in solving the dynamic problem with Monte Carlo procedures no assumptions are needed on the level-crossings nor use is made of the SRSS rule. This contributes to make the results of the two approaches significantly different, as shown next.

This problem was solved using the following set of values (after [131]): $m = 100$ t, $m_{\rm b} = 66$ t, $\omega_{\rm s} = 5\pi$ rad/s, $\omega_{\rm b} = \pi$ rad/s, $\nu_{\rm s} = 0.02$, $\nu_{\rm b} = 0.1$. A total of $11^3 = 1331$ stratified samples of the set $\boldsymbol{x} = \{\omega_{\rm g}, \nu_{\rm g}, A_{\rm g}\}$ were used for both the theoretical random vibration approach, on the one hand, and for the Monte Carlo simulation, on the other. Failure was defined as the exceeding of a threshold value $\bar{v}_{\rm b}(\boldsymbol{x}) = 0.25$m by the base displacement. The Monte Carlo runs implied the generation of artificial accelerograms, each one comprising $J = 2^{10} = 1,024$ random variables, to which the three random variables defining the power spectrum are added to yield $1,027$ random variables. Since in using the analytical approach the estimations are dependent on the probability of exceeding the threshold (see Eq. 3.9), which is unknown at this stage, it was assumed $R = 0.95$. In the second step 8,669 additional runs of the analytical approach were performed to yield a total of $10,000$ samples. For the application of Eqs.(4.7, 4.8) six classes were defined as follows:

$$\mathcal{C}_1 = \{\boldsymbol{x} : v_{\rm b,1}(\boldsymbol{x}) < 0.25\}$$

$$\mathcal{C}_2 = \{\boldsymbol{x} : 0.25 \leq v_{\mathrm{b},1}(\boldsymbol{x}) < 0.30\}$$

$$\mathcal{C}_3 = \{\boldsymbol{x} : 0.30 \leq v_{\mathrm{b},1}(\boldsymbol{x}) < 0.35\}$$

$$\mathcal{C}_4 = \{\boldsymbol{x} : 0.35 \leq v_{\mathrm{b},1}(\boldsymbol{x}) < 0.4\}$$

$$\mathcal{C}_5 = \{\boldsymbol{x} : 0.4 \leq v_{\mathrm{b},1}(\boldsymbol{x}) < 0.45\}$$

$$\mathcal{C}_6 = \{\boldsymbol{x} : 0.45 \leq v_{\mathrm{b},1}(\boldsymbol{x})\}$$

In order to compute the exact failure probability for comparison purposes only, 200,000 samples were used in Monte Carlo simulation. The result is

$$P_{\mathrm{f}} = 0.0367$$

The application of the proposed method is illustrated in Fig. 4.8. Notice that despite the number of samples scheduled for the first approximation given by Eq. (4.7) was $11^3 = 1331$, the total number of solutions of the differential equation of motion (4.12) with artificial accelerograms was only 152, due to application of the stopping criteria described above with $N_{\mathrm{tol}} = 100$. This means that of the $11^3 = 1,331$ Monte Carlo samples scheduled in the first run, 1,179 were never actually computed, indicating an efficiency of the proposed procedure of 89% in this particular case. These non computed samples correspond to the samples in Zone 3 of the illustrative Fig. 4.6 and appear as a horizontal line of dots with a fictitious value of the vertical coordinate, while the horizontal coordinate corresponds to the actual estimate obtained with the analytical approach.

The crude estimation with the random vibration and SRSS approach yields an estimate

$$\hat{P}_{\mathrm{f}} = \frac{179}{1331} = 0.1345$$

which is in very bad agreement with the exact value. This illustrates the limitations of analytical random vibration analysis for estimating the system reliability. The application of Eq.(4.7) yields an approximation of the failure probability equal to

$$\hat{P}_{\mathrm{f}} = \frac{0}{1152} \times \frac{1152}{1331} + \frac{8}{103} \times \frac{103}{1331} + \frac{11}{37} \times \frac{37}{1331} + \frac{21}{25} \times \frac{25}{1331} + \frac{9}{11} \times \frac{11}{1331} + \frac{3}{3} \times \frac{3}{1331} = 0.0391$$

which is a much better estimate. However, by the refining procedure proposed herein, an estimate very close to the exact value is obtained by means of Eq.(4.8) as

$$\hat{P}_{\mathrm{f}} = \frac{0}{1152} \times \frac{8598}{10000} + \frac{8}{103} \times \frac{816}{10000} + \frac{11}{37} \times \frac{347}{10000} + \frac{21}{25} \times \frac{165}{10000} + \frac{9}{11} \times \frac{57}{10000} + \frac{3}{3} \times \frac{10}{10000} = 0.0369$$

which differs from the exact value only 0.54%.

Chapter 5

Reliability-based seismic optimization

5.1 Introduction

As stated in Chapter 3, Reliability-Based Design Optimization (RBDO) is aimed at minimizing a cost function with probabilistic constraints. This problem can be formulated in a general form as [89]:

$$\begin{aligned} \text{find}: &\quad \boldsymbol{y} \\ \text{minimizing}: &\quad C(\boldsymbol{y}) \\ \text{subject to}: &\quad f_i(\boldsymbol{y}) \leq 0, \quad i = 1, 2, \ldots, R \\ &\quad \mathrm{P}[g_j(\underline{\boldsymbol{x}}, \boldsymbol{y}) \leq 0] \leq Q_j, \quad j = 1, 2, \ldots, T \end{aligned} \tag{5.1}$$

where $\boldsymbol{y}$ is the vector of design variables, $C(\boldsymbol{y})$ is the cost function, $\underline{\boldsymbol{x}}$ is a set of random variables (also called basic variables) obeying a distribution $p_{\underline{\boldsymbol{x}}}(\boldsymbol{x})$, $\mathrm{P}[A]$ the probability of the random event A and Q_j its limiting value. Functions $g_j(\underline{\boldsymbol{x}}, \boldsymbol{y})$ are the limit state functions, which in this context become a function of the basic as well as of the design variables in this case. The quantity $\mathrm{P}[g_j(\underline{\boldsymbol{x}}, \boldsymbol{y}) \leq 0]$ defines the probability of failure, which can also expressed as

$$
\begin{aligned}
P_{\mathrm{f}}(\boldsymbol{y}) &= \mathrm{P}[g(\underline{\boldsymbol{x}}, \boldsymbol{y}) \leq 0] && (5.2)\\
&= \int_{\mathcal{F}(\boldsymbol{y})} p_{\underline{\boldsymbol{x}}}(\boldsymbol{x}) \mathrm{d}\boldsymbol{x} && (5.3)\\
&= \int I[g(\boldsymbol{x}, \boldsymbol{y}) \leq 0] p_{\underline{\boldsymbol{x}}}(\boldsymbol{x}) \mathrm{d}\boldsymbol{x} && (5.4)\\
&= \mathrm{E}\left(I[g(\boldsymbol{x}, \boldsymbol{y}) \leq 0]\right) && (5.5)
\end{aligned}
$$

where $\mathcal{F}(\boldsymbol{y})$ is the region in the $\boldsymbol{x}-$space corresponding to failure situations determined by the model $\boldsymbol{y}$ and $I[\cdot]$ is the indicator function equal to one if the situation in brackets holds and zero otherwise. On the other hand, $f_i(\boldsymbol{y})$ are system responses constituting equality and inequality constraints, respectively, posed upon stresses and displacements. Note that a constraint of the form $h(\boldsymbol{y}) \geq 0$ can be formulated as $-h(\boldsymbol{y}) \leq 0$, and an equality constraint $h(\boldsymbol{y}) = 0$ can be doubled as $-h(\boldsymbol{y}) \geq 0$ and $h(\boldsymbol{y}) \leq 0$. Therefore, the formulation in Eq. (5.1) is general. The models satisfying all constraints are labeled as feasible while those violating at least one of them a labeled as unfeasible. Other formulations of RBDO are possible, but this is sufficient for the purposes of present paper.

The relevance of RBDO for assuring economical and safe structural designs has fostered an intensive research in the last years. It comprises approximate methods [132, 133], alternative formulations [134], methodological approaches [97, 135, 136, 137, 138], computational techniques [139, 140, 141], software development [142, 143] and applications [144, 145, 146, 147].

In essence the RBDO is a nested problem, as for each trial model to be tested in the optimization process it is necessary to estimate probabilities of failure $\mathrm{P}_{\mathrm{f},j} = \mathrm{P}[g_j(\underline{\boldsymbol{x}}, \boldsymbol{y}) < 0]$. Thus, if the optimization calculation requires K trials with populations of size N and each reliability analysis needs L samples, then the number of calls of the numerical solver of the structure is $K \times N \times L$. Therefore it is crucial to reduce each of all these factors as much as possible.

The aim of present chapter is twofold. First, to propose a numerical technique to tackle the RBDO problem with an economical computational cost based on the pattern recognition paradigm. This is justified by noting that in Eq. (5.1) all inequalities, including the one defining the random event whose probability is to be computed, define four classes of samples: safe and unsafe in the $\underline{\boldsymbol{x}}-$space and feasible and unfeasible in the $\boldsymbol{y}-$space. For the reliability component of the problem use is made of the method of Support Vector Machines (SVM) successfully adapted by the author to the field of Structural Reliability [14, 148, 15, 149, 150].

Upon the experience derived in this research a novel approach for generating the training set of the machines based on Markov chain concepts in the $\boldsymbol{x}-$space is proposed. In addition, the SVM method is also used for discriminating the feasible and unfeasible domains in the design space $\boldsymbol{y}$, allowing a classification of incoming trial models without the need of calculating the failure probabilities from a given iteration onwards.

For the optimization part of the problem, the numerical method known as Particle Swarm Optimization [151] has been selected after the benchmark comparison among five optimization algorithms with biological inspiration (Genetic Algorithms, Evolutionary Algorithms, Memetic Algorithms, Ant-Colony Optimization and Particle Swarm Optimization) reported in [152]. In this report the authors conclude that the PSO method performs better than the others in terms of success rate and solution quality, while being second best in terms of processing time. It also features easy implementation, good memory and feedback capabilities, small number of parameters and robustness.

There are few fields of application of structural reliability concepts and procedures as challenging as well as interesting as Earthquake Engineering. This is because of the large uncertainties involving the event occurrence, its intensity, its duration, its spatial distribution and its realization signals. In spite of this, seismic design codes include only a few basic probabilistic specifications on the base excitation and normally pose no probabilistic requirements on the structural responses. In practice, however, there is an old concern about the stochastic response of the system and an increasing interest on the control of the failure probability [86, 100, 153, 123]. The second aim of the chapter is thus to apply the proposed RBDO method in the field. First a discussion on the random modeling that adequately describes the problem in hand while subjecting to control the number of variables. It is shown that this can be easily done by means of well established theories of random vibration. The proposed numerical method for solving RBDO is then applied to a complex seismic problem, which is a base isolated building with steel-rubber devices using a highly uncertain power spectrum as input.

5.2 A new algorithm for generating SVM training samples

The classification approach to solve the reliability problem was introduced upon recognizing the simple act that in the context of Monte Carlo simulation the sign

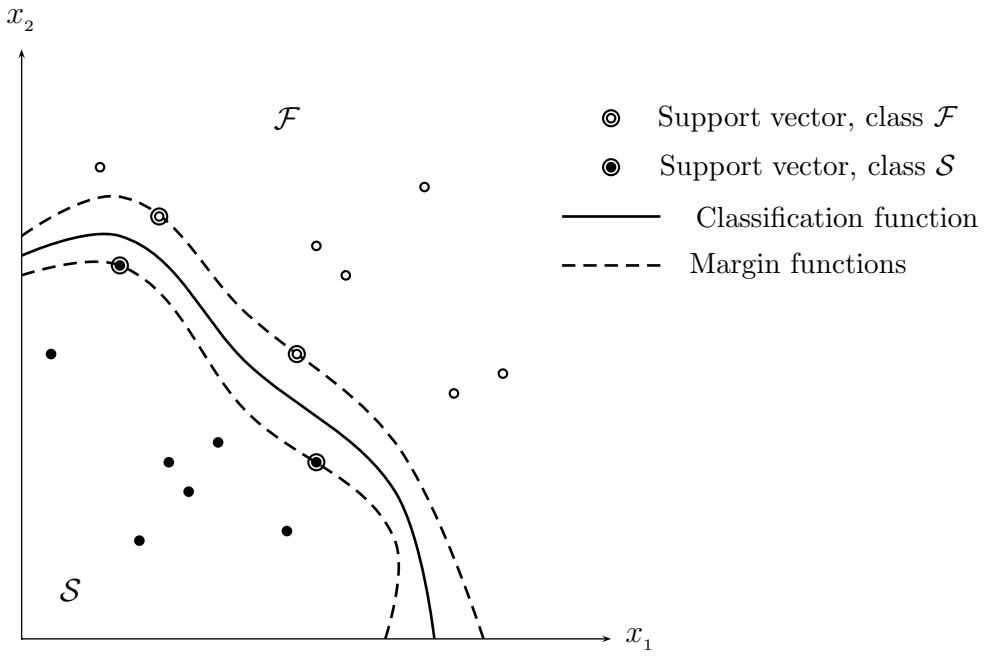

Figure 5.1: Support Vector Machine applied to the reliability problem.

of the limit state function $g(\boldsymbol{x})$ is all that matters for estimating the probability of failure [54]. Thus the function $g(\boldsymbol{x}) = 0$ can be interpreted as a function discriminating two classes, namely the safe and failure ones. This authorizes the use of pattern recognition approach for the case when the function is known only implicitly. Under this orientation Neural Classifiers were first successfully applied [54]. Support Vector Machines (SVM) [56], however, offers an important feature that helps in the selection of new training samples for improving its accuracy in a sequential program, which is the availability of ancillary functions known as margins (Fig. 5.1). The classification function $c(\boldsymbol{x})$ is defined only in terms of the support vectors as

$$c(\boldsymbol{x}) = \text{sgn}\left[\sum_{k=1}^{S} \alpha_k c_k K(\boldsymbol{x}, \boldsymbol{x}_k) - b\right] \tag{5.6}$$

where S is the number of support vectors, c_k the class sign of each of them $(-1, +1)$, α_k a Lagrange multiplier, $K(\boldsymbol{x}, \boldsymbol{x}_k)$ a kernel function and b a threshold [56]. The expression in brackets can be regarded as the SVM approximation of the limit state function:

$$\hat{g}(\boldsymbol{x}) = \sum_{k=1}^{S} \alpha_k c_k K(\boldsymbol{x}, \boldsymbol{x}_k) - b \tag{5.7}$$

The relevant feature of the methodology is that among the training samples only the support vectors, which are the samples closest to the unknown discriminating function, have non-zero Lagrange multipliers. Upon the basis of the cumulated experience on the use of this method in the field of structural reliability [14, 148, 15, 149, 150] an improved algorithm for the sequential refinement of the classifier is proposed next. Figure 5.1 illustrates the application of the SVM method for reliability analysis.

Firstly, it is necessary to consider that at a difference to the pattern recognition problem, in which the available samples are given by nature, in the structural reliability problem the samples are synthetic, i.e. generated by the computer. Thus, in order that the number of samples be as low as possible due to their high computational cost in many cases, the generation of the training set must be made with close regard to the nature of the reliability problem, whose main characteristics are the following two: (a) it is such that the number of samples is much lower in the failure class than in the safe class; (b) the failure samples tend to concentrate in a zone whose amplitude is strictly problem-dependent. A concept that can be of assistance in identifying such zone is that of the Importance Sampling, in which the original reliability problem

$$P_{\mathrm{f}} = \int I[g(\boldsymbol{x}) \leq 0](\boldsymbol{x}) p_{\underline{\boldsymbol{x}}}(\boldsymbol{x}) \mathrm{d}\boldsymbol{x}, \tag{5.8}$$

where $I[\cdot]$ is the indicator function, is replaced by an equivalent one

$$P_{\mathrm{f}} = \int I[g(\boldsymbol{x}) \leq 0](\boldsymbol{x}) \frac{p_{\underline{\boldsymbol{x}}}(\boldsymbol{x})}{f(\boldsymbol{x})} f(\boldsymbol{x}) \mathrm{d}\boldsymbol{x} \tag{5.9}$$

where $f(\boldsymbol{x})$ is the so-called Importance Sampling Density. By minimizing the variance of the Monte Carlo P_{f} estimate, it is found that its optimal value is [35]

$$f(\boldsymbol{x}) = (P_{\mathrm{f}})^{-1} I[g(\boldsymbol{x}) \leq 0] p_{\underline{\boldsymbol{x}}}(\boldsymbol{x}) \tag{5.10}$$

In practice the application of this formula is limited by the implication of the sought-after failure probability P_{f} in its expression. In spite of this it can be effectively sampled by means of a Markov chain method proposed by Au and Beck [40], which exploits the fact the denominator of Eq. (5.10) cancels out in a ratio of densities required in applying the Markov chain family of simulation methods derived from the original Metropolis algorithm [154].

The Metropolis algorithm is used in [40] to sample the Optimal Importance Sampling Density (OISD) and then an estimate of it is built using Gaussian mixtures. As shown in [15], such an estimate is subject to the so-called curse of dimensionality. However, the Markov chain sampling part of the method constitute a very good basis for developing a method oriented specifically to the generation of samples in the important zone useful for training statistical classification learning devices. To this end, the only difficulty in applying the Au and Beck algorithm lies in that the samples generated with it will lie exclusively in the failure zone. Such a difficulty is simply overcome by generating some samples from the ancillary density

$$s(\boldsymbol{x}) = ZI[g(\boldsymbol{x}) > 0]p_{\underline{\boldsymbol{x}}}(\boldsymbol{x}) \tag{5.11}$$

which mirrors the OISD in the safe domain. Here Z is an unknown normalizing constant whose value is irrelevant if use is made of Markov chain Monte Carlo algorithms, as done in the following. In addition, it is advisable to soften the indicator function in order to avoid rejection of highly relevant samples, i.e. samples lying very close to the actual boundary for which the indicator function may yield zero. To this end use is made of the sigmoid function, given by

$$\zeta\left[g(\boldsymbol{x})\right] = \frac{1}{1 + \exp\left(-\alpha g(\boldsymbol{x})\right)} \tag{5.12}$$

where α is a parameter defining the steepness of the function, such that the larger α, the steeper the function. In plugging this function into a Markov chain algorithm the value of α affects the probability of rejection or acceptance of new samples, in such a way that a large α induces very large or very low such probabilities, while low values provoke a stationary probability around 0.5. Thus a moderate value is necessary. Some tests conducted with the algorithm suggest using $\alpha = 2$.

Accordingly, an essential step of the proposed algorithm for generating the training population of Support Vector Machines is to produce a sample after either $f(\boldsymbol{x})$ or $s(\boldsymbol{x})$ with probability 0.5 each, where the final expressions of these densities are as follows:

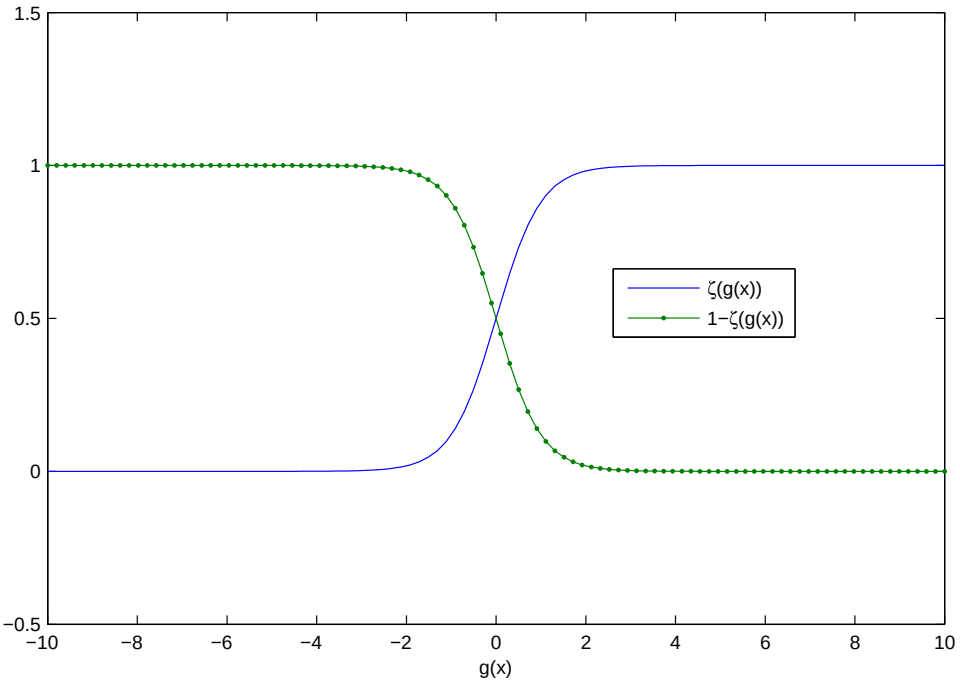

Figure 5.2: Sigmoid functions used for producing Markov chain samples in safe and failure domains.

$$\begin{aligned} s(\boldsymbol{x}) &= \zeta\left[g(\boldsymbol{x})\right] p_{\underline{\boldsymbol{X}}}(\boldsymbol{x}) \\ f(\boldsymbol{x}) &= \left(1-\zeta\left[g(\boldsymbol{x})\right]\right) p_{\underline{\boldsymbol{X}}}(\boldsymbol{x}) \end{aligned} \tag{5.13}$$

For the sake of clarity, Figure 5.2 depicts functions $\zeta\left(g\right)$ and $1-\zeta\left(g\right)$ for $\alpha=2$.

On the other hand, the Metropolis Markov chain sampling algorithm is based on a proposal distribution $q(\boldsymbol{x})$ from which a sample is generated and accepted as the new chain state with a certain probability. In [40] use is made of a uniform density on a hyperbox of width $L_d, d=1,\ldots,D$, where D is the number of dimensions, dependent on the parameter σ_d defining the standard deviation in dimension d of the OISD, which is not known in advance and may be difficult to estimate in

practice. However, in using Markov chains for sequential training of SVM it is important to note that since the goal is no longer an accurate building of a model of the OISD density but merely the sampling in safe and failure domains according to the densities given by Eq. (5.13), there is no need to estimate the spreads σ_d. Thus, instead of using the equation proposed in [40]

$$L_d = 6\sigma_d N_{\mathrm{c}}^{-1/(D+4)} \tag{5.14}$$

where N_{c} is the number of Monte Carlo samples constituting the chain, the box widths can be put in relation to the span covered by the support vectors in each dimension after the first trial as follows:

$$L_d = 6\left[\max_k(\boldsymbol{x}_k^{(d)}) - \min_k(\boldsymbol{x}_k^{(d)})\right],\ k = 1, 2, \ldots, S \tag{5.15}$$

where $\boldsymbol{x}_k^{(d)}$ denotes the d coordinate of $k-$th current support vector $\boldsymbol{x}_k$. Notice that this renders the algorithm adaptive to the information gained as the iteration advances.

In addition, the SVM building algorithm reported in [14], based upon the concept of active learning developed in [155], performs the sequential training in a sample-by-sample scheme by generating them exclusively inside the margin band, because the samples beyond it yield little information. In order to know if a sample $\boldsymbol{x}$ lies inside the margin, it is sufficient to check if

$$-1 \leq \sum_{k=1}^{S} \alpha_k c_k K(\boldsymbol{x}, \boldsymbol{x}_k) - b \leq +1 \tag{5.16}$$

holds. An improvement of this approach can be made if an exception to this rule is made for those samples among the current training population that may not be correctly classified by the current SVM classifier in each step. The exception is justified in that such classifying errors point out to a deficiency in the local curvature of the classification function in the vicinity of the respective samples. These samples constitute the seeds of small Markov chains generated as indicated in the preceding. If there are no such classification errors, the chain is generated from a point inside the margin band.

Finally, the SVM algorithm as reported in [14] was initiated with only two samples, one in each domain, which in some applications can be a cause of rapid convergence to a non satisfactory approximation of the limit state function. Thus the improved algorithm is initiated with three samples in each class.

According to the above said and incorporating the essentials of the Markov chain method for sampling the OISD as proposed in [40], the pseudo-code of the improved algorithm for the sequential generation of training samples for Support Vector classifiers reads as follows:

ALGORITHM 1: SVM ESTIMATION OF FAILURE PROBABILITY:
• Generate a pool of unlabeled patterns
(i.e. realizations of $\boldsymbol{x}$ after the original density $p_{\underline{\boldsymbol{x}}}(\boldsymbol{x})$).
• Initialize the training set with three safe and failure samples.
• Set $STOP = 0$
while $STOP = 0$
    • Train SVM with the current training set.
    • Classify the training set with the trained SVM.
    • Let E be the wrongly classified set.
    if E is non empty **then**
        • Generate a Markov chain from each sample in set E
        by sampling $s(\boldsymbol{x})$ or $f(\boldsymbol{x})$ with probability 0.5 in each step
        using ALGORITHM 2.
        • Incorporate the chain into the training set.
        else
        • Extract from the pool a sample $\boldsymbol{x}$ lying inside the margins (Eq. 5.16).
        • Generate a Markov chain using $\boldsymbol{x}$ as seed
        by sampling $s(\boldsymbol{x})$ or $f(\boldsymbol{x})$ with probability 0.5 in each step.
        • Incorporate the chain into the training set and reduce the pool.
    end if
    if pool is empty **or** P_{f} estimate stabilizes **then**
        • Set $STOP = 1$
    end if
end while

Finally, for the sake of completeness it is necessary to present the pseudo-code for the Markov chain step comprised in the above procedure for producing samples in both the safe and failure domains:

ALGORITHM 2: MARKOV CHAIN GENERATION STEP
• Initialize the seed $\boldsymbol{x}$ of the Markov chain.
• Set $i = 0$
while $i \leq N$

• Set $i = i + 1$
• Generate a sample $\boldsymbol{\xi}$ from the Uniform density
in a hyperbox of widths $L_d,\ d = 1, 2, \ldots, D$ (Eq. 5.15).
• Calculate the limit state function $g(\boldsymbol{\xi})$
• Calculate the limit state function $g(\boldsymbol{x})$
(if not already calculated)
• Generate a uniform random number w in the range $(0, 1)$.
if $w \leq 0.5$ **then**
• Set $r = s(\boldsymbol{\xi})/s(\boldsymbol{x})$ (Eq. 5.13)
else
• Set $r = f(\boldsymbol{\xi})/f(\boldsymbol{x})$ (Eq. 5.13)
end if
• Set $t = \min(r, 1)$.
• Generate a uniform random number v in the range $(0, 1)$.
if $t \geq v$ **then**
• Accept $\boldsymbol{\xi}$ as the next sample in the chain
else
• Keep $\boldsymbol{x}$ as the next sample in the chain and continue
end if
end while

5.2.1 Example 5.1. Two dimensional function

As an illustration on the application of the proposed algorithm, consider the limit state function

$$g(x_1, x_2) = -3.8 + \exp(x_1 - 1.7) - x_2 = 0 \tag{5.17}$$

where the x_1, x_2 are independent standard Normal variables, drawn from [15]. The problem was solved using the homogeneous polynomial kernel of degree 3, which has been found very useful in structural reliability applications, as it does not need parameters to tune. The chain length was set $N = 3$ in all cases. Figure 5.3 shows the initial Markov chains generated in the analysis. It is observed that they wander in the important region from the classification point of view. Figure 5.4 displays the entire training set together with the final support vectors. Notice the balanced distribution of the samples amongst the safe and failure classes. On the other hand Figure 5.5 displays the entire history of support vectors. Comparing the last two figures it can be observed the sequential approach of the support vectors

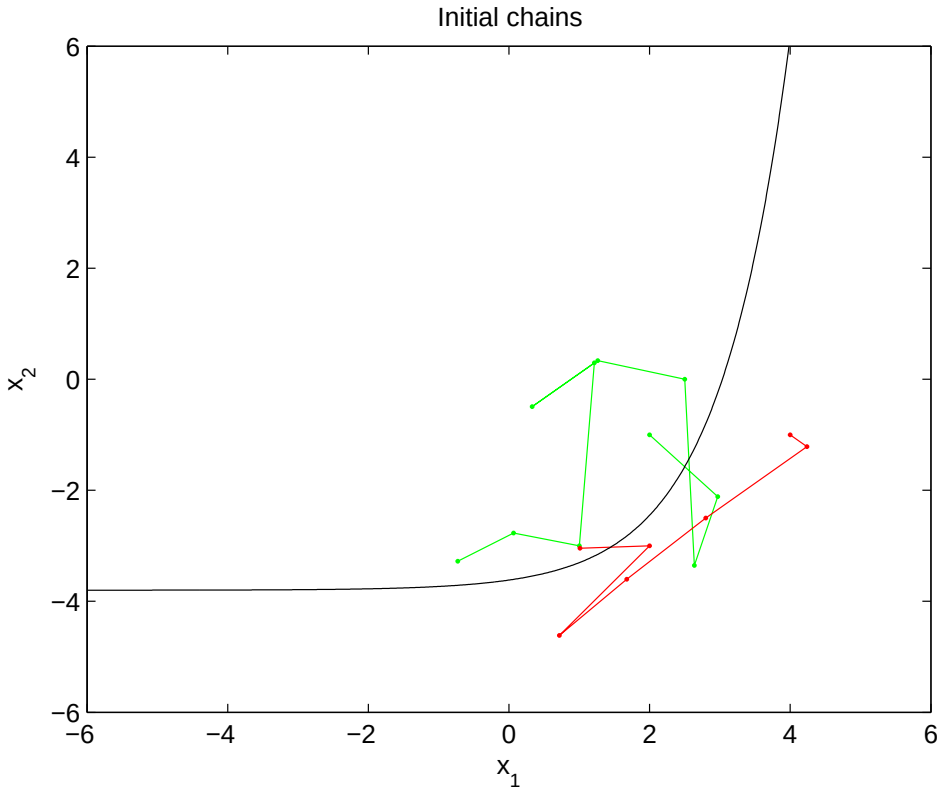

Figure 5.3: Initial Markov chains for Example 1.

to the actual class boundary. Also, it is important to note that while the end number of training samples is 39 the total number of $g-$ function calls is 102, due to the use of the Markov chains that implies the rejection of some samples whose $g-$value is actually evaluated, as illustrated by the respective algorithm. However, the Markov chain approach assures sampling in the important region, which is a very important prerogative when dealing with implicit limit state functions and, besides, the total number of solver calls is anyhow low. The probability of failure was calculated with 100,000 using both Monte Carlo simulation and the fitted SVM obtaining the same value (0.0024).

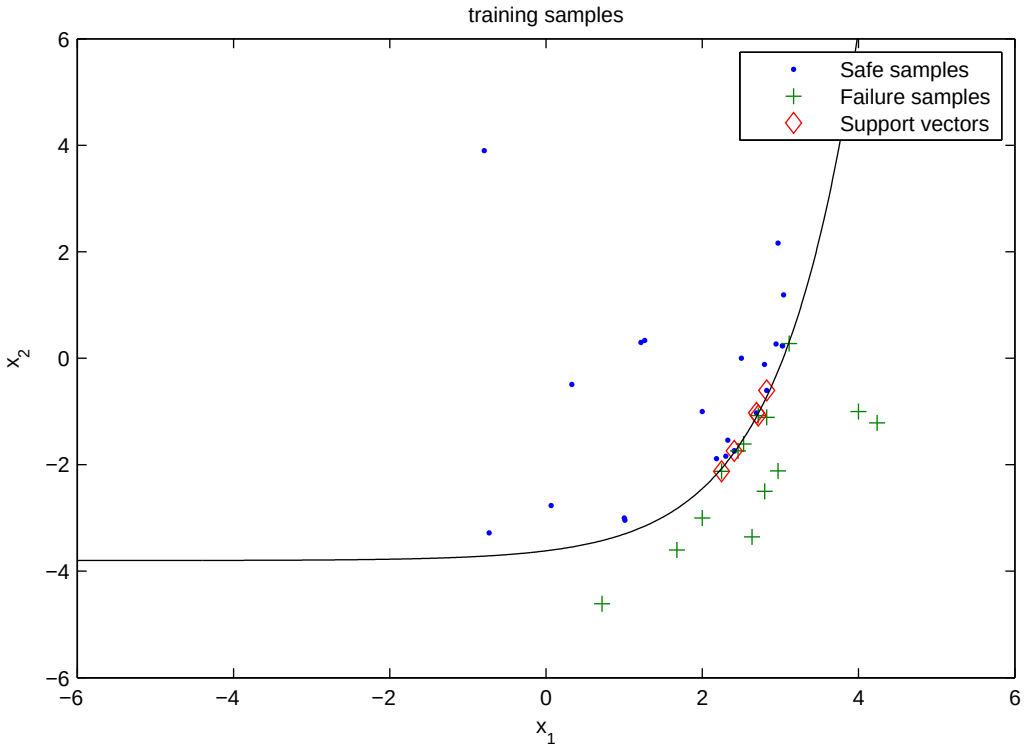

Figure 5.4: Training samples and end support vectors in Example 1.

5.2.2 Example 5.2. Two dimensional function with small P_{f}

It must be observed that the estimation of failure probabilities using Support Vector Machines is pretty independent of the value of the failure probability because the relevant issue is the availability of samples in both domains, their corresponding probability notwithstanding. to show this consider the limit state function [40]

$$g(x_1, x_2) = \begin{cases} 5 - \sqrt{x_1^2 + x_2^2} & \text{if } |x_1| \leq 5/\sqrt{2}, x_2 > 0 \\ 5\sqrt{2} - |x_1| - x_2 & \text{if } |x_1| > 5/\sqrt{2} \end{cases} \tag{5.18}$$

where the two variables are standard independent Normal. This function has a contour of equal probability so that there is an infinity of points at equal distance

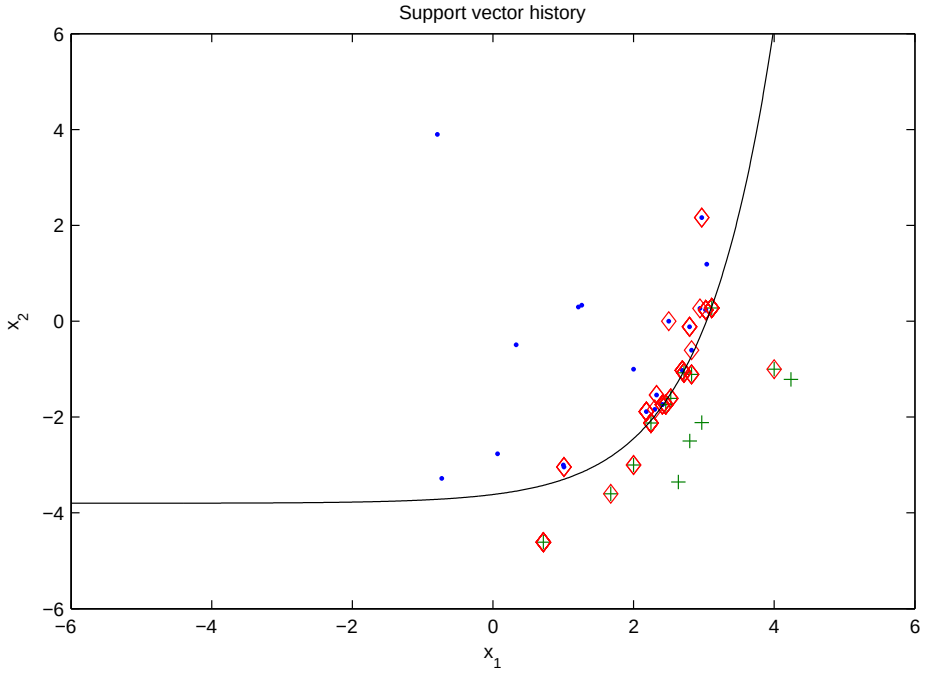

Figure 5.5: Support vector history in Example 5.1.

from the origin making it difficult the application of several structural reliability methods as in the previous case.

The problem was solved with the same SVM as in Example 1. The training population and the final support vectors are displayed in Figure 5.6. Considering the fact that the shortest distance from the function to the origin is large, the calculation of the failure probability with Monte Carlo simulation and the trained Support Vector Machine was performed with 5,000,000 samples. The results coincide at 2×10^{-6}.

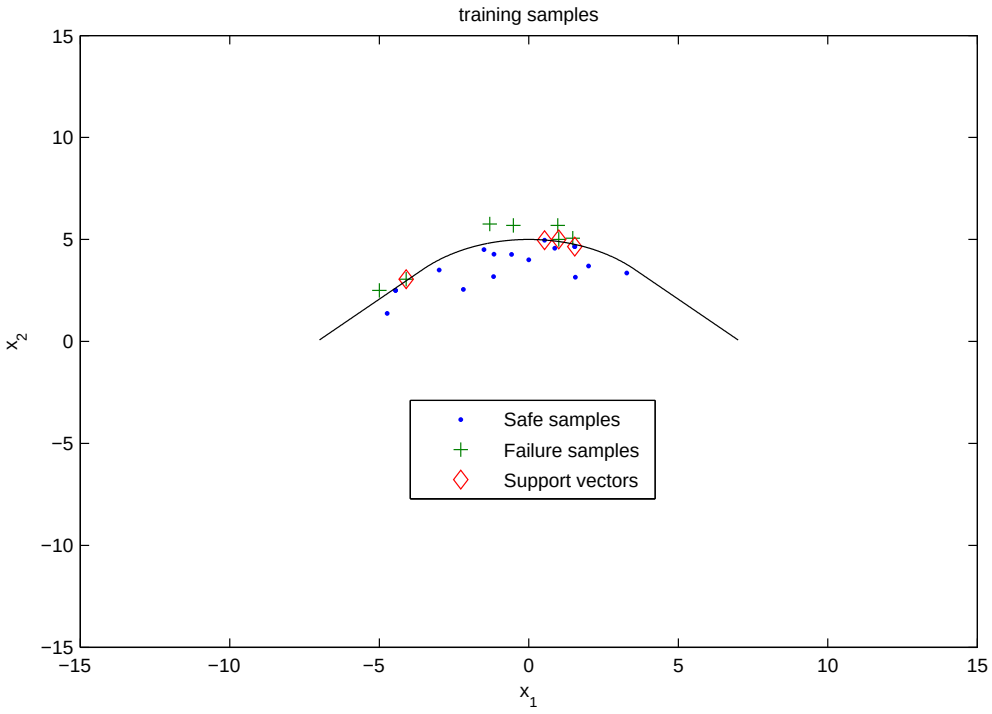

Figure 5.6: Results of Example 5.2.

5.3 Methodology for RBDO

As stated above, in reliability-based design optimization it is necessary to compute one or several failure probabilities for each trial model, with the consequence that the number of calls of the set of equations defining the structural model tends to be very large. Previous section dealt with a method for reducing such a number of the structural reliability computations. A similar goal should guide the specification of the optimization algorithm.

As said in the Introduction, the Particle Swarm method for optimization [151] (PSO) has been selected after the benchmark comparison published in [152]. Though inspired in biological processes, similarly to Genetic Algorithms and evolutionary Strategies, PSO differs from them in using as a paradigm the social behavior of

groups of species instead of their evolution. PSO has been successfully applied in structural reliability [156] as well as in structural optimization [157, 158, 159], , earthquake engineering [95] and others.

Consider several structural models as particles in the $\boldsymbol{y}-$design space. The motion of the i-th individual particle in iteration $k+1$ to a new position y_i^{k+1} is [151]

$$y_i^{k+1} = y_i^k + v_i^{k+1} \tag{5.19}$$

where v_i^{k+1} is the so-called velocity given by

$$v_i^{k+1} = \chi\left(wv_i^k + Z_1 r_i^k\left(P_i^k - y_i^k\right) + Z_2 s_i^k\left(P_{\mathrm{g}}^k - y_i^k\right)\right), \quad i = 1, 2, \ldots, N \tag{5.20}$$

In this equation the leading roles are those of P_i^k and P_{g}^k, which are respectively the best historical position of the i-th particle and the best current position amongst all particles of the group. Parameters Z_1 and Z_2 are positive constants called respectively cognitive and social parameters due to their relationship to P_i^k and P_{g}^k. Besides χ is a factor that controls the velocity, w is an inertial weight giving impulse to the particles, r_i^k and s_i^k are random numbers uniformly distributed in the range $[0, 1]$ that operate a perturbation and N is the population size.

The constituting ingredients elements of the algorithm are, therefore, the following:

- The experience of each individual, expressed by $\left(P_i^k - y_i^k\right)$ and representing the direction taken by the particle with respect to its best historical position.
- The experience of the group, $\left(P_g^k - y_i^k\right)$, representing a magnetic vector towards the best position recorded by the collective memory.
- The inertia of particles motion, such that a large inertia factor gives impulse to find global solutions while a small factor facilitates finding local minima. Thus it is recommended to initiate the optimization process with a large value and decreasing it as the solution advances.

Notice that Eq. (5.20) can be represented as a sum of vectors with directions v_i^k, $P_i^k - y_i^k$ and $P_g^k - y_i^k$ and magnitudes w, $Z_1 r_i^k$ and $z_2 s_i^k$, respectively. Such a sum determines the next position of the particle.

The application of this algorithm for RBDO requires handling deterministic and probabilistic constraints. To this end use is made of a penalty method proposed

in [160] was used. With reference to Eq. (5.1), it consists in minimizing the cost function

$$C_1(\boldsymbol{y}) = \begin{cases} C(\boldsymbol{y}) & \text{if } \boldsymbol{y} \in \mathcal{A} \\ C(\boldsymbol{y}) + k\sqrt{k}\, V(\boldsymbol{y}) & \text{if } \boldsymbol{y} \in \mathcal{U} \end{cases} \tag{5.21}$$

where $\mathcal{A}$ is the class of feasible solutions, $\mathcal{U}$ that of the unfeasible ones, k is the iteration counter and $V(\boldsymbol{y})$ a penalization function given by

$$V(\boldsymbol{y}) = \sum_{i=1}^{R} \Theta(q_i(\boldsymbol{y}))\ [q_i(\boldsymbol{y})]^{\beta(q_i(\boldsymbol{y}))} \tag{5.22}$$

where $q_i(\boldsymbol{y}) = \max\{0, f_i(\boldsymbol{y})\}$, $\Theta(\cdot)$ is a multistage penalization functional and $\beta(\cdot)$ a power functional. Since the components of penalty functions are problem dependent [161], the details are exposed in the application example. It is presently more relevant to discuss the link of this optimization method with the SVM classification approach for the specific case of RBDO. Firstly, by noticing that the constraints define a partition of the design variable space into feasible and unfeasible models, it is evident that the advantages of Support Vector Machines can be applied also in the $\boldsymbol{y}-$space, besides the random variable space. These two classifiers are identified as $\boldsymbol{y}-$SVM and $\boldsymbol{x}-$SVM, respectively. At a difference with respect to classifier in the random variable space, no special considerations are presently introduced for training the classifier in the design variable space. Secondly, notice that the margins of the current SVM in the design variable space provide a means of focalizing the search driven by the PSO, so that a penalization could be added for those particles lying beyond the current margins with the aim of accelerating convergence. Therefore, the presence of any constraint in Eq. (5.22) is two-fold: (a) a penalization for exceeding the limiting value and (b) a penalization for lying beyond the margins of the $\boldsymbol{y}-$SVM. Notice that for the specific case of probabilistic constraints, the availability of the $\boldsymbol{y}-$SVM classifier render unnecessary the calculation of failure probabilities for trial models tested after the classifier has been accurately trained, specifically for those models lying beyond the margins. In particular, if the feasible and unfeasible classes are perfectly separable, which is the case in many structural problems, the $\boldsymbol{y}-$SVM can be used for avoiding the calculation of failure probabilities after having a sufficient number of models for its learning.

The proposed RBDO algorithm is then a three-staged procedure described as follows:

ALGORITHM 3: RBDO WITH SVM IN TWO SPACES AND PSO
STAGE 1:
• Initialize randomly the $\boldsymbol{y}$ PSO population.
• Define a number of iterations K
• Set $k = 0$
while $k < K_1$
    • Set $k = k + 1$
    for each particle $i = 1, 2 \ldots, N$:
        • Train a $\boldsymbol{x}-$SVM (ALGORITHM 1).
        • Calculate P_{f} with the $\boldsymbol{x}-$SVM.
    end for
    • Apply penalizations to those samples exceeding any constraint
    • Generate the new population
end while
STAGE 2:
• Classify the cumulated populations into feasible and unfeasible classes
• Train a SVM for these classes ($\boldsymbol{y}-$SVM).
• Initialize randomly a new $\boldsymbol{y}$ PSO population of size N
about the best position found in STAGE 1.
• Set $k = 0$
STAGE 3:
while $k < K_2$
    • Set $k = k + 1$
    for each particle $i = 1, 2 \ldots, N$:
        • Classify the particle as feasible or unfeasible with $\boldsymbol{y}-$SVM.
    end for
    • Update the $\boldsymbol{y}-$SVM with the cumulated populations.
    • Apply penalizations to those samples exceeding any constraint,
    including penalization for lying beyond the current $\boldsymbol{y}-$SVM margins.
    • Generate the new population
end while
• Deliver the final population as the result and mark the optimum

5.4 Earthquake Engineering application example

The application of the RBDO concept in Earthquake Engineering implies the consideration of random variables corresponding to the structural materials and dimensions as well as to the ground motion excitation. However, the latter group is by far the most important because the uncertainty of its variables is typically much larger. For this reason, our interest will be focussed on this uncertainty source exclusively.

The way of defining the seismic action in probabilistic terms is critical in determining the realism but also the complexity of the RBDO solution, even in the case of linear problems. To illustrate this consider the linear equation of motion given by [98]

$$\boldsymbol{m}\ddot{\boldsymbol{u}} + \boldsymbol{c}\dot{\boldsymbol{u}} + \boldsymbol{k}\boldsymbol{u} = -\boldsymbol{m}\boldsymbol{r}\ddot{u}_{\mathrm{g}} \tag{5.23}$$

where $\boldsymbol{m}$, $\boldsymbol{c}$ and $\boldsymbol{k}$ are respectively the mass, damping and stiffness matrices, respectively, $\ddot{u}_{\mathrm{g}}$ is the ground motion acceleration, $\boldsymbol{r}$ a vector of static responses to a unit static ground motion and $\boldsymbol{u}$ the vector of structural displacement responses. As is well known, several design codes recommend the so-called SRSS solution (square-root of the sum of squares) given by

$$u_i = \sqrt{\phi_{i1}^2 b_1^2 + \phi_{i2}^2 b_2^2 + \ldots \phi_{ip}^2 b_p^2} \tag{5.24}$$

where ϕ_{ij} is the value of the $j-$th mode shape in the degree of freedom i, p is the total number of modes relevant for the calculation and the responses b_j are proportional to the design spectrum $S_{\mathrm{d}}(\omega_j, \nu_j)$:

$$b_j = L_j S_{\mathrm{d}}(\omega_j, \nu_j) \tag{5.25}$$

where ω_j and ν_j are respectively the frequency and damping of the $j-$th mode shape and L_j is the modal participation factor [98]. At this point it should be said that there are several alternatives for incorporating the ground motion uncertainties into the design optimization, as follows:

1. Random variables defining the design code spectrum. The most important of these is the maximum ground acceleration A_{g}, which is typically defined as that having a 10 percent probability of being exceeded in 50 years. In this approach there seems to be no clear way of making random the dominant

frequencies of the ground motion besides altering the periods of intersecting functions in a random way, but in most cases this would be meaningless. Anyhow notice that even if only the maximum ground acceleration A_g is modeled as random, there arises a nonlinear relationship between this variable and the estimate of the maximum design displacement, according to Eq. (5.24).

2. Uncertain spectrum defined by means of random vibration theories. In this case the ground motion is specified with an evolutionary power spectral density function, for which there are several proposals (see [162, 163, 164]), and the maximum response of the generic single degree of freedom system by means of the theory of the first passage problem [104]. This is a sophisticated as well as elegant stochastic formulation of the seismic action, not only because of the use of stochastic models but also for the consideration of random parameters in it. These parameters are the dominant frequency, the spectral shape, the strong motion duration and the maximum ground acceleration. The relationship linking these variables and the structural responses is highly nonlinear, as shown in the sequel.

3. Artificial accelerograms, which may be compatible with a design spectrum or not. In any case the accelerograms should be generated after the stochastic model using the random parameters just mentioned because otherwise the realism of this Monte Carlo procedure is doubtful. For this reason the method inherits the highly nonlinear relationship between the seismic model random parameters and structural responses and makes it even more complex. For linear structures this Monte Carlo procedure allows overcoming the approximations linked to approximate solutions of the first passage problem and the SRSS procedure, among others. This alternative is even more relevant for accurate solutions in the case of nonlinear systems, as it is obvious.

According to this discussion, it is evident that the last alternative is the most accurate, but also the most computationally expensive, for RBDO analysis, which requires computation of a large number of failure probabilities. In addition, it implies a very large increase of the number of random variables (normally hundreds or thousands) represented by those needed for generating the random signal used by each Monte Carlo sample. This makes difficult the understanding of the uncertainty propagation inside the structural system. On the contrary, in the second approach an adequate description of the problem can be made in terms of only

three independent random variables and two dependent ones defining the uncertain power spectrum, as shown next. In this way the entire uncertainty is lumped in only three variables, thus allowing a good understanding of the problem of designing in a highly uncertain environment. A similar approach has been adopted in [165] for studying the peak response of MDOF structures.

5.4.1 Stochastic spectrum

The spectral displacement $S_{\mathrm{d}}(\omega,\nu)$ will be defined in terms of a power spectral density model using random vibration theories [104]. The power spectrum adopted is that of Clough-Penzien given by [98]

$$G(\omega)=\frac{\omega_{\mathrm{g}}^4+4\nu_{\mathrm{g}}^2\omega_{\mathrm{g}}^2\omega^2}{(\omega_{\mathrm{g}}^2-\omega^2)^2+4\nu_{\mathrm{g}}^2\omega_{\mathrm{g}}^2\omega^2}\cdot\frac{\omega^4}{(\omega_{\mathrm{f}}^2-\omega^2)^2+4\nu_{\mathrm{f}}^2\omega_{\mathrm{f}}^2\omega^2}G_0 \tag{5.26}$$

where ω_{g} and ν_{g} are parameters associated to the dominant soil mass frequency and damping, respectively, ω_{f} and ν_{f} give the spectrum a necessary decreasing shape in the low frequency region, and G_0 is the one-sided power spectrum of the underlying white noise. This parameter can be related to the peak ground acceleration A_{g} by [99, 100]

$$G_0=2\left(\frac{A_{\mathrm{g}}}{28.4}\right)^2 \tag{5.27}$$

On the other hand the spectral displacement is given by

$$S_{\mathrm{d}}(\omega,\nu)=\lambda(s,R)\,\sigma_u \tag{5.28}$$

where σ_u is the standard deviation of the displacement response and $\lambda(s,R)$ the so-called peak factor, which is a function of the duration of the motion in its stationary phase s and R the probability of the system to remain below the level $S_{\mathrm{d}}(\omega,\nu)$ in the interval $(0,s)$. In other words, R is the reliability that the designer intends to confer to the system and thus it is given by $R=1-Q$, where Q is the limiting failure probability in the optimization (see Eq. e2q). The peak factor is approximately given by

$$\lambda(s,R)\approx\sqrt{2\ln\left(-\frac{\omega s}{\pi\ln R}\left[1-\exp\left\{-\sqrt{4\nu_{\mathrm{s}}\ln\left(-\frac{\omega s}{\pi\ln R}\right)}\right\}\right]\right)} \tag{5.29}$$

where

$$\nu_{\mathrm{s}} = \frac{\nu}{1 - \exp(-2\nu\omega s)} \tag{5.30}$$

For the duration of the strong motion phase s, the following regression will be applied [105, 106]:

$$s = 30 \exp\left(-3.254 A_{\mathrm{g}}^{0.35}\right) \tag{5.31}$$

Finally, the standard deviation of the displacement can be obtained from the following expression:

$$\sigma_u^2 = \frac{1}{\omega^4} \left[\omega G(\omega) \left(\frac{\pi}{4\nu_{\mathrm{s}}} - 1 \right) + \int_0^{\omega} G(\Omega) \mathrm{d}\Omega \right] \tag{5.32}$$

In this study, the set of basic random variables is defined as

$$\boldsymbol{x} = \{\omega_{\mathrm{g}},\, \nu_{\mathrm{g}},\, A_{\mathrm{g}}\} \tag{5.33}$$

Table 5.1: Probabilistic definition of independent spectral random variables

Parameter	Distribution	Mean	c.o.v.
ω_{g}	Gamma	20.3 rad/s	0.448
ν_{g}	Lognormal	0.32	0.421
A_{g}	Lognormal	0.25 g	0.6

The probabilistic definition of the first two random variables appearing in Table 1 follows reference [106]. The peak ground acceleration is modeled as a Lognormal variable with mean 0.25 g and a coefficient of variation 0.6, according to the research reported in [109]. Note that the uncertainty of all these variables is quite large, thus making significant the reliability-based optimization of structures in which the nonstructural damage as well as the overall stability depends on the lateral displacements. This is evidently more crucial for base isolation systems. It most be noted, however, that the randomness of the peak ground acceleration may be larger, since according to a study quoted in [81] its coefficient of variation lies in the range from 0.56 to 1.38. In addition, there are two dependent random variables, namely G_0 and s , given respectively by Eqs. (5.27) and (5.31).

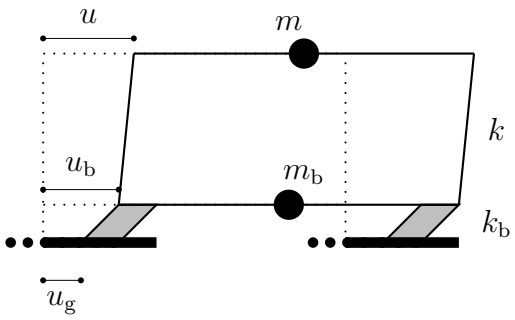

Figure 5.7: Base isolated building model.

5.4.2 Discussion on a base isolated building case

Seismic base isolation is an interesting case for testing structural reliability concepts and methods because of the critical dependence of the overall system safety on the lateral displacement of the supporting base. In this section the proposed algorithm for RBDO is applied for optimizing the design of a base isolated building subject to a earthquake design defined by means of random vibration theories.

Consider a two-floor base isolated building depicted in Figure 5.7, whose equations of motion were specified in the previous Chapter.

In order to illustrate the advantages of applying the pattern recognition paradigm in stochastic optimization, which justify the introduction of the $\boldsymbol{y}-$SVM in Algorithm No. 3, one hundred models of this building were randomly generated and analyzed with the stochastic spectrum described above, using the random variable definitions given in Table 1. Each model was identified by the set $\boldsymbol{y} = \{M, \omega_{\mathrm{s}}, \omega_{\mathrm{b}}\}$, where $M = m + m_{\mathrm{b}}$ with $m = 100$ t. In order to facilitate visualization, parameter ω_{s} was set equal to 13 rad/s. For each model the probability of exceeding 0.02 m

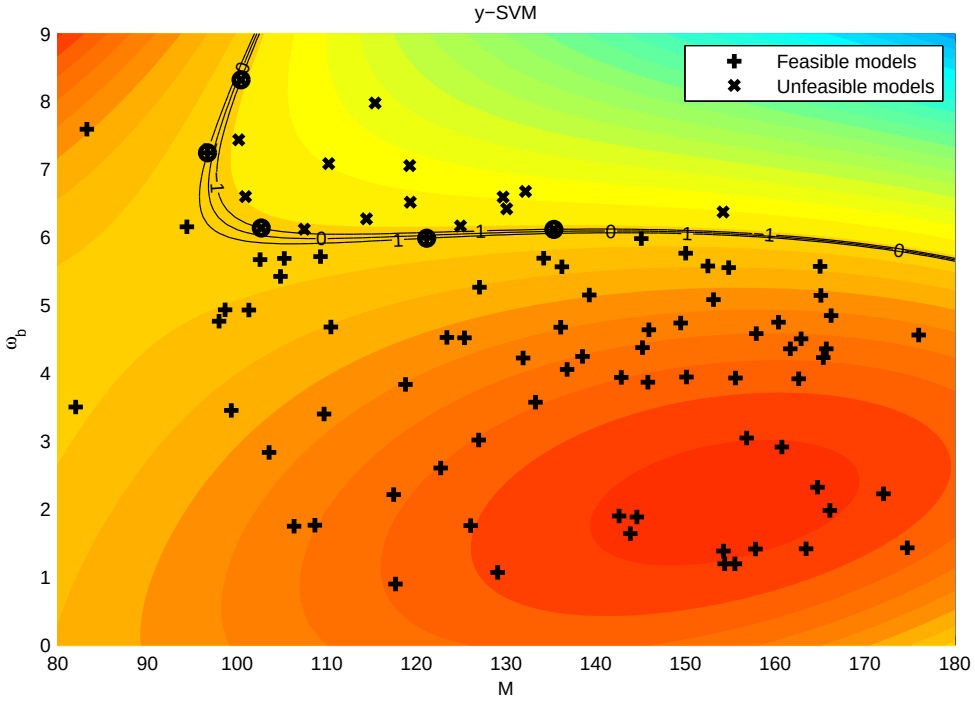

Figure 5.8: Two dimensional SVM fitted in $\boldsymbol{y}$ space for feasible and unfeasible domains.

by the base displacement v_{b}, considered as the failure condition, was calculated using 5,000 samples of the random variable set $\boldsymbol{x} = \{\omega_{\mathrm{g}}, \nu_{\mathrm{g}}, A_{\mathrm{g}}\}$. Finally, the models were labeled as feasible if their failure probability was lower than or equal to 0.03 and unfeasible otherwise and a SVM with polynomial kernel of degree 3 was trained with the labeled samples. The result is displayed in Figure 5.8. It can be seen that the SVM can be confidently used to avoid the costly calculation of the failure probability of each model after a sufficient number of samples allows its adequate training. In this respect it must be noted that the optimal characteristics of the SVM allow a reasonably good generalization capacity (i.e. high probability of correct class prediction for samples not used in the training phase) when trained with a reduced number of samples. This is an involved subject for which the in-

terested reader is referred to [56, 15]. In addition, the margins of the $\boldsymbol{y}-$SVM can be used for restricting the search space of the PSO algorithm, as explained in the preceding.

5.4.3 RBDO of a base isolated building

For the base isolated building model depicted in Figure 5.7 the RBDO problem is defined as follows:

$$\begin{aligned} \text{find}: \quad & \boldsymbol{y} \\ \text{minimizing}: \quad & C(\boldsymbol{y}) = y_1 + \tfrac{1}{\pi^2}\left(y_2^2 + 2y_3^2\right) && (5.34) \\ \text{subject to}: \quad & \mathrm{P}[0.035\mathrm{m} - \max|v_\mathrm{b}| \leq 0] \leq 0.03 && (5.35) \\ & \omega_\mathrm{s} \geq 11\mathrm{rad/s} && (5.36) \end{aligned}$$

where

$$\boldsymbol{y} = \{y_1,\, y_2,\, y_3\} = \{M,\, \omega_\mathrm{s},\, \omega_\mathrm{b}\} \tag{5.37}$$

In words, the goal is to minimize a cost function construed as the base slab mass plus the squared structural stiffness and twice the squared base isolation stiffness. The factor for the latter is introduced with a regard to the high cost of the isolation devices. The probabilistic constraint corresponds to a restriction posed on the base displacement to a maximum of 0.035 m, which is judged to be a threshold beyond which the overall stability of the structure is under risk. The limiting probability is $Q = 0.03$. The deterministic constraint corresponds to a limit posed on the natural frequency of the structure to avoid excessive flexibility.

For each calculation of the failure probability use was made of Markov chains with 10 samples. The three-stage algorithm was applied with $K_1 = 10, K_2 = 10$ (corresponding respectively to the number of iterations in the first and third stages) and $N = 10$ particles. The penalization of the constraints corresponds to $R = 2$ in Eq. (5.22) with the following specifications:

$$\begin{aligned} q_1(\boldsymbol{y}) &= \max\{0, (11 - \omega_\mathrm{s})\} && (5.38) \\ q_2(\boldsymbol{y}) &= \max\{0, (P_\mathrm{f} - Q)\} && (5.39) \end{aligned}$$

where $P_\mathrm{f} = \mathrm{P}[0.035 - \max|v_\mathrm{b}(\underline{\boldsymbol{x}}, \boldsymbol{y})| \leq 0]$. In addition

$$\Theta(q_1(\boldsymbol{y})) = \begin{cases} 1 & \text{if } q_1 < 0.001 \\ 2 & \text{if } 0.001 \leq q_1 < 0.01 \\ 3 & \text{if } 0.01 \leq q_1 < 0.1 \\ 4 & \text{otherwise} \end{cases} \tag{5.40}$$

$$\Theta(q_2(\boldsymbol{y})) = \begin{cases} 0.1 & \text{if } q_2 < 0.001 \\ 0.2 & \text{if } 0.001 \leq q_2 < 0.01 \\ 0.3 & \text{if } 0.01 \leq q_2 < 0.1 \\ 0.4 & \text{otherwise} \end{cases} \tag{5.41}$$

$$\beta(q_1(\boldsymbol{y})) = \begin{cases} 1 & \text{if } q_1 < 0.5 \\ 2 & \text{otherwise} \end{cases} \tag{5.42}$$

$$\beta(q_2(\boldsymbol{y})) = \begin{cases} 1 & \text{if } q_2 < 0.005 \\ 2 & \text{otherwise} \end{cases} \tag{5.43}$$

However, after the first $\boldsymbol{y}-$SVM was fitted (i.e. after the first K_1 iterations), the penalization of the probabilistic constraint changed simply to

$$\begin{aligned} q_2(\boldsymbol{y}) &= \max\{0, -c(\boldsymbol{y})\} \\ \Theta(q_2(\boldsymbol{y})) &= 0.03 \\ \beta(q_2(\boldsymbol{y})) &= 2 \end{aligned} \tag{5.44}$$

where $c(\boldsymbol{y})$ is the label given by the $\boldsymbol{y}-$SVM to the particle, given by

$$c(\boldsymbol{y}) = \operatorname{sgn}\left[r(\boldsymbol{y})\right] = \operatorname{sgn}\left[\sum_{k=1}^{S} \alpha_k c_k K(\boldsymbol{y}, \boldsymbol{y}_k) - b\right] \tag{5.45}$$

where $r(\boldsymbol{y})$ measures the distance of the particle $\boldsymbol{y}$ to the discriminating function. Clearly, if the particle is feasible, $c(\boldsymbol{y}) = +1$, $-c(\boldsymbol{y}) = -1$, and $q_2(\boldsymbol{y}) = \max\{0, -c(\boldsymbol{y})\} = 0$, while the opposite holds for an unfeasible particle. In addition, as said in the preceding, the position of the particle beyond the current $\boldsymbol{y}-$SVM margin is penalized in the third stage. To this end use was made of the following penalization:

$$q_3(\boldsymbol{y}) = \max\{0, |r(\boldsymbol{y})| - 1\} \tag{5.46}$$

$$\Theta(q_3(\boldsymbol{y})) = \begin{cases} 0.001 & \text{if } q_3 < 0.1 \\ 0.01 & \text{if } 0.1 \leq q_3 < 1 \\ 0.03 & \text{otherwise} \end{cases} \tag{5.47}$$

$$\beta(q_3(\boldsymbol{y})) = \begin{cases} 1 & \text{if } q_1 < 1 \\ 2 & \text{otherwise} \end{cases} \tag{5.48}$$

The constraint in Eq. (5.46) stems from the fact that a value of $|r(\boldsymbol{y})|$ greater that one corresponds to a sample beyond the margin.

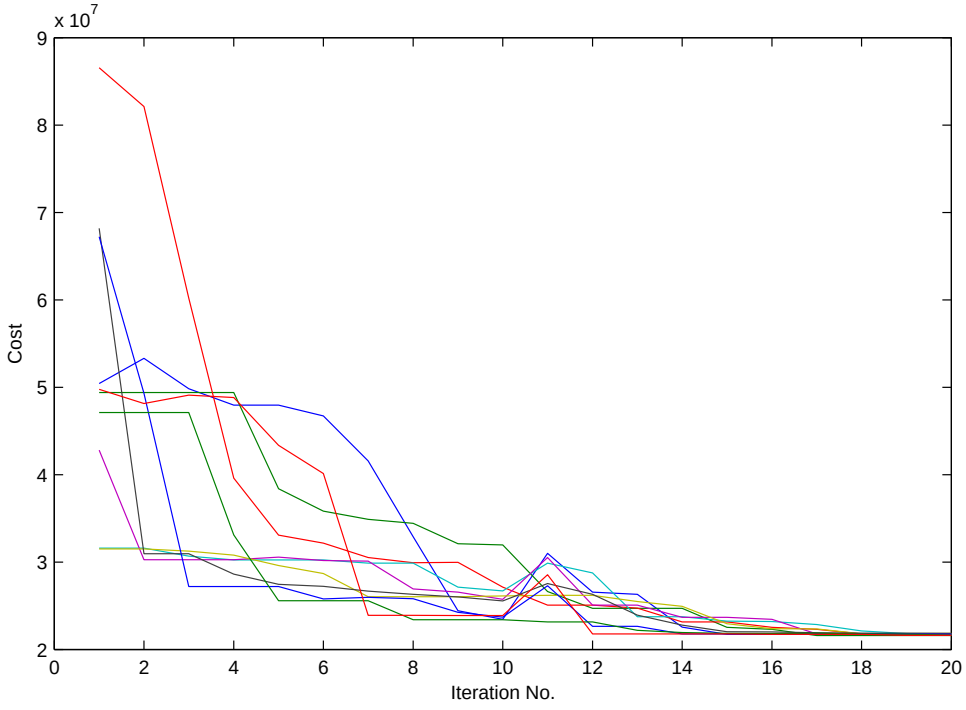

Figure 5.9: Evolution of cost function of the base isolated building. (Each line corresponds to a trial model).

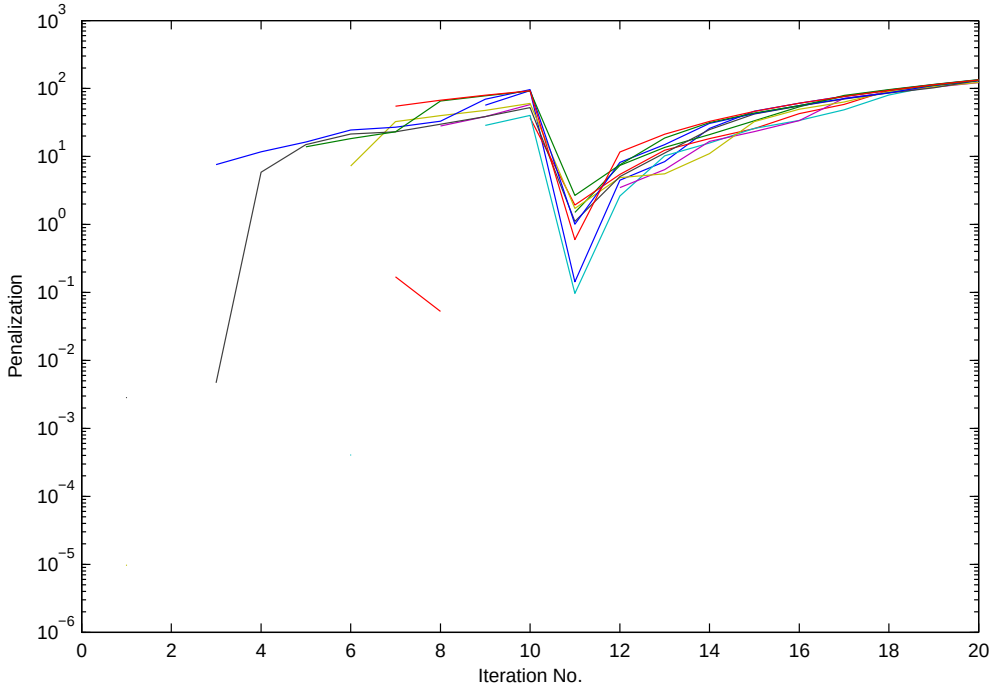

Figure 5.10: Evolution of penalization cost for the base isolated building.

Figure 5.9 shows the evolution of the structural cost function $C(\boldsymbol{y})$ for the ten particles along the $K_1 + K_2 = 20$ iterations. It can be observed that the algorithm converges rapidly. The minimum cost corresponds to $\boldsymbol{y} = \{M, \omega_{\mathrm{s}}, \omega_{\mathrm{b}}\} = \{186.6207\mathrm{t},\ 11.9679\mathrm{rad/s},\ 3.2567\mathrm{rad/s}\}$. Figure 5.10 shows the total penalization applied to the particles. The lines are broken for those particles which at certain iterations are not penalized. Notice that the penalization cost increases and becomes similar for all particles. Notice also the sudden reduction of the penalization cost when passing from the first stage to the third. This is not only due to the introduction of the third constraint concerning the violations of the margins of the newly calculated $\boldsymbol{y}-$SVM, but also to the change of initial population before starting the third stage, thus indicating that the generation of a new population in the vicinity of the best particle arising from the first stage is beneficial. On the

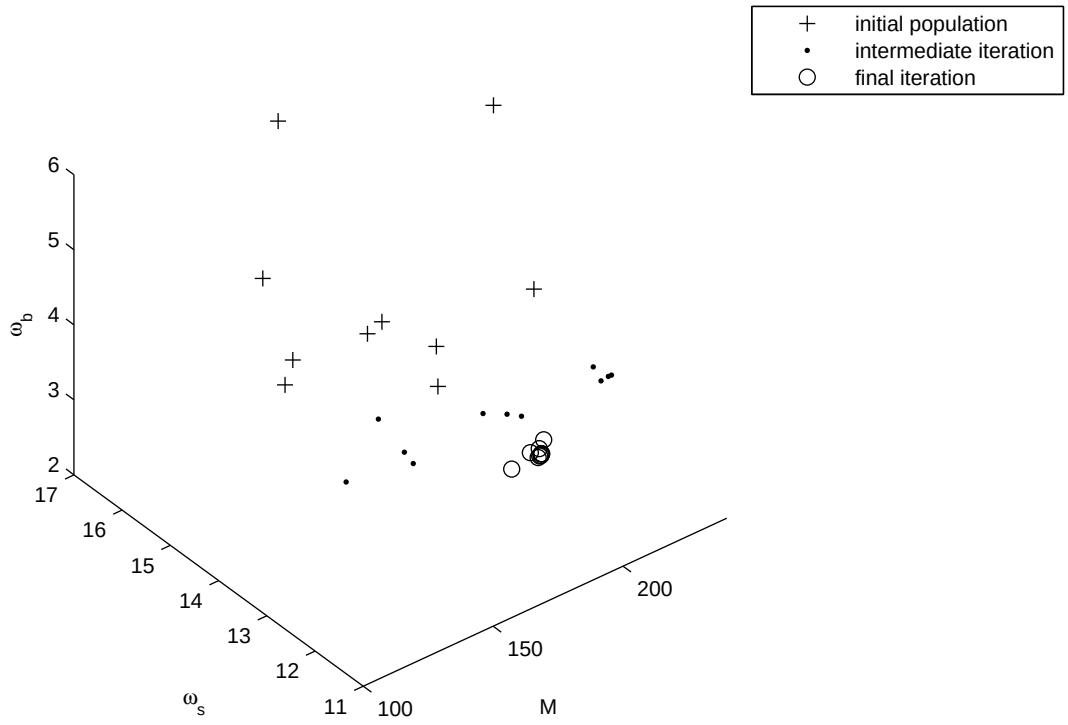

Figure 5.11: Snapshots of PSO convergence of base isolated building.

other hand, Figure 5.11 shows that the entire final population cluster in a small region close to the limiting value of $\omega_s = 11$ rad/s. Finally, Figure 5.12 displays the evolution of the failure probability estimates of all the particles through the first $K_1 = 10$ iterations. The figure interrupts at this point because of the introduction of the $\boldsymbol{y}-$SVM, which henceforth reports the feasibility or unfeasibility of the particle with labels $\{+1, -1\}$, respectively, without giving any estimate of the failure probability. Comparing this Figure with Fig. 5.9, it can be observed that as the cost diminishes the spread of the failure probability also reduces and, at the end of the first stage, almost all failure probabilities become lower than the imposed constraint. These figures demonstrate that the penalization technique succeeds in submitting the particles to the constraints.

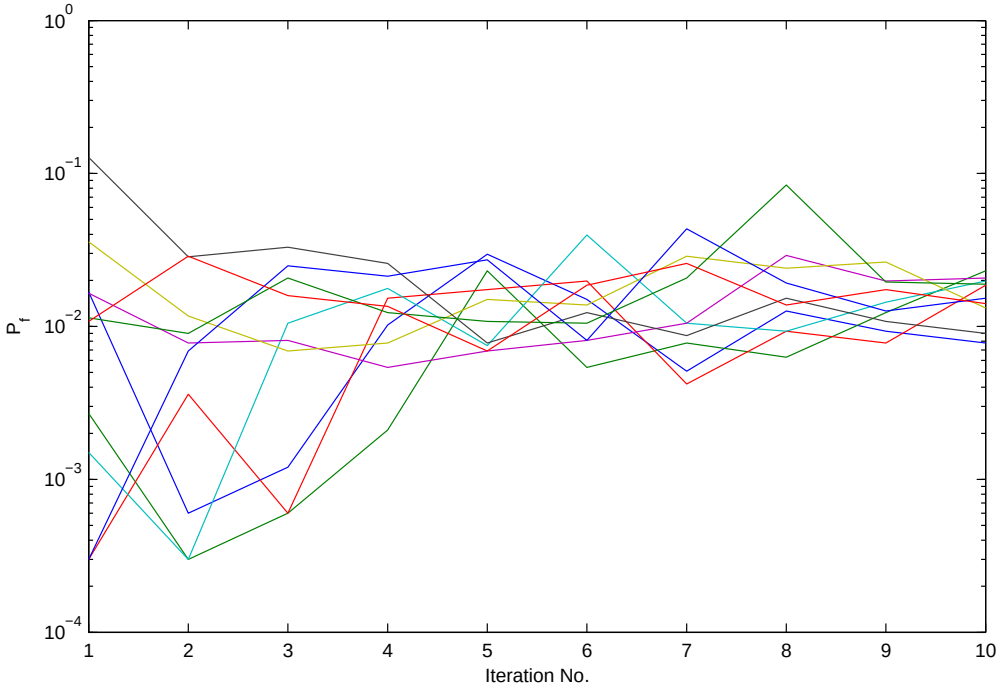

Figure 5.12: Evolution of the failure probability of the base isolated building.

5.5 Final remarks

This section is devoted to some comments about the limitations and hurdles of the methodologies proposed in the present paper.

First, with respect to the proposed algorithm for RBDO (Algorithm 3), it is important to note that the limiting numbers of iterations K_1 and K_2 are fixed on heuristic basis according to the international experience in SVM classification. Besides, they are given different names because of the dimensionality of $x-$SVM is in general different from that of the $\boldsymbol{y}-$SVM. Alternatively, the proposed algorithm can be modified by absorbing the training of the $\boldsymbol{y}-$SVM in Stage 1 and stopping its training according to a suitable stopping criterion. For instance, when the margin band becomes so narrow that the likelihood of misclassification of new

samples becomes little.

Also, improvements should be made to avoid the tend of flexible learning classifiers to produce fake twists and sometimes loops that may affect the prediction in both the $\boldsymbol{x}-$ and $\boldsymbol{y}-$spaces. An alternative using random numbers with a high entropy for the initial population is presently being evaluated by the authors.

Finally, in all uses of flexible classifiers it is important to incorporate methods for selecting its parameters (such as the number of neurons in Neural Networks of the kernel parameters in Support Vector Machines). The proposals for performing this task found in the international literature can be grouped into two categories: (a) the use of resampling techniques, in which several classifiers are evaluated with subsets of the given training population and (b) optimization techniques for finding the best parameters. Note that in applying these methods the training population is the same, so that the only increase in computational cost is that represented by the application of the resampling or optimization method.

Bibliography

[1] R. L. Iman and W. J. Canover. Small sample sensitivity analysis techniques for computer models with an application to risk assessment. *Communications in Statistics, Theory and Methods*, A9:1749 – 1842., 1980.

[2] A. Florian. An efficient sampling scheme: Updated Latin Hypercube Sampling. *Probabilistic Engineering Mechanics*, 7:123 – 130, 1992.

[3] D.E. Huntington and C.S. Lyrintzis. Improvements to and limitations of Latin Hypercube Sampling. *Probabilistic Engineering Mechanics*, 13:245 – 253, 1998.

[4] K. Ziha. Descriptive sampling in structural safety. *Structural Safety*, 17:33 – 41, 1995.

[5] A. Harbitz. An efficient sampling method for probability of failure calculation. *Structural Safety*, 3:109 – 115., 1986.

[6] G. I. Schuëller, C. G. Bucher, U. Bourgund, and W. Ouypornprasert. On efficient computational schemes to calculate failure probabilities. *Probabilistic Engineering Mechanics*, 4:10 – 18, 1989.

[7] O. Ditlevsen and H. O. Madsen. *Structural Reliability Methods*. John Wiley and Sons, Chichester, 1996.

[8] S. K. Au and J. L. Beck. Estimation of small failure probabilites in high dimensions by subset simulation. *Probabilistic Engineering Mechanics*, 16:263 – 277, 2001.

[9] A. Olsson, G. Sandberg, and O. Dahlblom. On Latin Hypercube sampling for structural reliability analysis. *Structural Safety*, 25:47–68, 2003.

[10] S. K. Au and J. L. Beck. Importance sampling in high dimensions. *Structural Safety*, 25:139 – 163, 2003.

[11] G. E. P. Box and N. R. Draper. *Empirical Model Building and Response Surfaces*. John Wiley and Sons, New York, 1987.

[12] D. C. Montgomery. *Design and Analysis of Experiments*. John Wiley and Sons, New York, 1991.

[13] J. E. Hurtado. Analysis of one-dimensional stochastic finite elements using neural networks. *Probabilistic Engineering Mechanics*, 17:35 – 44, 2002.

[14] J. E. Hurtado and D. A. Alvarez. A classification approach for reliability analysis with stochastic finite element modeling. *Journal of Structural Engineering*, 129:1141 – 1149, 2003.

[15] J. E. Hurtado. *Structural Reliability. Statistical Learning Perspectives*. Springer, Heidelberg, 2004.

[16] J. E. Hurtado and D.A. Alvarez. An optimization method for learning statistical classifiers in structural reliability. *Probabilistic Engineering Mechanics*, 25:26 – 34, 2010.

[17] O. Ditlevsen. Principle of Normal tail approximation. *Journal of the Engineering Mechanics Division*, 107:1191 – 1207, 1981.

[18] R. Rackwitz and B. Fiessler. Structural reliability under combined load sequences. *Computers and Structures*, 9:489 – 494, 1978.

[19] M. Hohenblicher and R. Rackwitz. Non-normal dependent vectors in structural reliability. *Journal of the Engineering Mechanics Division*, 107:1127 – 1138, 1981.

[20] S. Kotz, N. Balakrishnan, and N. L. Johnson. *Continuous Multivariate Distributions, Vol. 1.* John Wiley and Sons, New York, 2000.

[21] A. Nataf. Determination des distributions dont les marges sont donées. *Comptes rendues de l'Academie des Sciences*, 225:42–43, 1962.

[22] P. L. Liu and A. DerKiureghian. Multivariate distribution models with prescribed marginals and covariances. *Probabilistic Engineering Mechanics*, 1:105 – 112, 1986.

[23] H. J. Pradlwarter, C. G. Bucher, and G. I. Schuëller. Nonlinear systems. In G. I. Schuëller, editor, *Structural Dynamics: Recent Advances*, pages 128 – 213. Springer-Verlag, Berlin, 1991.

[24] A. DerKiureghian, H. Z. Lin, and S. J. Hwang. Second-order reliability approximations. *Journal of Engineering Mechanics*, 113:1208–1225, 1987.

[25] Y. G. Zhao and T. Ono. New approximations for SORM: Part I. *Journal of Engineering Mechanics*, 125:79–85, 1999.

[26] A. Haldar and S. Mahadevan. *Reliability Assessment using Stochastic Finite Element Analysis*. John Wiley and Sons, New York, 2000.

[27] W. K. Liu, T. Belytschko, and Y. J. Lua. Probabilistic finite element method. In C. (Raj) Sundararajan, editor, *Probabilistic Structural Mechanics Handbook*, pages 70–105. Chapman & Hall, New York, 1995.

[28] R. G. Ghanem and P. D. Spanos. *Stochastic Finite Elements: A Spectral Approach*. Springer Verlag, New York, 1991.

[29] B. Sudret and A. DerKiureghian. Stochastic finite element methods and reliability. a state-of-the-art report. Technical report, Report UCB/SEMM-2000/08, Department of Civil and Environmental Engineering, University of California, Berkely, 2000.

[30] G. I. Schuëller and R. Stix. A critical appraisal of methods to determine failure probabilities. *Structural Safety*, 4:293 – 309, 1987.

[31] J. C. Mitteau. Error evaluations for the computation of failure probability in static structural reliability problems. *Probabilistic Engineering Mechanics*, 14:119 – 135, 1999.

[32] Y. G. Zhao and T. Ono. A general procedure for first/second-order reliability method (FORM/SORM). *Structural Safety*, 21:955 – 112, 1999.

[33] Y. G. Zhao and T. Ono. New approximations for SORM: Part II. *Journal of Engineering Mechanics*, 125:86–93, 1999.

[34] R. Y. Rubinstein. *Simulation and the Monte Carlo Method*. John Wiley and Sons, New York, 1981.

[35] R. E. Melchers. *Structural Reliability: Analysis and Prediction*. John Wiley and Sons, Chichester, 1999.

[36] C. G. Bucher, H. J. Pradlwarter, and G. I. Schuëller. Computational stochastic structural analysis. In G. I. Schuëller, editor, *Structural Dynamics: Recent Advances*, pages 285 – 300. Springer-Verlag, Berlin, 1991.

[37] R. E. Melchers. Importance sampling in structural systems. *Structural Safety*, 6:3 – 10, 1989.

[38] G. L. Ang, A. H-S. Ang, and W. H. Tang. Optimal importance sampling density estimator. *Journal of Engineering Mechanics*, 118:1146 – 1163, 1991.

[39] C. G. Bucher. Adaptive Sampling: An Iterative Fast Monte-Carlo Procedure. *Structural Safety*, 5:119 – 126., 1988.

[40] S. K. Au and J. L. Beck. A new adaptive importance sampling scheme for reliability calculations. *Structural Safety*, 21:135 – 158, 1999.

[41] C. P. Robert and G. Casella. *Monte Carlo Statistical Methods*. Springer, New York, 1999.

[42] D. W. Scott. *Multivariate density estimation*. John Wiley and Sons, New York, 1992.

[43] G. McLachlan and D. Peel. *Finite Mixture Models*. John Wiley and Sons, New York, 2000.

[44] P. Bjerager. Methods for structural reliability computation. In F. Casciati and J. B. Roberts, editors, *Reliability Problems: General principles and Applications in Mechanics of Solids and Structures*, pages 89–136. Springer-Verlag, Wien, 1991.

[45] J. S. Liu. *Monte Carlo Strategies in Scientific Computing*. Springer, New York, 2001.

[46] H. J. Pradlwarter and G. I. Schuëller. Assessment of low probability events of dynamical systems by controlled Monte Carlo simulation. *Probabilistic Engineering Mechanics*, 14:213 – 227, 1999.

[47] N. Harnpornchai, H. J. Pradlwarter, and G. I. Schuëller. Stochastic analysis of dynamical systems by phase-space controlled Monte Carlo simulation. *Computer Methods in Applied Mechanics and Engineering*, 168:273–283, 1999.

[48] P. G. Melnik-Melnikov and E. S. Dekhtyaruk. Rare events probabilities estimation by "Russian Roulette and Splitting" simulation technique. *Probabilistic Engineering Mechanics*, 15:125 – 129, 2000.

[49] C. Bucher. A fast and efficient response surface approach for structural reliability problems. *Structural Safety*, 7:57–66, 1990.

[50] L. Faravelli. Response-surface approach for reliability analysis. *Journal of the Engineering Mechanics*, 115:2763 – 2781, 1989.

[51] M. R. Rajashekhar and B. R. Ellingwood. A new look at the response surface approach for reliability analysis. *Structural Safety*, 12:205–220, 1993.

[52] S. H. Kim and S. W. Na. Response surface method using vector projected sampling points. *Structural Safety*, 19:3–19, 1997.

[53] X. L. Guan and R.E. Melchers. Effect of response surface parameter variation on structural reliability estimates. *Structural Safety*, 23:429 – 444, 2001.

[54] J. E. Hurtado and D. A. Alvarez. Neural network-based reliability analysis: A comparative study. *Computer Methods in Applied Mechanics and Engineering*, 191:113 – 132, 2001.

[55] C. M. Bishop. *Neural Networks for Pattern Recognition*. Oxford University Press, Oxford, 1995.

[56] V. N. Vapnik. *Statistical Learning Theory*. John Wiley and Sons, New York, 1998.

[57] M. Papadrakakis, V. Papadopoulos, and N.D. Lagaros. Structural reliability analysis of elastic-plastic structures using neural networks and Monte Carlo simulation. *Computer Methods in Applied Mechanics and Engineering*, 136:145 – 163, 1996.

[58] T. Sasaki. A neural network-based response surface approach for computing failure probabilities. In R. B. Corotis, G. I. Schuëller, and M. Shinozuka, editors, *Structural Safety and Reliability - Proceedings of the International Conference on Structural Safety and Reliability, ICOSSAR 01, Newport Beach, California, 17-22 June 2001*, page 257, Lisse, The Netherlands, 2001. A.A.Balkema, Publishers.

[59] S. V. S. Cabral and L. S. Katafygiotis. Neural network based response surface method and adaptive importance sampling for reliability analysis of large structural systems. In R. B. Corotis, G. I. Schuëller, and M. Shinozuka, editors, *Structural Safety and Reliability - Proceedings of the International Conference on Structural Safety and Reliability, ICOSSAR 01, Newport Beach, California, 17-22 June 2001*, page 46, Lisse, The Netherlands, 2001. A.A.Balkema, Publishers.

[60] J. E. Hurtado. Neural networks in stochastic mechanics. *Archives of Computational Methods in Engineering*, 8:303 – 342, 2001.

[61] A. Sen and M. Srivastava. *Regression Analysis*. Springer Verlag, New York, 1990.

[62] B. D. Ripley. *Pattern Recognition and Neural Networks*. Cambridge University Press, Cambridge, 1996.

[63] B. Schölkopf and A. Smola. *Learning with Kernels*. The M. I. T. Press, Cambridge, 2002.

[64] K. Sobczyk and J. Trębicki. Maximum entropy principle in stochastic dynamics. *Probabilistic Engineering Mechanics*, 5:102 – 110, 1990.

[65] J. Trębicki and K. Sobczyk. Maximum entropy principle and non-stationary distributions of stochastic systems. *Probabilistic Engineering Mechanics*, 11:169–178, 1996.

[66] J. E. Hurtado and A.H. Barbat. Fourier-based maximum entropy method in stochastic dynamics. *Structural Safety*, 20:221 – 235, 1998.

[67] G. K. Er. A method for multi-parameter PDF estimation of random variables. *Structural Safety*, 20:25 – 36, 1998.

[68] C. A. Kennedy and W. C. Lennox. Solution to the practical problem of moments using non-classical orthogonal polynomials with applications for probabilistic analysis. *Probabilistic Engineering Mechanics*, 15:371 – 379, 2000.

[69] C. A. Kennedy and W. C. Lennox. Moment operations on random variables, with applications for probabilistic analysis. *Probabilistic Engineering Mechanics*, 16:253 – 259, 2001.

[70] G. A. Athanassoulis and P. N. Graviladis. The truncated hausdorff moment problem solved with kernel density functions. *Probabilistic Engineering Mechanics*, 17:273 – 291, 2002.

[71] H. P. Hong and N. C. Lind. Approximate reliability analysis using normal polynomial and simulation results. *Structural Safety*, 18:329 – 339., 1996.

[72] A. M. Hasofer. Non-parametric estimation of failure probabilities. In F. Casciati and B. Roberts, editors, *Mathematical Models for Structural Reliability Analysis*, pages 195–226. CRC Press, Boca Ratón, 1996.

[73] Y. G. Zhao and T. Ono. Moment methods for structural reliability. *Structural Safety*, 23:47 – 75, 2001.

[74] L. Xu and G. Cheng. Discussion on: moment methods for structural reliability. *Structural Safety*, 25:193 – 199, 2003.

[75] M. L. Shooman. *Probabilistic Reliability: An Engineering Approach*. McGraw-Hill, New York, 1968.

[76] M. E. Harr. *Reliability-based Design in Civil Engineering*. Dover Publications, New York, 1987.

[77] E. T. Jaynes. Information Theory and Statistical Mechanics. *The Physical Review*, 106:620 – 630, 1957.

[78] F. M. Reza. *An Introduction to Information Theory*. Dover Publications, New York, 1994.

[79] A. Papoulis. *Probability, Random Variables and Stochastic Processes*. McGraw-Hill, New York, 1991.

[80] F. Grooteman. Adaptive radial-based importance sampling method for structural reliability. *Structural Safety*, 30:533 – 542, 2008.

[81] R. D. Bertero and V. V. Bertero. Performance-based seismic engineering: the need for a reliable conceptual comprehensive approach. *Earthquake Engineering and Structural Dynamics*, 31:627 – 652, 2002.

[82] R. G. Sexsmith. Probability-based safety analysis – value and drawbacks. *Structural Safety*, 21:303 – 310, 1999.

[83] I. Elishakoff. *Safety Factors and Reliability: Friends or Foes?* Kluwer, New York, 2005.

[84] I. Doltsinis and A. Kang. Robust design of structures using optimization methods. *Computer Methods in Applied Mechanics and Engineering*, 193:2221 – 2237, 2004.

[85] H. G. Beyer and B. Sendhoff. Robust Optimization. A comprehensive survey. *Computer Methods in Applied Mechanics and Engineering*, 196:3190–3218, 2007.

[86] E. Rosenblueth and E. Mendoza. Reliability optimization in isostatic structures. *Journal of the Engineering Mechanics Division ASCE*, 97:1625–1640, 1971.

[87] M. Gasser and G. I. Schuëller. Reliability-based optimization of structural systems. *Mathematical Methods of Operations Research*, 46:287–307, 1997.

[88] N. C. Nigam and S. Narayanan. *Applications of Random Vibrations*. Springer Verlag - Narosa Publishing House, Berlin, New Delhi, 1994.

[89] D. Frangopol. Reliability-based structural design. In C. (Raj) Sundararajan, editor, *Probabilistic Structural Mechanics Handbook*, pages 352–387. Chapman & Hall, New York, 1995.

[90] B. Ellingwood, J. C. MacGregor, and C. A. Cornell. Probability-based load criteria: load factors and load combinations. *Journal of Structural Engineering*, 108:978–997, 1982.

[91] Y. Ben-Haim. *Robust Reliability in the Mechanical Sciences*. Springer Verlag, Berlin, 1996.

[92] M. Papadrakakis, N.D. Lagaros, and Y. Tsompanakis. Structural optimization using evolution strategies and neural networks. *Computer Methods in Applied Mechanics and Engineering*, 156:309 – 333, 1998.

[93] N. Lagaros, M. Papadrakakis, and G. Kokossalakis. Structural optimization using evolutionary algorithms. *Computers and Structures*, 80:571–579, 2002.

[94] N. Lagaros and M. Papadrakakis. Soft computing methodologies for structural optimization. *Applied Soft Computing*, 3:283–300, 2003.

[95] J. E. Hurtado. Optimal reliability-based design using support vector machines and artificial life algorithms. In Y. Tsompanakis and N. D. Lagaros, editors, *Intelligent Computational Paradigms in Earthquake Engineering*. Idea Group Inc., Hershey, 2006.

[96] I. Doltsinis, A. Kang, and G. Cheng. Robust design of non-linear structures using optimization methods. *Computer Methods in Applied Mechanics and Engineering*, 194:1779 – 1795, 2005.

[97] J. O. Royset, A. Der Kiureghian, and E. Polak. Reliability-based optimal structural design by the decoupling approach. *Reliability Engineering and System Safety*, 73:213–221, 2001.

[98] R. W. Clough and J. Penzien. *Dynamics of Structures*. McGraw-Hill, New York, 1993.

[99] P. Moayyad and B. Mohraz. A study of power spectral density of earthquake accelerograms. Technical report, Civil and Mechanical Engineering Department, Southern Methodist University, Dallas, TX, 1982.

[100] R. H. Sues, Y. K. Wen, and A. H. S. Ang. Stochastic evaluation of seismic structural performance. *Journal of Structural Engineering*, 111:1204–1218, 1985.

[101] N. C. Nigam. *Introduction to Random Vibrations*. The M. I. T. Press, Cambridge, 1983.

[102] T. T. Soong and M. Grigoriu. *Random Vibration of Structural and Mechanical Systems*. Prentice Hall, Englewood Cliffs, 1993.

[103] L. D. Lutes and S. Sarkani. *Stochastic Analysis of Structural and Mechanical Vibrations*. Prentice Hall, Upper Saddle River, 1997.

[104] E. Vanmarcke. Structural response to earthquakes. In C. Lomnitz and E. Rosenblueth, editors, *Seismic Risk and Engineering Decisions*, pages 287–337. Elsevier, Amsterdam, 1976.

[105] E. H. Vanmarcke and S. P. Lai. Strong-motion duration and rms amplitude of earthquake records. *Bulletin of the Seismological Society of America*, 70:1293–1307, 1980.

[106] S. P. Lai. Statistical characterization of strong ground motions using power spectral density function. *Bulletin of the Seismological Society of America*, 72:259–274, 1982.

[107] M. Shinozuka and Y. Sato. Simulation of nonstationary random processes. *Journal of Engineering Mechanics*, 93:11–40, 1967.

[108] M. Amin and A. H. S. Ang. A nonstationary stochastic model for strong motion earthquakes. Technical report, Structural Research Series, 306, Dept. of Civil Engineering, University of Illinois, Urbana-Champaign, Illinois, 1966.

[109] K.A. Ahmed, J. Kanda, and R. Iwasaki. Estimation of uncertainties in the dynamic response of urban soils in Japan. In *Proceedings of the Eleventh World Conference on Earthquake Engineering*, Rotterdam, 1996. Elsevier Science.

[110] J. B. Roberts and P. D. Spanos. *Random Vibration and Statistical Linearization.* John Wiley and Sons, Chichester, 1990.

[111] F. Casciati and L. Faravelli. *Fragility Analysis of Complex Structural Systems.* Research Studies Press Ltd., Taunton, 1991.

[112] L. Socha. *Linearization Methods for Stochastic Dynamic Systems.* Springer, Berlin, 2008.

[113] C. A. Schenk and G. I. Schuëller. *Uncertainty Assessment of Large Finite Element Systems.* Springer, Berlin, 2005.

[114] Y. K. Wen. Method for random vibration of hysteretic systems. *Journal of the Engineering Mechanics Division*, 102:248–262, 1976.

[115] T. S. Atalik and S. Utku. Stochastic linearization of multi-degree of freedom non-linear systems. *Earthquake Engineering and Structural Dynamics*, 4:411–420, 1976.

[116] J. E. Hurtado and A.H. Barbat. Equivalent linearization of the Bouc-Wen hysteretic model. *Engineering Structures*, 20:1121 – 1132, 2000.

[117] K. Kimura, H. Yasumuro, and M. Sakata. Non-gaussian equivalent linearization for nonstationary random vibration of hysteretic system. *Probabilistic Engineering Mechanics*, 9:15–22, 1994.

[118] J. N. Yang and S. C. Liu. Distribution of maximum and statistical response spectra. *Journal of Engineering Mechanics*, 107:1089–1102, 1981.

[119] L. Socha. The sensitivity analysis of stochastic non-linear dynamical systems. *Journal of Sound and Vibration*, 110:271 – 288, 1986.

[120] L. Socha and G. Zasucha. The sensitivity analysis of stochastic hysteretic dynamic systems. In P. D. Spanos and C. A. Brebbia, editors, *Computational Stochastic Mechanics*, pages 71–80. Elsevier Applied Science, London, 1991.

[121] E. Rosenblueth. Point estimates for probability moments. *Proceedings of the National Academy of Sciences of the USA*, 72:3812 – 3814, 1975.

[122] H. P. Hong, J. A. Escobar, and R. Gómez. Probabilistic assessment of the in seismic response of structural asymmetric models. In *Proceedings of the Tenth European Conference on Earthquake Engineering, Paris, 1998*, Rotterdam, 1998. Balkema.

[123] Y. G. Zhao, T. Ono, and H. Idota. Response uncertainty and time-variant reliability analysis for hysteretic MDF structures. *Earthquake Engineering and Structural Dynamics*, 28:1187 – 1213, 1999.

[124] J. E. Hurtado. Structural robustness and its relationship to reliability. In Y. Tsompanakis, N. D. Lagaros, and M. Papadrakakis, editors, *Structural Design Optimization Considering Uncertainties*. Taylor and Francis, Leiden, 2007.

[125] M. Ordaz. On the use of probability concentrations. *Structural Safety*, 5:317 – 318, 1988.

[126] J. T. Christian and G. B. Baecher. Point-estimate method and numerical quadrature. *Journal of Geotechnical and Geoenvironmental Engineering*, 125:779 – 786, 1998.

[127] M.E. Harr. Probabilistic estimates for multivariate analysis. *Applied Mathematical Modelling*, 13:313 – 318, 1989.

[128] H. P. Hong. An efficient point estimate method for probabilistic analysis. *Reliability Engineering and System Safety*, 59:261–267., 1998.

[129] J. Ohser and F. Mücklich. *Statistical analysis of microstructures in materials science*. John Wiley and Sons, Chichester, 2000.

[130] W. H. Press, S. A. Teukolsky, W. T. Vetterling, and B. P. Flannery. *Numerical Recipes in FORTRAN*. Cambridge University Press, Cambridge, 1992.

[131] J. M. Kelly. *Earthquake-Resistance Design with Rubber*. Springer-Verlag, London, 1993.

[132] J. H. Lee and B. M. Kwak. Reliability-based structural optimal design using the Neumann expansion technique. *Computers and Structures*, 55:287 – 296, 1995.

[133] R. V. Grandhi and L. Wang. Reliability-based structural optimization using improved two-pont adaptive nonlinear approximations. *Finite Elements in Analysis and Design*, 29:35–48, 1998.

[134] X. Qu and R. T. Haftka. Reliability-based design optimization using probabilistic sufficiency factor. *Structural and Multidisciplinary Optimization*, 27:314–325, 2004.

[135] J. O. Royset and E. Polak. Reliability-based optimal design using sample average approximations. *Probabilistic Engineering Mechanics*, 19:331–343, 2004.

[136] J. O. Royset and E. Polak. Reliability-based design optimization of structural systems. In *Proceedings of the 9th ASCE Speciality Conference on Probabilistic Mechanics and Structural Reliability*, Albuquerque, 2004. ASCE.

[137] K. K. Choi, J. Tu, and Y. H. Park. Extension of design potential concept for reliability-based design optimization to nonsmooth and extreme cases. *Structural and Multidisciplinary Optimization*, 22:335–350, 2001.

[138] H. Argawal and J. E. Renaud. Decoupled methodology for probabilistic design optimization. In *Proceedings of the 9th ASCE Speciality Conference on Probabilistic Mechanics and Structural Reliability*, Albuquerque, 2004. ASCE.

[139] Y. Tsompanakis and M. Papadrakakis. Robust and efficient methods for reliability-based structural optimization. In *IASS-IACM 2000 Computational Methods for Shell and Spatial Structures*, ATHENS, 2000. ISASR-NTUA.

[140] C. Papadimitriou and E. Notsios. Robust reliability-based optimization in structural dynamics using evolutionary algorithms. In *Proceedings of the 9th ASCE Speciality Conference on Probabilistic Mechanics and Structural Reliability*, Albuquerque, 2004. ASCE.

[141] J. E. Hurtado. Optimal reliability-based design using support vector machines and artificial life algorithms. In Y. Tsompanakis and N. D. Lagaros, editors, *Intelligent Computational Paradigms in Earthquake Engineering*. Idea Group Inc., Hershey, 2006.

[142] I. Kaymaz and C. A. McMahon. A probabilistic design system for reliability-based design optimization. *Structural and Multidisciplinary Optimization*, 28:416–426, 2004.

[143] M. Kleiber, A. Siemaszko, and R. Stocki. Interactive stability-oriented reliability-based design optimization. *Computer Methods in Applied Mechanics and Engineering*, 168:243 – 253, 1999.

[144] G. Kharmanda, N. Olhoff, A. Mohamed, and M. Lemaire. Reliability-based topology optimization. *Structural and Multidisciplinary Optimization*, 26:295–307, 2004.

[145] B. F. Spencer, M. K. Sain, C. H. Won, D. C. Kaspari, and P. M. Sain. Reliability-based measures of structural control robustness. *Structural Safety*, 15:111–129, 1994.

[146] M. Allen and K. Maute. Reliability-based optimization of aerolastic structures. *Structural and Multidisciplinary Optimization*, 27:228–242, 2004.

[147] S. Barakat, K. Bani-Hani, and M. Q. Taha. Multi-objective reliability-based optimization of prestressed concrete beams. *Structural Safety*, 26:311–342, 2006.

[148] J. E. Hurtado. An examination of methods for approximating implicit limit state functions from the viewpoint of statistical learning theory. *Structural Safety*, 26:271 – 293, 2004.

[149] J. E. Hurtado, F. Zrate, and E. Oate. Reliability estimation of the sheet stamping process using support vector machines. *International Journal of Vehicle Design*, 39(1-2):110–124, 2005.

[150] J. E. Hurtado. Filtered importance sampling with support vector margin: a powerful method for structural reliability analysis. *Structural Safety*, 29:2 – 15, 2007.

[151] J. Kennedy and R. C. Eberhart. *Swarm Intelligence*. Morgan Kaufmann, San Francisco, 2001.

[152] E. Ebeltagi, T. Hegazi, and D. Grierson. Comparison among five evolutionary-based optimization algorithms. *Information Sciences*, 19:43–53, 2005.

[153] Y. K. Wen. Building reliability and code calibration. *Earthquake Spectra*, 11:269–296, 1995.

[154] N. Metropolis, A. W. Rosenbluth, M. N. Rosenbluth, A. H. Teller, and E. Teller. A new algorithm for adaptive multidimensional integration. *Journal of Chemical Physics*, 21:1087 – 1092, 1953.

[155] Simon Tong and Daphne Koller. Support vector machine active learning with applications to text classification. In Pat Langley, editor, *Proceedings of ICML-00, 17th International Conference on Machine Learning*, pages 999–1006, Stanford, 2000. Morgan Kaufmann Publishers, San Francisco.

[156] C. Elegbede. Structural reliability assessment based on particle swarm optimization. *Structural Safety*, 27:171 – 186, 2005.

[157] P. C. Fourie and A. A. Groenwold. The particle swarm optimization algorithm in size and shape optimization. *Structural and Multidisciplinary Optimization*, 23:259–267, 2002.

[158] G. Venter and J. Sobieszczanski-Sobieski. Multidisciplinary optimization of a transport aircraft wing using particle swarm optimization. *Structural and Multidisciplinary Optimization*, 26:121–131, 2004.

[159] J.F. Schutte and A.A. Groenwold. Sizing design of truss structures using particle swarms. *Structural and Multidisciplinary Optimization*, 25:261–269, 2003.

[160] K. E. Parsopoulos and M. N. Vrahatis. Particle swarm optimization method for constrained optimization problems. Technical report, Department of Mathematics, University of Patras, Greece, 2001.

[161] R. T. Haftka, Z. Gurdal, and M. P. Kamat. *Elements of Structural Optimization*. Kluwer Academic Publishers, Dordrecht, 1990.

[162] D. M. Boore. Stochastic simulation of high-frequency ground motions based on seismological models of the radiated spectra. *Bulletin of the Seismological Society of America*, 73:18651894, 1983.

[163] G. M. Atkinson ans W. Silva. Stochastic modelling of California ground motions. *Bulletin of the Seismological Society of America*, 90:255274, 2000.

[164] C. H. Yeh and Y. K. Wen. Modeling of nonstationary ground motion and analysis of inelastic structural response. *Structural Safety*, 8:281–298, 1990.

[165] H. P. Hong and S. S. Wang. Probabilistic analysis of peak response of MDOF systems with uncertain PSD function. *Earthquake Engineering and Structural Dynamics*, 31:1719 – 1733, 2002.

CENTRO INTERNACIONAL DE METODOS NUMERICOS EN INGENIERIA

Lista de monografías publicadas en la Serie de Ingeniería Sísmica

Las monografías pueden adquirirse dirigiéndose al Departamento de Publicaciones del Centro Internacional de Métodos Numéricos en Ingeniería, Edificio C1, Campus Norte UPC, c/ Gran Capitán s/n, 08034 Barcelona, teléfono: 93-401.60.37, Fax: 93-401-65-17.

IS-1 *Qualitative Reasoning for Earthquake Resistant Buildings,* Luís M. Bozzo, 149 pp., ISBN 84-87867-36-7, 1993.

IS-2 *Control predictivo en sistemas de protección sísmica de estructuras,* R. Andrade Cascante, J. Rodellar, F. López Almansa, 143 pp., ISBN 84-87867-37-5, 1993.

IS-3 *Simulación numérica del comportamiento no lineal de presas de hormigón ante acciones sísmicas,* M. Galindo, J. Oliver, M. Cervera, 255 pp., ISBN 84-87867-38-3, 1994.

IS-4 *Simulación del daño sísmico en edificios de hormigón armado,* A. Hanganu, A.H. Barbat, S. Oller, E. Oñate, 96 pp., ISBN 84-87867-40-5, 1994.

IS-5 *Edificios con aislamiento de base no lineal,* N. Molinares, A.H. Barbat, 96 pp., ISBN: 84-87867-41-3, 1994.

IS-6 *Vulnerabilidad sísmica de edificios,* C. Caicedo, A.H. Barbat, J.A. Canas, R. Aguiar, 100 pp., ISBN 84-87867-43-X, 1994.

IS-7 *Análisis de terremotos históricos por sus efectos,* J. R. Arango González, 119 pp., ISBN 84-87867-44-8, 1994.

IS-8 *Control activo no lineal de edificios con aislamiento de base,* A.H. Barbat, N. Molinares, J. Rodellar, 124 pp., ISBN 84-87867-46-4, 1994.

IS-9 *Análise estocástica da resposta sísmica nao-linear de estructuras,* A.M. F. Cunha, 199 pp., ISBN: 84-87867-47-2, 1994

IS-10 *Definición de la acción sísmica,* A.H. Barbat, L. Orosco, J.E. Hurtado, M. Galindo, 122 pp., ISBN: 84-87867-448-0, 1994

IS-11 *Sismología y peligrosidad sísmica,* J.A. Canas Torres, C. Pujades Beneit, E. Banda Tarradellas, 87 pp., ISBN: 84-87867-49-9, 1994

IS-12 *Riesgo, peligrosidad y vulnerabilidad sísmica de edificios de mampostería,* F. Yépez, A.H. Barbat, J.A. Canas, 104 pp., ISBN: 84-87867-50-2, 1999

IS-13 *Estudios de ingeniería sismológica y sísmica*, J.A. Canas, ISBN: 84-87867-57-X, 13 pp., 1995

IS-14 *Simulación de escenarios de daño para estudios de riesgo sísmico*, F. Yépez, A.H. Barbat y J.A. Canas, ISBN: 84-87867-58-8, 103 pp., 1995

IS-15 *Diseño sismorresistente de edificios de hormigón armado*, L. Bozzo, A.H. Barbat, ISBN: 84-87867-59-6, 185 pp., 1995

IS-16 *Modelo tridimensional de atenuación anelástica de las ondas sísmicas en la Península Ibérica*, J.O. Caselles, J. A. Canas, Ll. G. Pujades, R.B. Herrmann, ISBN: 84-87867-60-X, 119 pp., 1995

IS-17 *Índices de daño sísmico en edificios de hormigón armado*, R. Aguiar ISBN: 84-87867-43-X, 99 pp., 1996

IS-18 *Experimental study of a reduced scale model seismically base isolated with Rubber-Layer Roller Bearings (RLRB),* D. Foti, J.M. Kelly ISBN: 84-87867-82-0, 112 pp., 1996

IS-19 *Modelos de evaluación del comportamiento sísmico no lineal de estructuras de hormigón armado,* F. Yépez Moya, ISBN: 84-87867-80-4., 96pp., 1996

IS-20 *Evaluación probabilista de la vulnerabilidad y riesgo sísmico de estructuras de hormigón armado por medio de simulación,* F. Yépez Moya, A.H. Barbat, J.A. Canas, ISBN: 84-87867-81-2, 1996

IS-21 *Modelización de la peligrosidad sísmica. Aplicación a Cataluña*, J.A. Canas, J.J. Egozcue, J. Miquel Canet y A.H. Barbat, ISBN: 84-87867-83-9, 101pp., 1996

IS-22 *Evaluación del daño sísmico global en edificios porticados de hormigón armado*, R. Aguiar, A.H. Barbat and J. Canas, ISBN: 84-87867-96-0, 173pp., 1997

IS-23 *Daño sísmico global en edificios con muros de cortante*, R. Aguiar, ISBN: 84-89925-00-3, 101 pp., 1997

IS-24 *Conceptos de cálculo de estructuras en las normativas de diseño sismorresistente*, A.H. Barbat y S. Oller, ISBN: 84-89925-10-0, 107pp., 1997

IS-25 *Stochastic dynamics of histeretic structures*, J.E. Hurtado, ISBN: 84-89925-09-7, 205pp., 1998

IS-26 *Análisis de los acelerogramas de la serie de Adra (Almería). Diciembre 1993 a Enero 1994,* R. Blázquez, A. Suárez, E. Carreño y A.J. Martín, ISBN: 84-89925-11-9,
1998

IS-27 *Respuesta de puentes frente a acciones sísmicas*, E. Maldonado, J.A. Canas, J.R. Casas, L.G. Pujades, ISBN: 84-89925-23-2, 107pp., 1998

IS-28 *Estudio de parámetros en la vulnerabilidad sísmica de puentes*, E. Maldonado, J.A. Canas y J.R. Casas, ISBN: 84-89925-16-X, 97pp., 1998

IS-29 *Metodologías para o cálculo sísmico não-linear de barragens de betão*, R. Faria ISBN: 84-89925-25-9, 113pp., 1998

IS-30 *Acciones para el diseño sísmico de estructuras*, R. Aguiar, ISBN: 84-89925-27-5, 122pp., 1998

IS-31 *Avaliação do comportamento sísmico de barragens de betão*, R. Faria, ISBN: 84-89925-28-3, 88pp., 1998

IS-32 *Vulnerabilidad sísmica de hospitales. Fundamentos para ingenieros y arquitectos*, O.D. Cardona, ISBN:84-89925-33-X, 165pp., 1999

IS-33 *Modelación estocástica de la acción sísmica*, J. E. Hurtado, ISBN:84-8925-34-8, 93pp., 1999

IS-34 *Earthquake simulator testing of a steel model seismically protected with friction energy dissipators,* D. Foti and J. Canas, ISBN: 84-89925-40-2, 110pp., 1999

IS-35 *Plasticidad y fractura en estructuras aporticadas, J.* Flórez López, ISBN: 84-89925-46-1, 90pp., 1999

IS-36 *Estimación de efectos locales con movimientos sísmicos y microtembl*ores, V. Giraldo, A. Alfaro, L. G. Pujades, J. A. Canas, ISBN: 84-89925-54-2, 83pp., 1999

IS-37 *Modelo numérico de elastómeros multi-fase y su aplicación al análisis de estructuras con aislamiento sísmico*, O. Salomón, S. Oller y A. H. Barbat, ISBN: 84-89925-54-2, 239pp.,1999

IS-38 *Dinámica de estructuras. Aplicaciones a la Ingeniería Sísmica*, J.E. Hurtado, ISBN:84-89925-59-3,177pp., 2000

IS-39 *Utilización de los conjuntos difusos en modelos de vulnerabilidad sísmica*, E. Maldonado Rondón, J.R. Casas Rius y J.A. Canas, ISBN:84-89925-61-5, 2000

IS-40 *Modelo de vulnerabilidad sísmica de puentes basado en " Conjuntos Difusos "*, E. Maldonado Rondón, J.R. Casas Rius, J. A.Canas, ISBN: 84-89925-64-X, 110pp, 2000

IS-41 *Vulnerabilidad de puentes de autopista. Un estado del arte*, C. Gómez Soberón, A. Barbat, S. Oller, ISBN: 84-89925-64-X, 168pp, 2000

IS-42 *Fuerzas sísmicas en los Países Bolivarianos*, R. Aguiar Falconí, ISBN: 84-89925-74-7, 101pp., 2000

IS-43 *Espectros de input de energía de aplicación en el proyecto sismorresistente estructuras en regiones de sismicidad moderada*, A. Benavent-Climent, L.G. Pujades, F. López-Almansa, ISBN: 84-89925-86-0, 85 pp., 2001

IS-44 *Capacidad límite última de disipación de energía de estructuras de hormigón Armado sometidas a acciones sísmicas,* A. Benavent- Climent, F. López-Almansa, L. G. Pujades, ISBN: 84-89925-88-7, 2001

IS-45 *Evaluación del daño en edificios y desempeño sísmico. Programa de ordenador CEINCI3,* R. Aguiar Falconí, ISBN: 84-89925-87-9, 107pp., 2001

IS-46 *Estudio analítico sobre el comportamiento sísmico de muros de mampostería confinada con aberturas,* J. J. Álvarez, S.M. Alcocer, ISBN: 84-89925-90-9, 119pp., 2002

IS-47 *Seismic vulnerability of bridges using simplified models*, C. Gómez Soberón, S. Oller, A. H. Barbat, ISBN: 84-89925-96-8, 135pp., 2002

IS-48 *Control de vibraciones en puentes. Un estado del arte y de la práctica,* M. Jara, J. R. Casas, ISBN: 84-95999-01-3, 120pp., 2002

IS-49 *Criterio de diseño de puentes con aisladores y disipadores de energía,* M. Jara, J. R. Casas, ISBN: 84-955999-02-1, 115pp., 2002

IS-50 *Ferrocemento: Un acercamiento al diseño sísmico,* D. A. Bedoya, J. Farbiarz, J. E. Hurtado, Ll. G. Pujades, ISBN: 84-95999-23-4, 76pp., 2002

IS-51 *Metodología para la evaluación del desempeño de la gestión del riego,* M. L. Carreño, O. D. Cardona, A. H. Barbat, ISBN: 84-95999-66-8, 2004

IS-52 *Sistema de indicadores para la evaluación de riesgos,* M. L. Carreño, O. D. Cardona, A. H. Barbat, ISBN: 84-95999-70-6, 200

IS-53 *Evaluación "ex-post" del estado de daño en los edificios afectados por un terremoto,* M. L. Carreño, O. D. Cardona, A. H. Barbat, ISBN: 84-95999-76-5, 2005

IS-54 *Identificação modal estocástica de estruturas de engenharia civil,* F. Magalhães, A. Cunha, E. Caetano, ISBN: 84-95999-89-7, 2005

IS-55 *Comportamiento sísmico de puentes articulados y disipación de energia adicional: Un estado del crecimiento,* G. E. Valdebenito, A. C. Aparicio, ISBN: 84-95999-87-0, 2005

IS-56 *Cálculo y diseño sismorresistente de edificios. Aplicación de la norma NCSE-02*, A.H. Barbat, S. Oller and J.C. Vielma, 2005

IS-57 Eval*uación rápida de la deriva máxima de piso para calcular la vulnerabilidad sísmica de estructuras,* R. Aguiar, ISBN: 84-95999-91-9, 2006

IS-58 *Factor de reducción de las fuerzas sísmicas en edificios de hormigón armado sin muros de corte,* R. Aguiar, ISBN: 978-84-96736-40-7, 2007

IS-59 *Herramientas necesarias para la evaluación sísmica de edificios,* R. Moreno, L. Pujades, A.C. Aparicio, A.H. Barbat, ISBN: 978-84-96736-53-5, 2007

IS-60 *Inelastic Analysis of Geometrically Exact Rods,* P. L. Mata, A.H. Barbat, S. Oller, R. Boroschek, ISBN: 978-84-96736-59-7, 2007

IS-61 *La gestión financiera del riesgo desde la perpectiva de los desastres,* M.C.Marulanda, O.D. Cardona, M.G. Ordaz, A.H.Barbat, ISBN:978-84-96736-60-3, 2008

IS-62 *Seismic protection of cable-stayed bridges applying fluid viscous dampers,* G.E. Valdebenito, A.C. Aparicio, ISBN:978-84-96736-84-9, 2009

Los autores interesados en publicar monografías en esta serie deben contactar con el editor para concretar las normas de preparación del texto.